



Roman Wilfinger, BSc.

Absolute positioning of vehicles in indoor environments using Wireless LAN and Bluetooth LE

MASTER'S THESIS

to achieve the university degree of

Diplom-Ingenieur

Master's degree programme: Geomatics Science

submitted to

Graz University of Technology

Supervisor

Ao.Univ.-Prof. Dipl.-Ing. Dr.techn. Manfred Wieser

Institute of Geodesy

Affidavit

I declare that I have authored this thesis independently, that I have not used other than the declared sources/resources, and that I have explicitly indicated all material which has been quoted either literally or by content from the sources used. The text document uploaded to TUGRAZonline is identical to the present master's thesis dissertation.

Date

Signature

Acknowledgments

First and foremost I would like to thank my supervisor Ao.Univ.-Prof. Dipl.-Ing. Dr.techn. Manfred Wieser. Despite his busy daily job routine, he somehow always managed to have an open ear for concerns, questions and ideas. My thanks go to him and the Institute of Geodesy for providing a pleasant working environment.

A great thanks is dedicated to Dipl.-Ing. Thomas Moder. Throughout the stages of the thesis he assisted me with valuable input and laid out a path for the directions this thesis took. His door is open at all times (apart from his occasional adventurous vacations, which is certainly nothing to begrudge him for!) and the collaboration with him was pleasant. This thesis would not have been possible without his effort and engagement.

My thanks go to Magna Steyr Engineering for having this thesis embedded in a larger project and thus providing monetary remuneration. Additionally I would like to thank Dipl.-Ing. Christian Payerl for his valuable feedback throughout our numerous meetings.

I am indebted to Fachoberinspektor Bernd Mölg for assisting me with my practical investigations and most importantly for helping with the tachymetric survey of the parking deck. I hereby also thank Dipl.-Ing. Stefan Lackner BSc. for helping me with the automated live-tracking of the test vehicle. Additionally, my thanks go to all other colleagues that supported me and my work in any way.

Last but not least, I have to thank my family and friends who always motivated me and endured my occasional whinings, although those have been surprisingly few throughout the past months.

Thank you!

Abstract

Exact position determination in indoor environments is crucial for many applications, including the aspiring field of self-driving vehicles. In the face of an autonomous parking pilot in indoor parking lots, the car's position must be determined in an accurate and reliable way in the absence of Global Navigation Satellite Systems (GNSS). Thus, electromagnetic waves emitted from Wireless LAN and Bluetooth Low Energy access points are investigated and their received signal strength is used as observations. This thesis introduces these network technologies and discusses wireless positioning techniques. In a number of practical investigations the characteristics of the signal and the capability of position determination using these technologies are inspected. To examine the theory, a large test setup is established in a public parking garage where tests with car-mounted antennas are performed. Since the observations are highly affected by signal attenuation and shadowing effects and are thus considerably noisy, the positioning result can be improved with suitable data filtering and interpolation. Throughout the tests it is shown that Bluetooth provides significantly better results than WLAN. Although the achievable accuracy is in the range of some meters, the presented position determination may nonetheless be valuable for autonomous driving when combined with other sensors. Since this thesis deals with absolute position determination only, follow-up investigations dealing with the integration of relative sensors are introduced.

Zusammenfassung

Die exakte Positionsbestimmung innerhalb von Gebäuden ist für eine Vielzahl von Anwendungen entscheidend und ist auch im aufstrebenden Fachgebiet der autonomen Fahrzeuge von Relevanz. Im Hinblick auf automatisiertes Einparken in Parkhäusern gilt es, die Position des Fahrzeuges unter Verzicht von globalen Satellitennavigationssystemen (GNSS) möglichst genau und zuverlässig zu bestimmen. Hierfür werden elektromagnetische Wellen von Wireless LAN und Bluetooth Low Energy Sendern untersucht und deren empfangene Signalstärken als Beobachtungen verwendet. Die vorliegende Arbeit stellt diese Netzwerktechnologien vor und bietet einen Einblick in die drahtlose Positionsbestimmung. In einer Reihe praktischer Versuchsanordnungen werden die Charakteristika der Signale und deren Befähigung zur Positionsbestimmung untersucht. Für realitätsnahe Ergebnisse wird eine ausgedehnte Testumgebung in einem öffentlichen Parkhaus etabliert, in welchem Tests mit am Fahrzeug montierten Antennen durchgeführt werden. Da die Beobachtungen maßgeblich von Signalabschwächung und Abschattungen betroffen sind und darum einen hohen Rauschanteil besitzen, kann das Positionierungsergebnis durch geeignete Datenfilterung und -interpolation verbessert werden. Im Laufe der durchgeführten Untersuchungen zeigt sich, dass Bluetooth signifikant bessere Ergebnisse liefert als WLAN. Obwohl die erreichbare Genauigkeit im Bereich einiger Meter liegt, kann die vorgestellte Positionsbestimmung dennoch von Nutzen für autonome Fahrzeuge sein, wenn sie mit anderen Sensoren kombiniert wird. Da die vorliegende Arbeit nur die absolute Positionierung zum Thema hat, werden Nachfolgeuntersuchungen, in welchen relativ messende Sensoren integriert werden, vorgestellt.

Contents

List of Figures	IX
List of Tables	XI
List of Acronyms	XII
1 Introduction	1
1.1 About this thesis	1
1.2 Motivation	2
1.3 Goals	3
1.4 State of the art analysis	4
1.4.1 Indoor positioning	5
1.4.2 Autonomous driving	6
2 Wireless networks	8
2.1 Wireless Local Area Network	8
2.1.1 History of Wireless LAN	9
2.1.2 IEEE standardization	9
2.2 Bluetooth	10
2.2.1 History of Bluetooth	11
2.2.2 Bluetooth Low Energy	12
2.2.3 iBeacon	13
2.3 Received signal strength	16
2.4 Signal interference and other disturbing factors	17
2.4.1 Influence of multiple access points	17
2.4.2 Shadowing and signal attenuation	19
3 Wireless positioning techniques	21
3.1 Indoor positioning	21
3.1.1 Applications	22
3.1.2 Precision	22

CONTENTS

3.2	General positioning techniques	23
3.2.1	Proximity detection	23
3.2.2	Lateration	24
3.2.3	Angulation	25
3.2.4	Fingerprinting	26
3.2.5	Dead reckoning	27
3.3	Suitability for WLAN and Bluetooth	28
3.4	Lateration	29
3.4.1	Concept	30
3.4.2	Mathematical algorithms	30
3.4.3	Relation between RSSI and distance	32
3.5	Fingerprinting	34
3.5.1	Concept	34
3.5.2	Positioning algorithms	36
3.5.3	Distance operators	39
3.6	Combination of multiple techniques	42
4	Practical investigations	45
4.1	Used hardware	45
4.2	Software for signal recording and evaluation	48
4.3	Relationship between distance and RSSI	49
4.3.1	Wireless LAN	50
4.3.2	Bluetooth Low Energy	52
4.4	Simple fingerprinting test bed	53
4.4.1	Test bed overview	53
4.4.2	Results	54
4.5	Setting up a radio map in a parking garage	57
4.5.1	Overview of the parking garage	57
4.5.2	Recording the radio map	59
4.5.3	Results	61
4.6	Measurement data processing	63
4.6.1	Applying a moving average filter	63
4.6.2	Data interpolation	64
4.6.3	RSSI truncation	66
4.6.4	Impact of data processing	67
4.7	Combination of BLE and WLAN	70
4.8	Vehicle positioning in a public parking garage	72
4.9	Lateration	75

CONTENTS

4.9.1	Lateration in A111 lecture room	76
4.9.2	Lateration in Thondorf parking garage	77
4.10	Time synchronization between different measurement systems	78
4.11	Comparison with a reference solution	82
5	Results	85
5.1	Static positioning	86
5.2	Kinematic positioning	88
5.3	Conclusion and future work	92
5.3.1	Valuation of the results	92
5.3.2	Outlook	93
	Bibliography	XIII

List of Figures

2.1	The Bluetooth logo	11
2.2	Photos of BLE beacons from different vendors	14
2.3	Official logo of Apple's iBeacon	14
2.4	Signal strength and standard deviation for various advertising intervals	15
2.5	Influence of multiple visible BLE access points on the RSSI	18
3.1	Schematic representation of lateration in 2D space	24
3.2	Schematic representation of angulation using two access points	25
3.3	Schematic representation of fingerprinting in a building	26
3.4	Schematic representation of dead reckoning using distance ρ and angle ϑ	27
3.5	2D feature space of WLAN fingerprints	36
3.6	Principle of the Kalman filter	43
4.1	Used USB adapters for receiving WLAN and BLE data	47
4.2	Linksys E2500 router with cables for an external, portable power source	47
4.3	Sample screenshot of the prompt-based application <i>Wireless Kit</i>	49
4.4	Arrangement for determining the relation between distance and RSSI	50
4.5	Empirically determined relation between distance and WLAN RSSI	51
4.6	Empirically determined relation between distance and Bluetooth RSSI	52
4.7	Overview of the positioning test bed at lecture room A111	54
4.8	Interpolated WLAN radio maps for lecture room A111	55
4.9	Static WLAN positioning on selected test points in lecture room A111	56
4.10	Outside view of the parking garage at Liebenauer Hauptstraße	58
4.11	Photograph showing the inside of the Thondorf parking garage	58
4.12	Schematic view of a steel girder in the parking garage	59
4.13	Bluetooth and WLAN radio maps in the parking garage	60
4.14	Interpolated radio map for Bluetooth access point 33 (parking garage)	62
4.15	Interpolated radio map for WLAN access point 10 (parking garage)	62
4.16	Example for two different moving average filters	64
4.17	Filtered and interpolated observations from BLE access point 28	65
4.18	Filtered and interpolated observations from WLAN access point 09	66

LIST OF FIGURES

4.19	Mean number of visible access points per reference point	67
4.20	Fingerprinting with raw BLE measurements	68
4.21	Fingerprinting with processed measurements	69
4.22	Trajectory obtained from combination of WLAN and BLE measurements	71
4.23	Fingerprinting with processed measurements (antennas inside the car) . .	73
4.24	Fingerprinting with processed measurements (antennas on the car's roof)	74
4.25	Count of different BLE access points throughout the test circuit	74
4.26	WLAN-based lateration in the A111 lecture room	76
4.27	Lateration results using BLE data in the Thondorf parking deck	77
4.28	Setup for time synchronization experiment	79
4.29	Results for time synchronization experiment	79
4.30	Time offset of the Lenovo Z580 relative to the GPS time	80
4.31	Time offset of the Asus Eee PC relative to the GPS time	81
4.32	Relationship between the geodetic coordinate system and the car system	83
5.1	Static positioning results on three selected test points	87
5.2	Time series of the PPE for test point 3	88
5.3	Kinematic positioning, exemplary BLE trajectories	89
5.4	Kinematic positioning, exemplary WLAN trajectories	90
5.5	Kinematic positioning, exemplary BLE+WLAN combined trajectories . .	90
5.6	Time series of the PPE for test trajectory 3	91

List of Tables

2.1	Specifications of members of the IEEE-802.11 family	10
2.2	Classes of Bluetooth devices	11
2.3	Proximity zones for iBeacons	13
2.4	Relation between dBm and mW	16
2.5	2.4 GHz signal attenuation	19
3.1	Suitability of positioning techniques w.r.t. WLAN and BLE	29
3.2	Example of a disadvantageous distance computation	41
3.3	Comparison of absolute and relative positioning	42
4.1	Used laptops	46
4.2	Used USB adapters for receiving WLAN and Bluetooth signals	46
4.3	Used infrastructure for the parking deck	61
4.4	Used parameters for the BLE measurement data processing	69
4.5	Comparison between data sets – dense example	71
4.6	Comparison between data sets – sparse example	72
4.7	Used parameters for the rearranged path loss model	75
4.8	Comparison of the time offsets between the two laptops	81
5.1	Used parameters for the final measurement data processing	85
5.2	PPE results for static positioning tests	86
5.3	PPE results for kinematic positioning tests	89

List of Acronyms

AFH	Adaptive Frequency Hopping
BIAS	Bluetooth Interference-Aware Scheduling
BLE	Bluetooth Low Energy
GNSS	Global Navigation Satellite System
GPS	Global Positioning System
IEEE	Institute of Electrical and Electronics Engineers
IMU	Inertial Measurement Unit
INS	Inertial Navigation System
LAN	Local Area Network
LOS	Line of Sight
PPE	Point Position Error
RF	Radio Frequency
RFID	Radio Frequency Identification
RSSI	Received Signal Strength Indicator
SIG	Special Interest Group
USB	Universal Serial Bus
UUID	Universally Unique Identifier
WLAN	Wireless Local Area Network
WPAN	Wireless Private Area Network

Chapter 1

Introduction

This preliminary chapter shall help the reader to get a picture of what to expect from the thesis at hand. Section 1.1 gives a quick overview of the content and its breakdown among the chapters of this thesis. In Section 1.2, the motivation for investigations regarding indoor-position determination with Wireless Local Area Network (WLAN) and Bluetooth is briefly described and, finally, Section 1.3 substantiates the ambitions and goals that were initially laid.

The practical work for this thesis was done between August 2014 and early April 2015, the actual writing of the thesis itself was concluded mid-April 2015.

1.1 About this thesis

This text was written as a Master's thesis and is separated into five chapters, whereas Chapter 1 serves as an introduction to clarify content breakdown as well as motivation and goals. Additionally, a state of the art analysis of indoor positioning, particularly using WLAN or Bluetooth, and of autonomous vehicles is given. The main goal is the investigation whether or not WLAN and Bluetooth are a suitable basis for absolute position determination of vehicles within underground parking lots or large parking decks, where no Global Navigation Satellite System (GNSS) is available. In the near future this positioning shall be the basis for an autonomous parking pilot which navigates through the building and finds a parking spot without human intervention.

In Chapter 2, wireless networks are discussed in general. Here, the two well known and widely spread wireless network technologies, WLAN and Bluetooth, are dealt with. The focus lies on standardization, historical facts as well as the general mode of operation. Additionally, the concept of received signal strength, which is of major impact within this

thesis, is examined. Its characteristics are discussed and verified in a number of tests. Measured signal strengths act as observations and are directly used for positioning, hence knowing their behavior and capabilities is crucial.

Chapter 3 deals with wireless positioning techniques. After a comparison of outdoor positioning and indoor positioning and the difficulties that arise with the latter, the general positioning techniques (i.e., proximity detection, lateration, angulation, fingerprinting and dead reckoning) are briefly discussed. Within the next section, the focus is laid on the suitability of these techniques for applications based on WLAN and/or Bluetooth. Since those concepts are then used to evaluate the observations taken for this thesis, their mathematical principles are covered in detail. In a closing section, the combination of multiple positioning techniques (both absolute and relative) is discussed.

Chapter 4 contains the practical investigations that were conducted throughout the development of this thesis. It contains a detailed description of the data acquisition itself as well as information regarding the evaluation of the gathered observations. Additionally, the chapter describes the devices and software products that were used to record and process the measurements.

The main results of the investigations performed in this thesis are presented within Chapter 5. For an objective assessment, they are compared with a reference solution of superior accuracy. The thesis is completed by interpreting the results and thereafter drawing a conclusion whether or not WLAN and Bluetooth are suitable as a basis for an indoor vehicle positioning system. Last but not least, an outlook is given of what subsequent constructive work might be and what to expect from the future.

1.2 Motivation

We live in a computer-driven world where nearly every aspect of our lives is somehow affected by computers. This applies to the automotive industry as well: Cars become smarter and smarter by being aware of their position and environment and self-driving cars are an excessive field of research. Thus, a reliable and accurate position determination and navigation in all possible conditions and environments is mandatory.

Position determination and navigation in outdoor environments can be considered trivial due to the great performance of GNSS, namely the Global Positioning System (GPS). However, in indoor environments GPS is not available and therefore positioning must rely on alternative technologies. This is often realized through an Inertial Measurement Unit (IMU), but those relative positioning techniques are known to be afflicted with large

drift errors and therefore the accuracy quickly worsens over time. To counteract this disadvantageous behavior, some form of absolute position determination is required.

This is where wireless positioning based on WLAN and Bluetooth comes into play. In case the required infrastructure is not already present anyway, the financial effort of installing such an array of network access points is rather insignificant, compared to other indoor positioning systems (e.g., pseudolites [8]).

The principle of WLAN-based fingerprinting has been around for several years and is greatly documented in relevant literature, e.g. [21]. However, this technique lacks in accuracy and is therefore mainly used for pedestrian localization, where room-level accuracy is considered satisfactory. To make fingerprinting useful for applications where a higher accuracy is mandatory, the basic fingerprinting algorithm has to be augmented and improved. Besides fingerprinting, the measured data could also be used for multilateration. Whether or not this addition is capable of enhancing the fingerprinting result or may yield feasible results on its own is to be investigated.

The second major part deals with Bluetooth, particularly Bluetooth Low Energy (BLE), which is at this time not as frequently used for ubiquitous position determination as WLAN. It is rather used as a proximity sensor to give an approximate distance of the user from the respective transmitter. The question arises whether or not Bluetooth fingerprinting yields equal or even better results than WLAN and if the two technologies can be combined into one positioning system.

Additionally, the integration of different, additional sensors (e.g., wheel sensors or accelerometers) has proven its value in other projects (see Section 1.4) and is expected to increase the quality of the position determination. The sensor integration is part of a number of follow-up investigations which are based on the findings and results of this thesis.

1.3 Goals

This section covers the goals and objectives for the scope of this Master's thesis. This includes both the final results as well as milestones during the work phase.

The fundamental goal is to effectively establish a positioning system for vehicles in environments where no GNSS is available, with an accuracy high enough for reliable position determination. Thus, a representative location (namely a public parking deck or parking garage) has to be found to provide meaningful results.

Positioning will be achieved using WLAN and Bluetooth. In an initial phase, those technologies are to be examined and a software tool for monitoring the signals is needed. Moreover, characteristics and advantages of different antennas and frequency bands have to be investigated.

After the preliminary tasks are completed, the next step is to perform a number of practical investigations. Those are intended to substantiate the requirements on both hardware and software for the use in a realistic environment.

For the main tests, a multistory parking deck will be used. For positioning and visualization purposes, the building has to be georeferenced by means of surveying. Also the reference point grid and the access point coordinates have to be well designed and their coordinates have to be known.

With utilizable measurements obtained, the last large working package is the data evaluation and thus the actual position determination. The goal is to effectively enhance the fingerprinting algorithm by a suitable data filtering or to combine its solution with other positioning methods to achieve an accuracy as best as possible. It is to be investigated whether or not the computed positioning is accurate enough to supplement accurate relative sensors and hence be the basis of an autonomous parking pilot.

1.4 State of the art analysis

This section covers recent and ongoing investigations regarding related topics such as projects aimed at fingerprinting positioning. Even though this thesis solely is about the position determination of vehicles (and not about navigation or controlling the vehicle), its findings are nevertheless within the context of an autonomous driving application. Thus, other autonomous driving systems (and especially their realization of the position determination) are of interest and hence discussed within this section.

Related work on indoor positioning is treated in Section 1.4.1 and autonomous driving is covered in Section 1.4.2. Note that this state of the art analysis does certainly not claim to be a complete listing of all relevant research projects or applications. It is rather an excerpt of some interesting projects that tackle problems which also appeared in the thesis at hand.

1.4.1 Indoor positioning

Indoor positioning based on WLAN fingerprinting is widely used due to the fact that it provides absolute positioning at a low cost to supplement relative sensors where no GNSS is available. An example where fingerprinting is combined with a variety of other sensors is given in [29]. The authors used basic WLAN fingerprinting to sustain an IMU-based dead reckoning alongside activity recognition. Via a suitable activity recognition, it was then possible to detect stairs in the movement pattern of the test subject. All the measurement data was then filtered in a two step process: In an initial Kalman filter, the user's height and thus the current floor are being evaluated (using absolute heights derived from 3D fingerprinting and height changes from activity recognition). With this information obtained, the 2D position is computed via a particle filter which integrates a navigable map with the measurements. The integration of all these measurement types effectively compensates their individual weaknesses.

When fewer observation types are at hand, the WLAN fingerprinting itself must be enhanced to provide more reliable results. Related investigations have been performed in [36], where the authors discuss the weaknesses of the Euclidean distance method and compare it with a probabilistic approach using Gaussian distribution. In practical investigations, they created four separate radio maps, each representing a different orientation (i.e., North, East, South and West) of the receiver. Additionally, the access points were placed in such a way that the antennas are aligned horizontally with respect to each other, which is claimed to result in higher accuracy and being more robust in terms of noise and other factors influencing the Received Signal Strength Indicator (RSSI). The orientation during the online phase was determined using the built-in digital compass of an ordinary smartphone, allowing the selection of the correct radio map.

Although the setup in [36] enhances the fingerprinting result, it is questionable whether or not it makes up for the additional expenditure of time for the radio map creation. Since the need of the radio map creation is a drawback of fingerprinting compared to other methods, modeling the RSSI database has been investigated in [31]. Here, the authors created a radio map by applying a cubic spline interpolation based on actual measurements. It turned out that in general, an interpolated radio map causes a loss of accuracy of 18% compared to a fully measured radio map. This number suggests that for applications where a high position accuracy is not essential, an artificial radio map is a viable option. Interestingly, the authors further found that for certain rooms of their test bed, the interpolated radio map performed better than the measured one. It is claimed in [31] that with a certain percentage of interpolated points, measured *bad* points are

being replaced, even causing an increased accuracy. Investigations on interpolated radio maps have also been conducted in [9].

Besides WLAN, also Bluetooth and especially BLE are commonly used for indoor positioning throughout the literature. An interesting alternative approach is presented in [1], where neural networks [15] instead of *classical* positioning methods (cf. Section 3.2) are used. The authors of [1] used multiple neural networks not only to deal with the high noise of the measurements but also with changes in RSSI values due to user orientation. Thus, besides Bluetooth base stations and a mobile receiver, also a compass module has been used. In case of a failure of one or more access points, suitable backup networks have been trained which are then automatically selected. Though the system performance is reduced in case of a node failure, it is still significantly better than a system without such a recovery mechanism (74% accuracy compared to only 48% in the case of only 60% of the access points being active). The overall positioning accuracy is significantly higher than any *classic* Bluetooth-based positioning method could achieve: During a walk through the test environment (i.e., a building with a corridor and some adjacent offices), an accuracy of 0.5 meters and a precision of 90% were achieved. It is questionable whether or not the method presented in [1] is suitable for large scale applications, because of the time-consuming nature of the establishment and training of the neural networks. Besides that, the system is lucrative due to its performance and its low cost infrastructure.

1.4.2 Autonomous driving

The backbone of an autonomous vehicle is a robust and precise position determination. In the thesis at hand, the designated goal is to partly realize this by means of WLAN and BLE¹. Throughout the literature the position determination is accomplished using a variety of different sensors, each with different advantages and drawbacks. In the U.S., the development of autonomous vehicles is pushed by the DARPA² Challenges, a racing event for autonomous cars held by the government. A report of 2007's urban challenge winning team is given in [35]. It provides a good overview of the challenge itself as well as detailed information regarding positioning and control of an autonomous vehicle. A good overview of recent development in autonomous driving is given in [6].

¹To actually meet the requirements of a positioning system for an autonomous vehicle, short-term accuracy is mandatory, e.g., provided by inertial sensors.

²Defense Advanced Research Projects Agency, a research organization within the U.S. Department of Defense — see <http://archive.darpa.mil/grandchallenge/>.

The Google driverless car [13][26] is presumably the most prominent example of an autonomous vehicle. Up to 2011, the fleet of Toyota Priuses has driven about 300 000 kilometers on public roads [13], without being guilty of an accident. The cars are packed with an array of different sensors, including a roof-mounted laser scanner, radar systems, a camera, a GPS receiver, an IMU and a wheel encoder. The last three sensors are – supported by a detailed navigable map – responsible for determining the vehicle’s position. Whether or not the vehicles are capable of driving in indoor environments has not been documented in aforementioned articles. The position combined with the readings of the laser scanner, the four radars, the optical camera and the digital road map produce enough information to navigate safely through complex urban road networks. A virtual 3D environment can be generated from the gathered data, including both the environment (with traffic lanes, lights and signs) and moving objects like other cars or pedestrians.

While many autonomous vehicles rely on GPS to determine their position, a system solely based on laser data and surface maps, which allows a car to autonomously maneuver through a multi-level parking garage, is introduced in [20]. While the position can be determined without the use of GPS, nevertheless a receiver is on board for outdoor positioning. In their work, the authors dealt with mapping, localization, SLAM³, path planning and navigation, all tailored to a complex test environment. Starting from outside the large parking garage, the car had to drive autonomously through several levels of the building to finally park in a designated parking spot. For the total distance of 375 meters the car took approximately three and a half minutes, resulting in an average speed of 6.6 km/h. According to the conclusions in [20], autonomous driving is possible in complex indoor environments like parking garages with the described sensors.

A rather different positioning approach is presented by the Swedish car manufacturer Volvo within one of their press releases⁴. With magnets embedded in the roads and suitable sensors mounted on a vehicle, the position shall be determined with an accuracy better than one decimeter. The major advantage of these magnetic roads lies within their independence of external conditions: Unlike *traditional* sensors like GNSS or cameras, the magnets are not affected by obstacles or bad weather. Although the project has been heavily criticized in several articles [10][28] mainly due to its exorbitant monetary expenses, the system performs as intended and might actually be a viable option for indoor positioning.

³Simultaneous Localization and Mapping

⁴Volvo car group (March 2014) — www.media.volvocars.com/global/en-gb/media/pressreleases/140760/volvo-car-group-tests-road-magnets-for-accurate-positioning-of-self-driving-cars

Chapter 2

Wireless networks

This chapter covers wireless network technologies, which can be considered as the basis of the investigations treated in this thesis. To be more precise, WLAN and Bluetooth are of particular interest. They are both based on electromagnetic waves. WLAN is discussed in Section 2.1 and Bluetooth in Section 2.2. For Bluetooth, the focus lies on a technology called Bluetooth Low Energy, which is covered within aforementioned section. To conclude, received signal strength (which serves as the measurement quantity for the investigations in this thesis) and signal interference along with other disturbing factors are introduced and discussed in Section 2.3 and Section 2.4, respectively.

2.1 Wireless Local Area Network

In this section, WLAN is briefly introduced. When talking about WLAN one usually refers to a standard of the Institute of Electrical and Electronics Engineers (IEEE) family, namely the IEEE 802.11. The technology is primarily used to connect nearby computers among each other or, when coupled with some sort of internet access, with the world wide web. In private households, a cable modem is often connected to a WLAN router by an Ethernet cable, which then spreads the data wirelessly throughout the house. A router is commonly referred to as an *access point* (though the term is usually more likely used for publicly available routers than for private devices).

Aside from the use case described in the preceding paragraph known as *infrastructure mode*, WLAN may also operate in the *ad-hoc mode*: Here, two hierarchically equal devices (e.g., two notebooks) are connected directly (peer to peer). Among this thesis, the ad-hoc mode is not of interest.

2.1.1 History of Wireless LAN

This section briefly covers the history of WLAN, from its early struggles up to its breakthrough and success in present times. The information in this section was taken from [30].

As an alternative to wired networks, WLAN first became a noticeable technology in the late 1990's. However, just a few years before, WLAN found almost no success due to its high cost, high power consumption and the fact that it was simply too slow compared to existing Ethernet Local Area Network (LAN). It had mainly evolved as a slow and unreliable emulation of conventional LAN, only without the need of wires. In fact, even at the end of the 20th century, WLAN had to face with skepticism if it will ever become a mainstream network interface. However, the importance of WLAN eventually grew with the standardization within the IEEE-802.11 family which took place in 1997 [33]. Details regarding this standardization process are exclusively treated in Section 2.1.2.

2.1.2 IEEE standardization

Being as well part of the history of WLAN, this section now covers the standardization through IEEE in the 802.11 standard family, see [30][33].

Especially one variant, the IEEE-802.11b (operating in the 2.4 GHz band), came out on top among other competitors such as HIPERLAN, 802.11a (operating in the 5 GHz band) and also Bluetooth (see Section 2.2). From then, the performance of WLAN was ever-increasing while getting cheaper at the same time. After 802.11g was released in 2003, the new 802.11n standard was added to the 802.11 family in 2009 and brought a massive boost in data rates. As an extension to 802.11n, the most recent release is 802.11ac, which is up to now only supported by a small amount of devices. Each standard features a number of available channels either in the 2.4 GHz or the 5 GHz band. To give an example (see Table 2.1), the standards IEEE 802.11g and 802.11n (which are, at the moment, the most commonly used) feature 13 different channels in the 2.4 GHz band, which are evenly spread across 83.5 MHz (from 2.4 GHz to 2.4835 GHz). Due to a certain channel width of usually 20 MHz (for the n standard also 40 MHz are possible), only a fraction of those channels should be used to prevent signal interference. The subject of signal interference is explicitly treated in Section 2.4.

Additionally, aside from the more publicly relevant WLAN standards, the 802.11p variant has been developed to provide reliable wireless access in vehicular environments. As

Table 2.1: Specifications of the most commonly used members of the IEEE-802.11 family, [33]. The number of available channels is region-dependent.

Standard	Spectrum	Channel width
802.11a	5.15 – 5.3500 GHz	20 MHz
802.11b	2.40 – 2.4835 GHz	22 MHz
802.11g	2.40 – 2.4835 GHz	20 MHz
802.11n	2.40 – 2.4835 GHz	20/40 MHz
	5.15 – 5.3500 GHz	20/40 MHz
802.11ac	5.15 – 5.3500 GHz	20/40/80/160 MHz
	5.47 – 5.7250 GHz	20/40/80/160 MHz
802.11p	5.85 – 5.9250 GHz	10 MHz

stated in [18], vehicle to vehicle connections require a very fast connection establishment to ensure low latencies so that vehicles are able to communicate with one another. Additionally, the physical layer must be adapted to handle data transmissions between fast moving devices. As connectivity between cars and monitoring systems increase, this standard is expected to gain in importance.

2.2 Bluetooth

This section covers the well-known Wireless Private Area Network (WPAN) technology Bluetooth [3]. In accordance to WLAN, Bluetooth is also part of the IEEE-802 standard, namely the IEEE-802.15.1 standard. Bluetooth is intended to easily establish secure connections between devices for data interchange. The classes of connectable devices is widely spread, ranging from mobile phones to computers, headsets, speakers, input devices (i.e., mice and keyboards), etc. The main purpose of Bluetooth is the reduction of wires when connecting devices.

Bluetooth operates at frequencies ranging from 2.4 GHz to 2.485 GHz, whereas the actually used frequency is dynamically selected based on other broadcasting devices within the aforementioned spectrum. This avoiding of occupied frequencies is called Adaptive Frequency Hopping (AFH) [12] and is intended to provide greater performance by reducing interference with other signals. It is again briefly discussed in Section 2.4.1.

Bluetooth operates at distances ranging up to approximately 100 meters and is subdivided into three classes [4], as shown in Table 2.2.

Table 2.2: Classes of Bluetooth devices

Class	Range	Usage
3	1 m	Battery-powered devices
2	10 m	Phones and computers
1	100 m	Industrial applications

Unlike WLAN, Bluetooth is intended to be used at fairly close distance, mostly in the magnitude of several meters. Therefore, its emitted power is low compared to WLAN. The range mentioned in Table 2.2 refers to a general environment including obstacles and not necessarily a Line of Sight (LOS) connection. In free-air conditions, class 3 devices are said to operate on ranges up to 10 m and class 2 devices on ranges up to 50 m. The maximum range of 100 m (class 1) however remains unchanged.

2.2.1 History of Bluetooth

This section shall give a brief overview about the history of Bluetooth. The origin of the name "Bluetooth" is found in Scandinavian history: The 10th century king Harald Blauzahn (which translates to Bluetooth) – who was known to be a very communicative leader – managed to unite many Danish tribes into a single kingdom. Therefore, the name shall reflect the ability of Bluetooth to connect different devices with each other. The logo itself consists of two Scandinavian runes – the initials of the aforementioned king.

**Figure 2.1:** The Bluetooth logo

The foundation for Bluetooth has been laid in 1998 with the founding of a Special Interest Group (SIG) driven by major computer companies like IBM and Toshiba. Even though infrared had been present as a replacement for wired connections for a couple of years, the need of inter-visibility was considered a significant downside and therefore the breakthrough of the infrared technology never came.

With Bluetooth however, a suitable technology for small, private networks (called *pi-conets*) had been found and its first iteration (1.0) was released in 1999 with a maximum

data rate of 732.2 kbit/s. In early 2001, Bluetooth 1.1 was released and, with it, a major reduction of the security issues from the first release came along. Furthermore, version 1.1 includes an indicator for received signal strength (cf. Section 2.3), which is of great importance in wireless positioning techniques.

In late 2004, Bluetooth 2.0 was released. The updated version almost tripled the achievable data rates (up to 2.1 Mbit/s) while maintaining downward compatibility. The next major step occurred in 2009 with the release of Bluetooth 3.0 and again a significant improvement in data transfer. This was achieved by establishing peer-to-peer connections between two devices and an additional high speed channel based on WLAN.

The 4th version of Bluetooth was released in 2010 with an update to Bluetooth 4.1 in 2013. The 4.0 release includes a technology called BLE, further discussed in Section 2.2.2, which consumes – as the name suggests – significantly less energy than *classic* Bluetooth. Unlike previous releases, this version does not support downward compatibility.

2.2.2 Bluetooth Low Energy

The concept of BLE was first developed by Nokia back in 2006 and finally merged into the main Bluetooth standard with the release of version 4.0 in 2010. Its marketing name is *Bluetooth Smart* [5]. BLE devices show a significantly reduced power consumption at the cost of providing a lower communication range as *normal* Bluetooth. BLE is not compatible with regular Bluetooth, therefore special transceivers are required (often denoted as *Bluetooth Smart Ready* if they support both Bluetooth and BLE). This implies that – even though the frequency domain is the same – not every Bluetooth 4.0 device is capable of communicating via BLE.

BLE features low power consumption; a device may be running for several months or even years with nothing more than a regular button cell. However, battery life depends on the rate at which the device transmits its advertising data and on the power of the emitted signals. Due to their simplicity, they are small in size and monetary effort but nevertheless compatible to many devices, including modern smartphones.

The usage of BLE ranges from various profiles (including health care and sports) to location based applications. The latter is realized as proximity sensing and is referred to as iBeacon (see Section 2.2.3). Basic proximity sensing uses only visibility information to detect whether a mobile user is within the range of a certain BLE source. A more sophisticated approach is to use the received signal strength to obtain a distance estimation. This technique is also subject of this thesis and is discussed in Section 3.4.3. To

give an example, proximity sensing is used in retail stores to send a targeted, location-based advertisement to users (e.g., one receives specific information on his phone when entering a certain area of a shop).

2.2.3 iBeacon

A BLE access point transmits its advertising data in a standardized way and is therefore recognized by a large number of BLE-capable devices. In 2013, Apple Inc. established this standard for indoor positioning and navigation, known as *iBeacon*. It was first supported by the iPhone 4S and is since then integrated in all subsequently released iOS devices as well as Macintosh computers with Bluetooth 4.0 and OS X Mavericks or later. Additionally, iBeacon is supported by Android 4.3 or later and some Windows phones, making it available for a broad spectrum of users.

The concept behind iBeacon is rather simple. A BLE-capable device broadcasts a predefined message at a specific interval and therefore notifies nearby receivers of its presence. This advertising protocol consists of

- an iBeacon prefix defined by Apple
- a variable Universally Unique Identifier (UUID)
- a Major/Minor part (containing additional customizable data, 2 bytes each)
- and data regarding the signal strength.

This data may then be used depending on the application (e.g., an appropriate mobile app displays content based on the proximity of a certain UUID and its Major/Minor data). For location-based applications, the distance to the beacon is expressed in four proximity zones [2], which is illustrated in Table 2.3.

Table 2.3: Proximity zones for iBeacons [2]. Due to the fact that the transmission power differs between various BLE beacon models, different zone ranges may be found throughout relevant sources.

Zone	Range	Description
Immediate	< 1 m	The device is likely to be held directly up to the beacon
Near	1 - 3 m	If granted LOS, the device is within a few meters of the beacon
Far	> 3 m	A low signal strength indicates large distance or non-LOS
Unknown	? m	If ranging has just begun or too little observations are available

Apple introduced this range classification to overcome the fact that the emitted signal is rather unstable. In [2] it is further pointed out that "Due to the issues around signal strength and the variabilities in deployment environments, iBeacon technology is not intended to be used for specific location identification. It should be capable of providing room-level accuracy, but there are many factors that need to be considered to build a successful deployment. Number of beacons, where they are positioned, expected use cases, and many more factors need to be examined to provide a good user experience".

BLE beacons are offered by a wide range of vendors and are available in many different shapes and sizes. Three different beacon models have been tested within this thesis: A device from a German company¹, a beacon manufactured in Spain² and a third device from a company located in Poland and the United States with the beacons being manufactured in Krakow³. Photographs of the beacons can be seen in Figure 2.2.

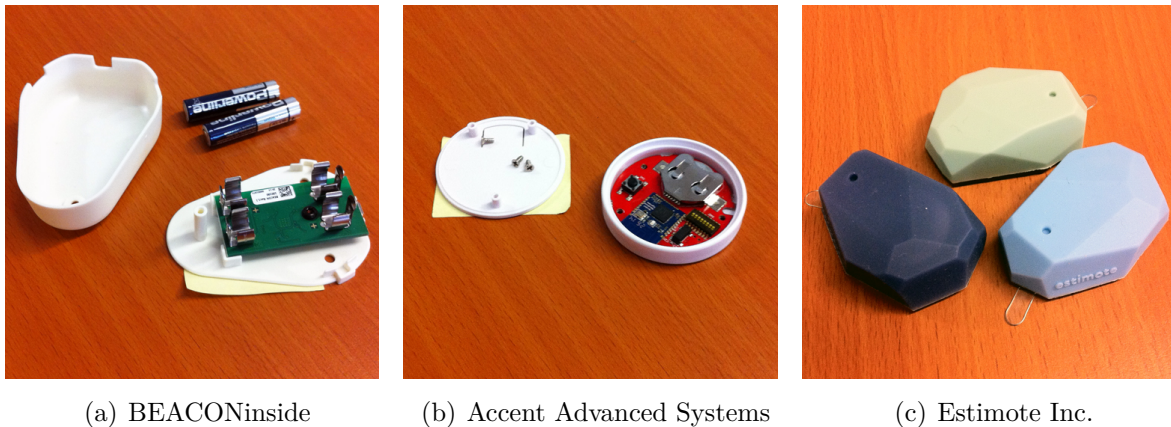


Figure 2.2: Photos of exemplary BLE beacons from different vendors showing different shape and power source



Figure 2.3: Official logo of Apple's iBeacon

¹BEACONinside GmbH — <http://shop.beaconinside.com>

²Accent Advanced Systems — <http://www.accent-systems.com>

³Estimote Inc. — <http://estimote.com/>

Besides their obvious differences such as size, shape and battery type, they also differ in configurability, transmission power and advertising interval. An in-depth analysis of the three beacons, shown in Figure 2.2, is given in Chapter 4. Furthermore, it shall be noted that some beacons also support additional sensors like thermometers or accelerometers. However, the performance and accessibility of those sensors is not of particular interest within this project and therefore has not been investigated.

Many beacons (including the three devices mentioned in Figure 2.2) allow a certain degree of customization. This is most conveniently done with appropriate mobile applications which are available for both iOS and Android. Usually, beacon manufacturers offer their own app which is intended to work best with their beacons, but may as well work flawlessly with other models. To give an example for configuration, minimizing the advertising interval (i.e., the rate at which the signal is broadcast) grants more observations within a certain period of time, which is of particular relevance for kinematic positioning applications. In a simple test setup it has been shown that increasing the advertising interval does not worsen the signal quality (in terms of standard deviation of the received signal strength). This can be seen in Figure 2.4.

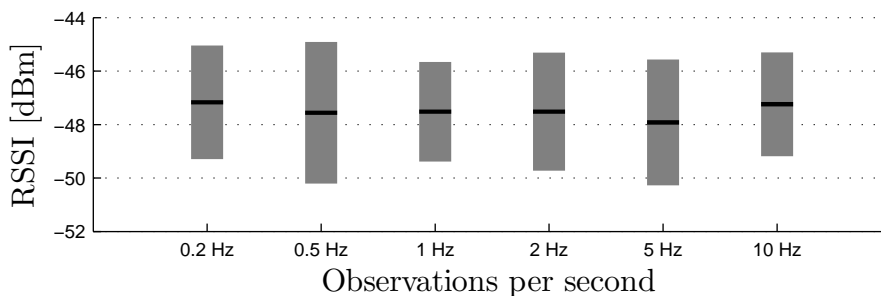


Figure 2.4: Signal strength and standard deviation for various advertising intervals of static observations for a total of 1 min each. The mean signal strength is drawn in black, the corresponding standard deviation as gray bars.

The measurement time was one minute each, ranging from advertising intervals of 0.2 Hz up to 10 Hz. Although Figure 2.4 suggests that maximizing the advertising interval has no drawbacks, it is important to note that a high advertising interval will obviously drain the beacon’s battery at a faster rate. For kinematic applications however, depending on the velocity of the receiver, it might be mandatory to have the beacons operate on a higher advertising rate. For long-term installations, certain beacons including the model shown in Figure 2.2(a) allow for an external power source, so that the beacon’s lifetime is no longer limited by a button cell.

2.3 Received signal strength

Received signal strength, or correctly denoted as Received Signal Strength Indicator or simply RSSI, is a measurement of the power being received by an antenna. It is most commonly expressed in units of dBm (Decibel-milliwatts), a logarithmic scale referring to the power of 1 mW. Therefore, a change of ± 30 dBm implies a change of $10^{\pm 3}$ on the milliwatts scale. This relation is exemplarily represented in Table 2.4.

Table 2.4: Relation between dBm and mW

dBm	Power
+30	1 W (watt)
0	1 mW (milliwatt)
-30	1 μ W (microwatt)
-60	1 nW (nanowatt)
-90	1 pW (picowatt)

A received signal strength of about -30 to -60 dBm is considered a good connection, a lower value might cause problems and lead to slow data transmissions and connection losses. Additionally, a weaker signal typically implies a worse signal-to-noise ratio which negatively influences the quality of the position determination.

For WLAN, the signal is typically emitted with approximately 200 mW, ranging up to even 1 W. BLE has a much smaller power emission and is usually situated at about 1 mW, but can be configured up to a certain degree (e.g., up to a value of +4 dBm in case of the devices used for this project). For comparison, regular Bluetooth is emitted at power levels similar to WLAN.

It is important to be mentioned that the percentual signal quality displayed by most operating systems (usually a percentual value) is not identical to the RSSI. To obtain the latter, one either has to use specific software packages⁴ or make use of specific system commands available for Linux operating systems. While both WLAN and Bluetooth allow the readout of the RSSI, their data acquisition is realized via very different methods and commands. For the measurement of RSSI values, a C++ application has been developed that utilizes these system commands (see Section 4.2).

⁴e.g., see www.netstumbler.com/downloads OR www.inssider.com/inssider

2.4 Signal interference and other disturbing factors

This section deals with signal interference and other potentially disturbing factors (such as walls or the human body) and how WLAN and Bluetooth are affected by them. Being in knowledge of those potential sources of signal manipulation is crucial for a RSSI-based position determination. Generally speaking, a higher number of observables (meaning a higher number of access points) acts beneficial for the quality of the computed position. Therefore, to work as intended, using multiple access points simultaneously must not have a negative impact on the observations.

2.4.1 Influence of multiple access points

Whether or not multiple access points broadcasting on the same channel have an impact on each other was investigated in [19]. The experimental arrangement included three WLAN access points, from which RSSI was recorded for the duration of one hour. It was found that the three obtained RSSI time series are not correlated among each other (correlation values of -0.02 , 0.13 and -0.03). Furthermore, in another test arrangement with two access points broadcasting on the same channel, it was proven in [19] that both signals are independent and thus do not interfere with each other. To prevent interference, a transmission is either not heard or delayed if another transmission currently exists. As stated in [33], it is always better to have multiple access points broadcast on the same channel rather than on overlapping channels. The reason for this is the following, as briefly explained in [33]: If two channels partly overlap, then the partially received signal of the other access point is considered as a disturbance and the access point amplifies its transmitting power to gain predominance within the channel. Respectively, the same phenomenon occurs for the other channel.

In the case of BLE, the channel may not be specifically assigned. Instead, AFH is used to automatically switch to an unoccupied channel or schedule the transmission. Alternatively, as explained in [12], a technology called Bluetooth Interference-Aware Scheduling (BIAS) is used, the key idea of which is to wait for a slot with a good⁵ frequency before transmitting data. If each available frequency is considered as bad, the transmission slot is skipped and the procedure is repeated in the next transmission opportunity. To avoid this, AFH replaces those bad frequencies with good ones so that the data transmission does not have to be delayed.

⁵Here, *good* refers to any arbitrarily defined criterion, such as a packet loss threshold.

To verify that multiple BLE access points do not negatively influence the RSSI, a simple test setup has been arranged. First, the signal strength of one access point has been observed for 60 seconds, with no other access points in range. After that, the same access point has been observed again, but this time with a total of 14 other access points in the immediate vicinity. The results in terms of mean RSSI (denoted by μ) and standard deviation (denoted by σ) can be seen in Figure 2.5. The test with only one access point is shown in the upper plot and the test with 15 access points is displayed below.

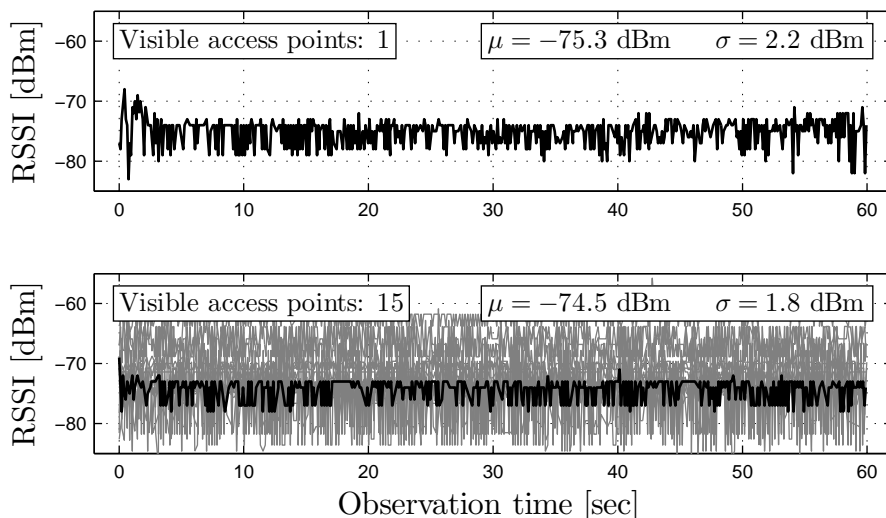


Figure 2.5: Influence of multiple visible BLE access points on the RSSI

The similarity of the statistic parameters μ and σ between the two test runs prove that signal interference is handled properly for BLE by means of the AFH. In the lower plot of Figure 2.5, the measurements of the other 14 access points are displayed as gray lines. As their RSSI suggests, all of them are placed in a similar range to the receiver, many of them even closer than the access point displayed in black. The higher variance at the beginning and the end of the time series is caused by the user being in the signal path while starting or ending the measurement process.

When WLAN and Bluetooth networks are running side by side, the AFH also reduces interference among each other and thus lessens packet loss. In addition, as further stated in [12], the packet loss of WLAN in case of a nearby Bluetooth network is generally low if the WLAN access point primarily acts as a transmitter and not a receiver. Hence, this behavior is beneficial for a WLAN-based positioning, where the connection is usually one-sided (the access points only transmit their beacon message containing –among other unused data – their identification and the received signal strength).

2.4.2 Shadowing and signal attenuation

The second aspect treated within this section is signal attenuation or manipulation caused by shadowing or other disturbing factors. As for the deployment of access points within parking decks – which is intended for the investigations in this thesis – one has to be aware that facing such effects is inevitable. While those effects are unpleasant for a lateration-based positioning (because the RSSI attenuation cannot be modeled correctly for obstructed signal paths in practice), it is not as painful in the case of fingerprinting. Local shadowing effects are simply part of the RSSI pattern and are – in the case of a non-changing environment – present in both the offline and the online phase. However, when the environment changes, the fingerprinting might fail as well due to different signal patterns. For a public parking deck, the environment obviously changes up to a certain degree due to traffic and parking vehicles.

As proven in [19], organic objects like the human body⁶ absorb a significant amount of the signal and thus lower the RSSI. For a generally weak signal, this can lead to the signal being completely absorbed. Therefore, when creating a radio map, one should avoid blocking the signal path with his own body because it is obviously not part of the constant environment. Aside from obstructing the signal path at a certain orientation, the orientation of the receiver only has a minor effect on the RSSI, as further found in [19]. The variations in the RSSI for different orientations are in the magnitude of ± 2 dBm or less and are treated as negligible compared to other error sources. Regarding different receiver orientations, similar numbers have also been found in [16, p. 6].

In [34], signal attenuation for the 2.4 GHz band was investigated for an indoor environment. The signal attenuation caused by various materials as shown in Table 2.5.

Table 2.5: 2.4 GHz signal attenuation (source: [34, p. 4])

Material	Attenuation
Window brick wall	2.0 dB
Metal frame glass wall into building	6.0 dB
Office wall	6.0 dB
Metal door in office wall	6.0 dB
Cinder block wall	4.0 dB
Metal door in brick wall	12.4 dB
Brick wall next to metal door	3.0 dB

⁶The human body roughly consists of 70% water, which has a resonance frequency of 2.4 GHz (source: [19]) and therefore the signal gets attenuated when the user obstructs the signal path

These numbers suggest that especially metal is critical for the signal propagation. Furthermore, in [34] an interesting phenomenon was documented when observing the signal propagation through multiple floors of a building. The path loss per floor behaves non-linearly, in fact the attenuation of each floor becomes less with an increasing number of floors. The author suggests that this phenomenon is explained by a diffraction of the radio waves through the windows and along the outside wall of a building, somehow yielding a quasi LOS connection.

Remark. Unfortunately, parking decks or underground parking lots are a difficult environment for the propagation of electromagnetic waves. Although there are large open spaces, the typical presence of metal, glass and concrete influences the signal enormously. Thus, close-range LOS observations should be preferred. This often implies the deployment of a high number of access point, so that obstructed observations can be omitted while still maintaining a high enough number of visible access points. This is especially relevant for a lateration-based positioning, where modeling of the signal attenuation is crucial. Having multiple access points which broadcast at the same location does not cause negative interference effects due to the capabilities of the underlying network technologies. Thus the decision for a higher amount of access points is mainly a matter of financial effort and not of a busy radio spectrum.

Chapter 3

Wireless positioning techniques

In this chapter, wireless positioning techniques are discussed. With the focus being laid on indoor positioning, potential use cases and associated accuracy requirements are presented. In Section 3.2, general positioning techniques suitable for wireless signals are examined. Subsequently, Section 3.3 narrows down this list to those techniques suitable for positioning with WLAN or Bluetooth signals, i.e., lateration and fingerprinting. Those are then discussed in detail within Section 3.4 and 3.5, respectively. Thereafter, in Section 3.6, a method of sensor integration/sensor fusion and therefore the combination of multiple observation types and techniques is presented. Note that the sensor integration is subject of follow-up investigations and is thus not treated practically within this thesis.

3.1 Indoor positioning

With the breakthrough of smartphones within the last few years, indoor positioning became a noteworthy field of expertise. Having a highly connected computer in one's pockets, the foundation was laid to make indoor positioning and applications like pedestrian navigation a technology of common interest. Unfortunately, GPS is not available in buildings (or at least far away from being reliable) and thus the position has to be obtained using alternative data sources and techniques (those techniques are introduced in Section 3.2). Indoor environments are typically more complex in terms of signal propagation than outdoor areas. Often, height information is required to correctly localize a user inside a building. This is either accomplished using 3D positioning techniques or by considering additional constraints, such as activity recognition combined with map information [29].

3.1.1 Applications

Indoor positioning features a versatile spectrum of use cases, both for commercial as well as for public applications. For the former, localization of goods in large fabrication halls or the positioning and navigation of forklift trucks in storage depots are prominent examples. In the public sector, pedestrian navigation within large buildings such as shopping centers or airports becomes more and more important. In [27, p. 11-14], the wide spectrum of applications for indoor positioning is presented. This ranges from private homes (ambient assistant living) over the navigation of visually impaired people to industry and underground construction sites.

Recently, indoor positioning is also used by companies to provide location-based advertisements (e.g., if a customer approaches a certain area in a shop he receives a contextual advertisement on his smartphone). As mentioned earlier, this is usually realized using BLE and a tailored smartphone application.

3.1.2 Precision

The achievable precision of indoor positioning highly depends on the underlying technique as well as the used hardware components and – for techniques involving radio waves – on the environment. The spectrum of achievable accuracy and coverage is presented in [27, p. 10]. Depending on the technology, the accuracy ranges from some μm (tactile and combined polar systems, cameras) up to hundreds of meters (cellular network methods).

In the context of indoor vehicle navigation, an accuracy in the magnitude of a few decimeters, combined with other sensors for collision avoidance, is assumed to be sufficient. To achieve a high accuracy in the magnitude of 1 meter or better, most likely the combination of different techniques is mandatory: An inertial measurement unit itself produces highly accurate relative positions, but the absolute position is likely to be negatively affected over time by drift effects. Thus, when combining the accurate position changes with frequent absolute position updates from another technique, a significantly higher and more stable position accuracy can be expected.

3.2 General positioning techniques

Within the field of position determination, one must distinct between five different techniques. Primarily, they differ in type of observable (and thus in hardware requirements) and in position type (i.e., absolute or relative coordinates). Aside from dead reckoning, all techniques are conceivable with using radio waves (or derived quantities) as observations. These techniques are:

- Proximity detection
- Lateration
- Angulation
- Fingerprinting
- Dead reckoning

Within the following sections, these positioning techniques are briefly introduced.

3.2.1 Proximity detection

Proximity detection (often referred to as *mobile phone tracking* or *Cell-ID positioning* [7, p. 49-50]) is the coarse localization of a receiver (e.g., a mobile phone) based on the coverage area of the transmitter it is currently in. In an idealized environment, this coverage area would be a sphere with the transmitter in its center. The receiver may now lie anywhere within that sphere. Consequently, the achievable accuracy of Cell-ID positioning equals the effective range of the signal transmitter. Hence, it may be in the magnitude of multiple kilometers. This technique is commonly used by mobile network operators to determine the amount of users in various cells (coverage areas of Radio Frequency (RF) transmitters).

Proximity detection may be further enhanced by considering the strength of the received signal: While a strong signal implies a short distance between receiver and transmitter, a weak signal may indicate a position further away. However, local shadowing effects may heavily deteriorate this proximity estimation.

3.2.2 Lateration

The concept of lateration [7][21] is based on distances between an unknown position and several known points. When given such a distance to a known point, the geometric locus of the unknown position, the so-called Line of Position (LOP) is a circle with the known point as its center and the distance as radius. The problem of lateration may therefore be broken down to an intersection of multiple circles. This is shown in Figure 3.1. In analogy to the common geodetic notation, points with known coordinates are marked as triangles while unknown points are marked as circles. A non-white colored point implies that a receiver (or generally speaking, a survey station) is located on that point.

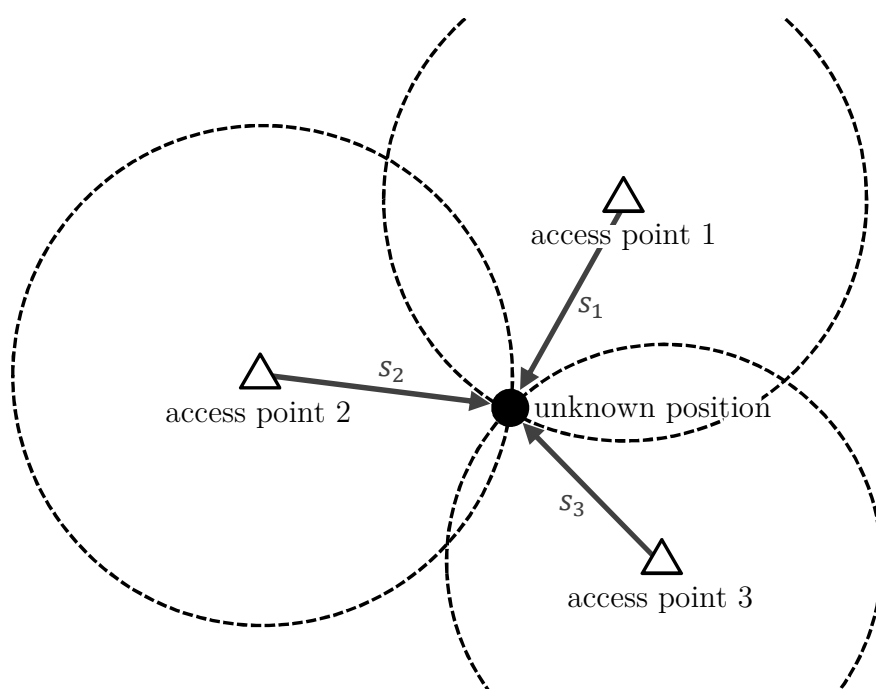


Figure 3.1: Schematic representation of lateration in 2D space

The observables are represented as dark gray arrows and define the radii of the individual geometrical loci. As Figure 3.1 suggests, the problem of a 2D lateration becomes uniquely solvable when at least three distances are observed. In 3D space, a geometrical locus as a result of a distance measurement would be a sphere; thus the position is determined by intersecting spheres. For that reason, a minimum of at least four observations is required to determine a position in 3D space. When given distance observations to three different known points (the minimum number to uniquely derive a position in 2D space), the technique is referred to as *trilateration*, with four or more observations, the term *multilateration* is used.

The concept of multilateration is used in GNSS: Due to the fact that the distance observations between satellite and receiver are affected by clock biases, they are referred to as *pseudoranges* ρ . The term suggests that the measured distances do not correspond with the actual distances. Because the clocks in both the satellite and the receiver are not synchronized, an additional observation (and thus an additional satellite) is required to overcome this problem. Technically, a total number of five satellites would then be required to derive a 3D position. However, four visible satellites are enough for practical applications because one of the two resulting points may be eliminated due to the fact that it lies approximately 40 000 km away from the Earth's surface.

3.2.3 Angulation

Contrary to previously introduced lateration, the concept of angulation [21] assumes known (measured) angles between a reference direction and the direction from an access point to an unknown position. The geometrical locus as a result of an angular measurement α_i is a straight semi-line, thus, the position is derived by an intersection of lines. The situation is illustrated in Figure 3.2.

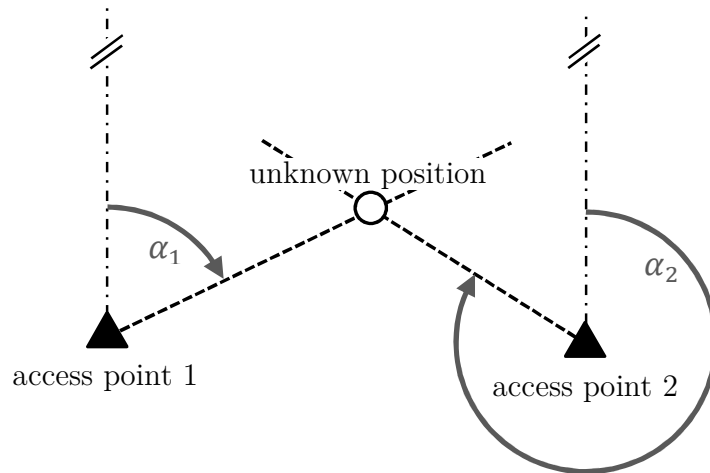


Figure 3.2: Schematic representation of angulation using two access points

Aside from the resolution of the angular measurement, the geometric constellation may additionally worsen the resulting position in case of a glancing intersection¹. This is the case if the access points and the unknown position roughly lie on a straight line. This

¹If geometric objects intersect each other under very flat angles and therefore no distinct point of intersection is apparent.

potential error source also applies to lateration, when the geometrical loci (i.e., circles) intersect at very flat angles.

The concept of angulation is used in classic geodetic surveying, where maps were created using triangulated irregular networks (i.e., partitioning of the landscape in aligned triangles). Today, angulation is mostly replaced by trilateration due to its advantage in terms of speed.

3.2.4 Fingerprinting

Position determination using fingerprinting [7][21] takes a rather different approach than the techniques previously introduced. The concept of fingerprinting is illustrated in Figure 3.3. The fingerprints are laid out across the room (not necessarily in a regular grid). To visually distinguish the fingerprints from the access points, they have been represented as circles (contrary to the usual geodetic notation), although their coordinates have to be known in the general case².

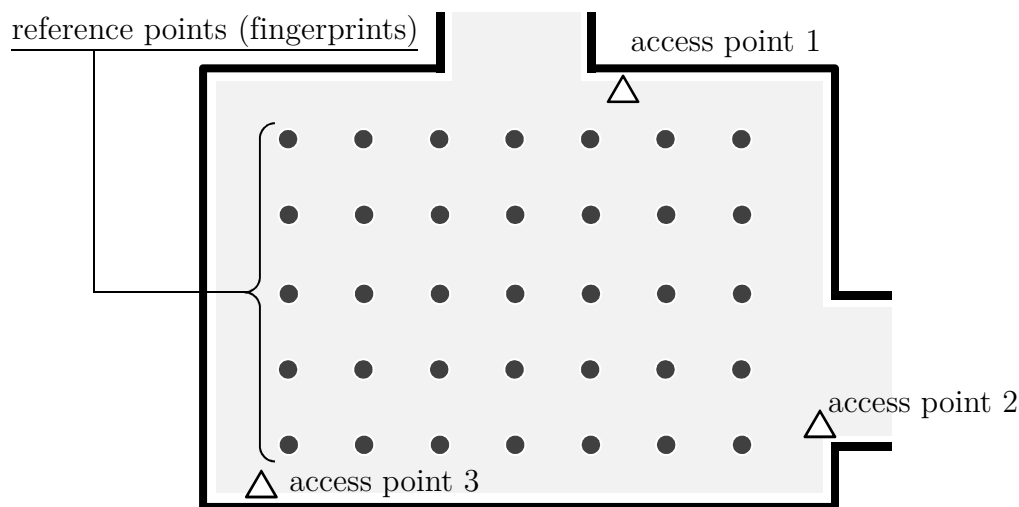


Figure 3.3: Schematic representation of fingerprinting in a building

In an initial phase, patterns of some measurable quantity (e.g., RSSI) emitted from numerous access points are recorded at each reference point and stored in a database for later use (this is referred to as *offline phase*). Subsequently, in the positioning

²If the number of nearest neighbors K equals 1, then one does not have to be in knowledge of the reference point coordinates. This implies that the result, however, can not be expressed in terms of coordinates as well.

phase or *online phase*, the current measurement pattern is compared with the reference points. Based on the assumption that similar patterns imply a short metrical distance, an estimation for the user position can be derived.

3.2.5 Dead reckoning

Unlike the other positioning techniques introduced in Section 3.2, dead reckoning only yields relative positions (position changes with respect to a former position). Therefore, a traveled distance and a corresponding course angle with respect to the last known position is required. Those quantities may be obtained from a variety of sensors. Dead reckoning, as well as other relative positioning techniques, are highly susceptible to drift effects, hence their long-term accuracy is low. On the other hand, the short-term accuracy is high, making it valuable for combinations with absolute techniques (see also Section 3.6). In Figure 3.4, the concept of dead reckoning is shown. At the current epoch t , the user position $P(t)$ has to be computed based on recent measurements and the position of the last epoch, i.e., $P(t-1)$. According to [17], the distance is denoted as ϱ and the course angle as ϑ , hence the technique is referred to as *rho-theta technique*.

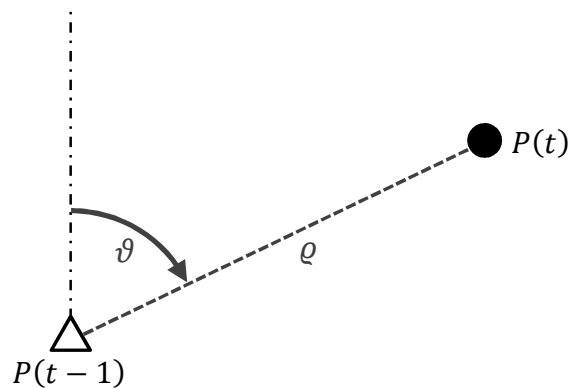


Figure 3.4: Schematic representation of dead reckoning using distance ϱ and angle ϑ

Since the technique is of relative nature, it is not further discussed here and the reader is referred to the explanations in [17].

3.3 Suitability for WLAN and Bluetooth

Among the positioning techniques introduced in Section 3.2, only a fraction of them are eligible in combination with WLAN or Bluetooth signals. In the following, their qualification with respect to the given signals is briefly discussed, followed by a summary in Table 3.1.

Proximity detection. Although proximity detection is technically conceivable, it is only of interest when it comes to a coarse localization³ rather than positioning up to a few meters or better. Thus, proximity detection is not of practical use within the examinations performed in this thesis.

Lateration. At first glance, the problem of lateration seems to be impossible to overcome with signals designed for wireless networks due to the fact that distances between access points and receivers are required. As discussed in Section 3.4.3 however, it turns out that a relation between distance and received signal strength (which may be observed directly) can be formulated. Thus, lateration is a conceivable technique in the scope of absolute positioning using WLAN or Bluetooth.

Angulation. For this technique, the angle of arrival of a radio wave has to be known. Thus, special loop antennas [17, p.139-140] capable of determining a signal's angle of arrival are required. Regular WLAN or Bluetooth receivers do not feature such an antenna, hence the technique of angulation is not of further concern within this thesis.

Fingerprinting. The concept of fingerprinting seems to be suited well for positioning with WLAN or Bluetooth and is also favored throughout relevant literature, including [21]. Its biggest advantage is the capability to deal with complex environments, where a lot of obstacles alter the radio signals. However, fingerprinting is expected to give poor results when dealing with environments changing over time. This is due to the fact that a previously recorded radio map can not reflect the current environment properly. Whether or not the changing environment in a parking deck (i.e., moving vehicles) do have a major impact so that fingerprinting becomes unfeasible is going to be investigated within the practical investigations in Chapter 4.

³Unlike positioning, the term *localization* refers to obtaining the topological circumstances (e.g., within the transmission range of access point *i*) of an object rather than its actual coordinates.

Dead reckoning. To perform dead reckoning, a traveled distance as well as an oriented direction is required. Both the traveled distance and the direction are, as previously stated, not accessible with conventional WLAN or Bluetooth receivers. Furthermore, dead reckoning is a technique yielding relative coordinates (referring to the last known position). Since this thesis deals with absolute positioning, the technique is not of interest.

Summary. To conclude this section, Table 3.1 shows a compact summary of the preceding listing. Whether or not a technique is *applicable* for positioning within this project is based on several criteria, including required parameters, expected accuracy, or the capability of providing absolute coordinates.

Table 3.1: Suitability of wireless positioning techniques with respect to radio signals from WLAN or Bluetooth

Positioning technique	Applicable?
Proximity detection	No
Lateration	Yes
Angulation	No
Fingerprinting	Yes
Dead reckoning	No

Within the subsequent sections, the positioning methods lateration and fingerprinting are discussed in more detail.

3.4 Lateration

This section deals with the positioning technique called lateration. Unlike angulation (cf. Section 3.2.3), lateration does not require the arrival angles of radio waves. Thus, no special antennas (i.e., loop antennas) are mandatory. However, the exact computation of distances based on electromagnetic waves is not trivial. An approximate estimate to obtain distances is presented in Section 3.4.3.

3.4.1 Concept

As introduced in Section 3.2.2, the measurement quantities of lateration are distances between the unknown position and a number of access points, whose coordinates have to be known. In Figure 3.1, the problem is shown graphically and it turns out that lateration is basically the intersection of multiple circles with each other. To uniquely solve the problem, observations to three different access points are required. If there are more observations available, the system of equations becomes over-determined and thus the problem is solved by means of least squares adjustment. In the following section, the mathematical relationship is presented.

3.4.2 Mathematical algorithms

This section presents the mathematical model of 3D lateration. For 2D operations, one simply has to omit terms and rows/columns that involve the z component from subsequent equations.

Definitions. As previously mentioned, the goal of lateration is the computation of the coordinates of an unknown point, denoted as P :

$$P = P(x, y, z) \tag{3.1}$$

with x , y and z being the 3D coordinates of that point. From P , distances to known access points H_i are being measured (or somehow computed). In the context of this thesis, the access points are either WLAN routers or BLE beacons. At the unknown point P , an antenna receives the radio signals emitted by all nearby access points. To obtain a distance estimation, the path loss model introduced in Section 3.4.3 is applied. In analogy to P , the access points are given by

$$H_i = H_i(x_i, y_i, z_i). \tag{3.2}$$

If the coordinates of such an access point are known, it is eligible for being a base station used for lateration. Any one of these access points is designated as the reference point, denoted by a subscript r . For the sake of simplicity, the first access point ($i = 1$) is used:

$$H_{i=1} = H_r = H_r(x_r, y_r, z_r). \tag{3.3}$$

Aside from a minimum number of four, the total count of access points is arbitrary. This count is denoted by the letter n during the further procedure. Having $n > 4$ yields an

over-determined system which has to be solved using the well-known methods of least squares adjustment. To conclude these preliminary symbol definitions, the distances from P to H_i are denoted as s_i .

Derivation of the functional model. Assume the true (but unknown) Euclidean distance between the unknown point P and the i^{th} access point, H_i :

$$d_i = \sqrt{(x - x_i)^2 + (y - y_i)^2 + (z - z_i)^2}. \quad (3.4)$$

When being squared, the square root vanishes and (3.4) may be written as

$$d_i^2 = (x - x_i)^2 + (y - y_i)^2 + (z - z_i)^2. \quad (3.5)$$

Now, subtracting and adding x_r (and as well y_r and z_r , respectively) yields

$$d_i^2 = (x - x_r + x_r - x_i)^2 + (y - y_r + y_r - y_i)^2 + (z - z_r + z_r - z_i)^2, \quad (3.6)$$

which may then be further expanded to

$$\begin{aligned} d_i^2 &= (x - x_r)^2 + 2(x - x_r)(x_r - x_i) + (x_r - x_i)^2 \\ &\quad + (y - y_r)^2 + 2(y - y_r)(y_r - y_i) + (y_r - y_i)^2 \\ &\quad + (z - z_r)^2 + 2(z - z_r)(z_r - z_i) + (z_r - z_i)^2. \end{aligned} \quad (3.7)$$

In the next step, (3.7) is rearranged by grouping all squared terms on the right side and the linear terms on the left side of the equation:

$$\begin{aligned} (x - x_r)(x_r - x_i) + (y - y_r)(y_r - y_i) + (z - z_r)(z_r - z_i) = \\ -\frac{1}{2} \left((x - x_r)^2 + (y - y_r)^2 + (z - z_r)^2 + (x_r - x_i)^2 + (y_r - y_i)^2 + (z_r - z_i)^2 - d_i^2 \right). \end{aligned} \quad (3.8)$$

Now, when considering the formula for the Euclidean distance in (3.4), (3.8) shortens to

$$(x - x_r)(x_r - x_i) + (y - y_r)(y_r - y_i) + (z - z_r)(z_r - z_i) = -\frac{1}{2} \left(d_r^2 + d_{ir}^2 - d_i^2 \right). \quad (3.9)$$

Here it is important to distinguish between measured and computed quantities: While d_{ir} is computed from the given access point coordinates, d_r and d_i are actual measurements. Therefore, we formally replace d by s and write

$$(x - x_r)(x_r - x_i) + (y - y_r)(y_r - y_i) + (z - z_r)(z_r - z_i) \approx -\frac{1}{2} \left(s_r^2 - s_i^2 + d_{ir}^2 \right). \quad (3.10)$$

Now this is the functional model used to compute a position based on lateration. A minimum of four access points H_i is required to explicitly solve the problem in case the measurements show no erroneous behavior. In practice, this is obviously not the case and therefore a least squares adjustment with an over-determined system of equations is preferred.

Matrix notation. To conclude this section, this set of observation equations as given in (3.10) is presented in matrix notation. Note that the subscript r has been changed to 1 for the sake of readability, as previously defined in (3.3).

$$\begin{pmatrix} x_2 - x_1 & y_2 - y_1 & z_2 - z_1 \\ x_3 - x_1 & y_3 - y_1 & z_3 - z_1 \\ \vdots & \vdots & \vdots \\ x_n - x_1 & y_n - y_1 & z_n - z_1 \end{pmatrix} \cdot \begin{pmatrix} x - x_1 \\ y - y_1 \\ z - z_1 \end{pmatrix} = -\frac{1}{2} \cdot \begin{pmatrix} s_1^2 - s_2^2 + d_{12}^2 \\ s_1^2 - s_3^2 + d_{13}^2 \\ \vdots \\ s_1^2 - s_n^2 + d_{1n}^2 \end{pmatrix}. \quad (3.11)$$

This, again, may finally be written as

$$\mathbf{A} \cdot \vec{x} = \vec{l} \quad (3.12)$$

and thus the over-determined system may be solved by means of least squares:

$$\hat{\vec{x}} = (\mathbf{A}^T \mathbf{A})^{-1} \cdot \mathbf{A}^T \vec{l}. \quad (3.13)$$

In accordance to the usual notation used in parameter estimation, the hat $\hat{}$ indicates an estimated quantity.

3.4.3 Relation between RSSI and distance

As previously mentioned, the positioning technique lateration requires distances to known access points to calculate an unknown user position. However, when dealing with radio signals, no such distance is available initially. It is therefore essential to somehow compute the distance between access point and receiver based on available information.

Many radio positioning systems (including GNSS and radar) overcome this problem by measuring the elapsed time Δt of the radio waves traveling from transmitter to receiver. When having knowledge of the propagation velocity (which is, for radio waves in vacuum, the speed of light c), one can easily compute the required distance d :

$$d = c \cdot \Delta t. \quad (3.14)$$

Unfortunately, these convenient circumstances are of no relevance when it comes to positioning with WLAN or Bluetooth. This is simply due to the fact that the receivers do not provide any information regarding the run time of the received signals. However, an alternative approach is found utilizing the measurable received signal strength (cf.

Section 2.3): A relation between signal strength and distance is given by the path loss model [14]

$$PL_d = PL_{d_0} + 10n \cdot \log_{10} \left(\frac{d}{d_0} \right). \quad (3.15)$$

The presented equation is a very basic relation and is only valid for free air conditions (i.e., no obstacles exist along the signal path and in the surrounding area). One must be aware of the fact that any obstacle that alters the signal immediately falsifies the relation between signal strength and distance. Therefore, various more sophisticated modifications of (3.15) do exist, such as presented in [21]. This advanced model is capable of incorporating obstacles such as walls and therefore provide a realistic result. However, such a model is of minor relevance for practical applications, because to work properly, any obstacle would have to be physically and geometrically modeled. Furthermore, the model would have to be aware of the position of all these obstacles relative to the unknown receiver position. Obviously, this is not achievable without knowing the receiver position.

Now back to Equation (3.15). d represents the unknown distance between access point and receiver, d_0 is an arbitrary reference distance. As in [14], $d_0 = 5$ m has been used for investigations within this thesis. PL indicates path loss, i.e. the received signal strength, expressed in relation to d (PL_d) and d_0 (PL_{d_0}). Its physical unit is dBm, as described in Section 2.3. The constant value n serves as an attenuation coefficient that helps adapting the model to the surrounding conditions. According to [21], a value of $n = 2$ is used for free air conditions and a value of $2 < n < 6$ for office buildings, where shadowing is likely to occur.

Now, if one wants to derive a distance from an observed signal strength, (3.15) is rearranged, yielding

$$d = 10^{(PL_d - PL_{d_0})/10n} \cdot d_0. \quad (3.16)$$

In this respect, it should be pointed out that even though a distance can be obtained from observed signal strength, the result is likely to be highly inaccurate. Thus, a lateration-based position determination using (3.16) is expected to yield worse results than a fingerprinting-based approach, as described in Section 3.5. This is illustrated by [21] as well as throughout other relevant literature.

3.5 Fingerprinting

In this section, fingerprinting is covered. Alongside lateration, it has been elected as one of the two suitable positioning techniques for WLAN or Bluetooth signals. As [21] points out, it can be considered as the best approach to obtain a position using WLAN and clearly outperforms approaches based on path loss [7]. Since Bluetooth shows similar characteristics and operates in the same frequency band, fingerprinting is therefore expected to perform best for Bluetooth as well.

The computation of a position based on reference points is usually realized via a WKNN (weighted K nearest neighbors) approach, with K being the number of reference points whose coordinates shall be considered for computing the unknown position. The principle will be described in more detail within the subsequent sections.

3.5.1 Concept

Fingerprinting takes a rather different approach than the other positioning methods introduced in Section 3.2. The position is obtained by comparison of current signal patterns with previously measured signal patterns in reference points, referred to as *fingerprints*. Those fingerprints are arbitrarily laid out (usually in a regular grid, however this is not mandatory) in an area where the positioning shall take place. The entirety of the stored reference points is denoted as a *radio map*. In Figure 3.3, the concept of fingerprinting is shown by means of a fictive building interior with three access points (e.g., WLAN routers) mounted on the walls. Note that for fingerprinting, the coordinates of the access points do not have to be known (aside from visualization purposes). The fingerprinting itself is divided into two phases, an *offline phase* where the fingerprints are measured and an *online phase* where the actual positioning takes place.

Offline phase. In the initial offline phase, the radio map is created. As mentioned before, it consists of the reference points that are later used to derive the user's position. One must be aware of the fact that a computed position compulsorily lies within the convex hull of all reference points. Thus, the reference points must be spread in a sufficient way to cover the whole area of possible user positions. For each reference point, the following data is acquired and stored:

- Coordinates of the reference point
- Received signal strength of all individual access points

Depending on the size of the site where fingerprinting shall be established and the chosen density of the reference points, the radio map creation can be a time consuming procedure: In practical applications, one would observe the signal strengths received at a certain reference point for a period of time (e.g., some minutes) to reduce noise and get a good estimation of the RSSI. To further enhance the fingerprint, different antenna orientations can be considered and then either merged into one fingerprint or separately saved. In the case of retaining four directions (i.e., 0° , 90° , 180° and 270°), this results in four times as many fingerprints as for the combined radio map.

Online phase. Once the radio map is created, the actual positioning may take place in a so called online phase. At an unknown position $P(x, y, z)$, the received signal strength of all access points in range is measured. This signal pattern is then compared with the pattern of each fingerprint stored in the radio map. In this comparison, the *nearest neighbors* are determined. Here, *near* refers to a high similarity between the signal patterns of both the unknown position and the fingerprint. Examples on how to express this similarity in a mathematical way are presented in Section 3.5.3.

With K nearest neighbors being selected, the coordinate determination may now be performed by means of the arithmetic average of all K neighbors. Additionally, each individual neighbor may be assigned a weight, depending on its similarity value. Thus, a fingerprint that is more similar receives a higher weight than one with less similarity. The weighting of fingerprints is covered in (3.20) in Section 3.5.2.

Remark. In practical applications, fingerprinting faces some difficulties that are worth being mentioned. Since the received signal strength is influenced by objects in the signal path, fingerprinting is best used in static environments. If obstacles change, the signal is not likely to come across the same conditions and therefore yield a different signal strength. This makes the mapping of reference points more complicated or even unfeasible. According to [21, p.66], one could decrease this effect by having a set of reference receivers installed at certain locations. The radio map is then adapted regularly based on the measurements at those reference points. The effect of changing conditions may also occur due to a different antenna orientation between offline phase and online phase. To overcome this, radio maps are sometimes measured in four directions, as conducted in [22]. The four observation sets are then either merged into one combined fingerprint or saved separately, yielding four fingerprints per reference point. However, as stated in [22], increasing the size of the sample used to compute a fingerprint seems to be most beneficial. This means that the combination of the different orientations

yields a better result. Furthermore, as stated in Section 2.4.2 based on the findings of [19], the orientation is not a severe error source. Hence the assumption arises that, from an economical point of view, considering receiver orientations might not be of much value.

One must be aware of the fact that the (theoretically) achievable accuracy of an unknown position is directly associated with the density of the reference points. However, establishing a too dense grid might result in too similar signal patterns between reference points and thus letting the noise predominate over the dissimilarity of the fingerprints. This, of course, has a negative impact on the positioning result since a correct determination of nearest neighbors might not be possible any more. In addition, increasing the amount of fingerprints consequently requires more effort within the offline phase.

3.5.2 Positioning algorithms

As stated before, position determination via fingerprinting is based on similarity between signal patterns. The positioning may either be realized using nearest neighbor algorithms or statistical methods. The problem is visualized in Figure 3.5.

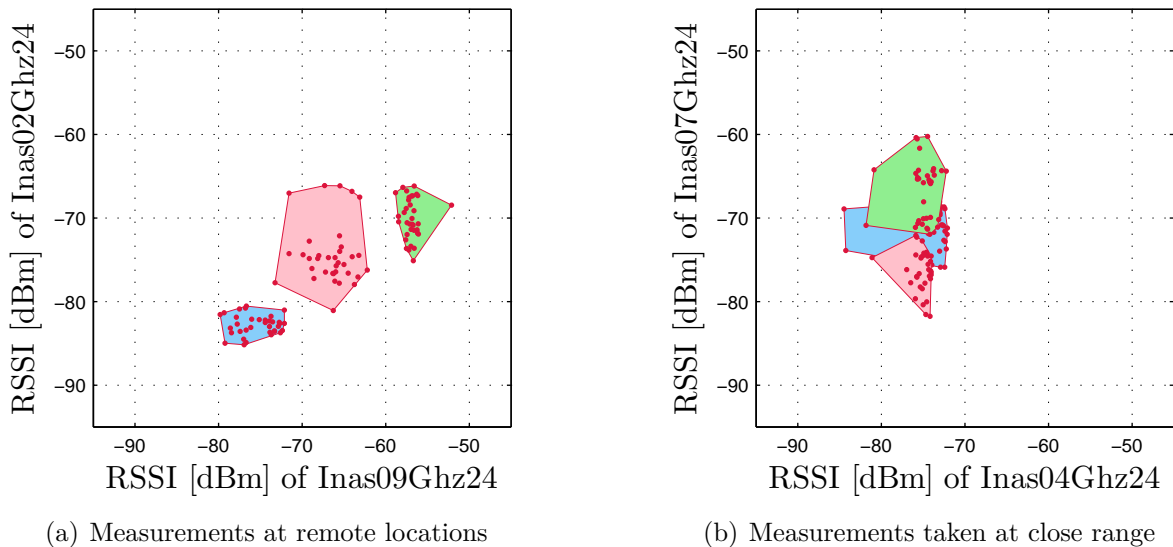


Figure 3.5: 2D feature space showing clustering of measurements from two WLAN access points, showing both an example for easily distinguishable fingerprints and an example for a similar feature representation (caused by a close spatial distance between fingerprints)

Here, measurements from three different fingerprints (obtained during a fingerprinting offline phase, cf. Section 3.5.1) are shown, whereas in Figure 3.5(a), those fingerprints have a considerably large distance (> 10 m) in between them, while in Figure 3.5(b), the displayed fingerprints are close to each other (a few meters apart). For visualization purposes, only measurements of two access points are shown, hence the feature space is 2-dimensional. In Figure 3.5(a), the clusters representing the individual fingerprints are clearly distinguishable and a nearest neighbor algorithm is likely to succeed in selecting the right fingerprint. However, in the example shown in Figure 3.5(b) however, the fingerprints are close to each other in the feature space and thus hardly distinguishable. By adding additional access points (resulting in a higher dimension feature space), a more obvious clustering is likely to occur.

Nearest neighbor algorithms. For an unknown point $P(x, y, z)$, assume a vector \vec{r}_P containing the current RSSI measurements to all n access points H_i in range. Thus, we write

$$\vec{r}_P = \begin{pmatrix} \text{RSSI}_{(H_1,P)} \\ \text{RSSI}_{(H_2,P)} \\ \vdots \\ \text{RSSI}_{(H_n,P)} \end{pmatrix}. \quad (3.17)$$

For each reference point, an analogous vector \vec{r}_i exists, containing the signal strength measurements observed at that reference point (typically, each of those RSSI values is the result of an average over multiple observations). The similarity of \vec{r}_P and \vec{r}_i is now illustrated as a scalar value, denoted as distance D_i , where the index i represents the i^{th} fingerprint: $D_i = \|\vec{r}_P - \vec{r}_i\|$.

Details on the computation of D_i may be found in Section 3.5.3. In the next step, the list of fingerprints is reordered based on their respective distance (ascending order), resulting in the assumed best reference point at the top of the list. Note that the variable i now refers to the sorted list of reference points. The most elementary approach would then be to take the coordinates of this topmost reference point and identify it with the coordinates of the unknown position (the vector \vec{x}_i represents the x, y, z coordinates of the i^{th} reference point):

$$\vec{\hat{x}}_{\text{NN}} = \vec{x}_{i=1}. \quad (3.18)$$

Setting $i = 1$ refers to the first reference point in the sorted list and thus the point with the smallest computed distance. The subscript $_{NN}$ denotes nearest neighbor, implying that only one reference point is considered. This method performs good if the number of fingerprints is sufficiently high and if the signal patterns can be assigned correctly to their respective fingerprint. If either of these conditions fails, then the approach is likely to yield poor results.

A more robust approach would be the consideration of multiple nearest neighbors (referred to as KNN-fingerprinting with K being the number of considered nearest neighbors) for the position computation. According to this, the position is computed from the first K fingerprints of the sorted list:

$$\vec{x}_{\text{KNN}} = \frac{1}{K} \cdot \sum_{i=1}^K \vec{x}_i. \quad (3.19)$$

The consideration of multiple nearest neighbors reduces the impact of nominating a completely wrong nearest neighbor. However, the result may also worsen depending on the arrangement of the fingerprints: If few fingerprints are situated in the vicinity of the unknown position, then the arithmetic average over K fingerprints forces \vec{x}_{KNN} into regions with a higher point density. A similar phenomenon occurs if the fingerprint distribution is not homogeneous around the unknown position (e.g., at the border area of the reference point grid).

To overcome these unwanted side effects, one may consider a weighted nearest neighbor fingerprinting, accordingly referred to as WKNN-fingerprinting. Therefore, a reference point with a small distance receives a high weight and vice versa, a more distant point is provided with a small weight. To achieve this behavior, the weights are represented by the inverse distances:

$$\vec{x}_{\text{WKNN}} = \sum_{i=1}^K \frac{1}{D_i} \vec{x}_i \cdot \left(\sum_{i=1}^K \frac{1}{D_i} \right)^{-1}. \quad (3.20)$$

Statistical methods for positioning. Another approach to compute the unknown location from measured signal patterns is given through the context of conditional probabilities [32]. In other words, the location probability shall be derived for a set of observations \vec{r}_P at the unknown position P . By applying the Bayes rule, we find the equation

$$p(\vec{x}|\vec{r}) = \frac{p(\vec{r}|\vec{x}) p(\vec{x})}{\sum_{i=1}^N p(\vec{r}|\vec{x}_i) p(\vec{x}_i)} \quad (3.21)$$

which describes the probability for the user being at the position \vec{x} under the condition of the observations \vec{r} . For the sake of readability, the notation has been adapted to previously used symbols in this chapter. $p(\vec{x})$ is the a priori probability of being at the position \vec{x} , without considering any observations. It may for example be derived from considering the last position(s) of a moving user. The sum in the denominator of (3.21) describes the probability $p(\vec{r})$ and contains the set of all possible positions \vec{x}_i . The term $p(\vec{r}|\vec{x})$ is referred to as likelihood function [32] and is currently unknown. It may be determined using different methods:

- using a histogram
- using a kernel function
- using models for radio wave propagation

These individual methods are not further discussed here; the interested reader is referred to [21][32].

3.5.3 Distance operators

The similarity of two points (current position P and reference point i) is expressed as a scalar value, referred to as *distance* D_i . It is important to note that in the context of this section, *distance* does not refer to a metrical separation, but to a degree of similarity in the signal domain. This means that if a signal pattern is very similar to another one, the distance between the two respective points becomes small, up to a value of 0 if the two patterns perfectly coincide. The distance is therefore computed via the difference of the two fingerprints, just as one would do with an actual geometrical distance, see (3.22). The following shall give an overview of commonly used measures of distance.

Generally speaking, the distance is computed via its norm

$$D_i = \|\vec{r}_P - \vec{r}_i\|. \quad (3.22)$$

One now has multiple options how to compute the norm $\|\cdot\|$ and therefore the distance. In order to do so, only RSSI values of access points found in both \vec{r}_P and \vec{r}_i are considered.

The number of access points observed at both points is denoted as N . For Euclidean distances, the ℓ^2 -norm is used:

$$\|\vec{r}_P - \vec{r}_i\|_2 = \sqrt{\sum_{n=1}^N (r_{P,n} - r_{i,n})^2} \quad (3.23)$$

Here, $r_{P,n}$ denotes the RSSI value measured at P of the n^{th} access point. The distance computation in (3.4) uses exactly this norm, applied for a 3-dimensional vector. Similar to the ℓ^2 -norm, the ℓ^1 -norm (referred to as *Manhattan distance*) reads

$$\|\vec{r}_P - \vec{r}_i\|_1 = \sum_{n=1}^N |r_{P,n} - r_{i,n}| \quad (3.24)$$

and thus, a generalized ℓ^p -norm may be formulated as

$$\|\vec{r}_P - \vec{r}_i\|_p = \left(\sum_{n=1}^N |r_{P,n} - r_{i,n}|^p \right)^{1/p} \quad (3.25)$$

with p being an arbitrary integer value. In the special case of $p \rightarrow \infty$, the norm reads

$$\|\vec{r}_P - \vec{r}_i\|_\infty = \max |r_{i,n}| \quad (3.26)$$

and is known as Chebyshev norm⁴ or maximum norm. Alternatively, one could also consider the variance of the RSSI observations at each reference point. This can be accomplished by using the Mahalanobis distance [25] given by

$$\|\vec{r}_P - \vec{r}_i\|_{\text{MD}} = \sqrt{(\vec{r}_P - \vec{r}_i)^T \mathbf{C}_r^{-1} (\vec{r}_P - \vec{r}_i)}, \quad (3.27)$$

where the matrix \mathbf{C}_r denotes the variance-covariance matrix of the fingerprint's observations. For training data with different and characteristic variance, the Mahalanobis distance often yields better results than the Euclidean distance.

⁴Named after the famous 19th century Russian mathematician Pafnuty Lvovich Chebyshev

Remark. The distance computations listed above share one common potential weakness. The fact that only observations occurring in both the fingerprint and the current position are considered might result in a falsified distance computation. This is best illustrated by means of an example:

Assume a given radio map with two reference points, R_1 and R_2 . At an arbitrary time t during the online phase, observations to several access points are given for an additional, yet unknown point P . The fictional observations with their corresponding distances to P (based on the ℓ^2 norm) are listed in Table 3.2. In the example, P shares four common access points with R_1 , while only one common access point is observed in both P and R_2 .

Table 3.2: Fictive observations for an unknown point P and two reference points to seven different access points. The computed distance is based on the ℓ^2 norm.

Access point	P [dBm]	R_1 [dBm]	R_2 [dBm]
AP1	-76	-73	
AP2	-80	-78	
AP3	-67	-69	
AP4	-89	-90	-93
AP5			-81
AP6			-83
AP7			-63
Distance to P :		4.24	4.00

If one had to instinctively determine which reference point better resembles P , the answer would certainly be R_1 . However, the ℓ^2 distance computation puts R_2 in favor. This is because the distance computation for R_2 is only based on AP4, which is the only common access point. Thus it becomes obvious that somehow the number of common access points (or even the number of diverse access points) should be considered to avoid erroneous assignments to reference points.

A potential solution to overcome this issue is implemented as follows: Each reference point R_i is complemented with a set of pseudo observations. For every access point that has not been recorded, a pseudo observation to that access point of -100 dBm is added to the radio map. For the example in Table 3.2 this results in an adaptations of the distance for R_2 to a value of 45.62. Hence, the correct fingerprint (R_1) is now selected properly. Another – yet experimental – approach would be to increase the weight of R_i for each common access point and to decrease it for each access point that is observed in R_i , but not in P .

3.6 Combination of multiple techniques

When it comes to position determination, the combination of multiple different positioning techniques is usually beneficial in favor of the achievable accuracy and reliability. The most effective setup would be the combination of an absolute technique (e.g., GNSS positioning or WLAN/BLE fingerprinting) and a technique yielding relative positions (such as an IMU or odometry). By combining absolute and relative positioning one overcomes the weaknesses of either technique. A comparison between those two positioning methods is given in Table 3.3. In [17, p. 288], the source table compares GNSS with an Inertial Navigation System (INS), however, most of it may be applied to absolute and relative systems in general. Most importantly, absolute and relative positioning differ in achievable accuracy: While an absolute system is stable over longer periods of time, its short-term accuracy is low compared to a relative system. On the other hand relative positioning is affected by drift effects, hence the long-term accuracy is low.

Table 3.3: Comparison between absolute and relative positioning [17, p. 288]

Feature	Absolute	Relative
Short-term accuracy	Low	High
Long-term accuracy	High	Low
Availability	Limited	Unlimited
Vulnerability	High	None

Absolute positioning techniques often suffer from limited availability, e.g. GNSS which is not available indoors. An INS does not face this problem: With the IMU being the only required infrastructure, the availability is unlimited and its use is independent of external conditions. Furthermore, due to its dependence on external infrastructure, an absolute positioning system is usually much more vulnerable in terms of errors or even manipulation⁵ than a relative, independent system.

A possible way of combining different measurements would be the utilization of a Kalman filter. It is an algorithm for the best⁶ estimation of time-dependent parameters under consideration of previous epochs. It is therefore closely related to the recursive parameter estimation. In layman's terms, the Kalman filter is an improvement of a measurement by considering previously gathered data as well as a model describing the object's behavior.

⁵A good example would be Selective Availability (SA), which was used to intentionally deteriorate the GPS signal until May 2000 [17, p. 191-192]

⁶In the context of parameter estimation, *best* usually implies an estimation with respect to BLUE (best linear unbiased estimation)

This *dynamic model* is responsible for modeling an object's expected movement, so that parameter estimation may be performed even if no measurements are available.

Generally speaking, the Kalman filter is subdivided into three computation steps:

- **Gain computation.** Subject of this step is the computation of the gain matrix (or Kalman matrix) \mathbf{K} . It acts as a weight for new observations based upon their accuracy in relation to the accuracy of the predicted parameters. Hence, if the new measurements are very accurate, \mathbf{K} approaches the unit matrix; contrary, if the prediction shows a high accuracy and the measurements are inaccurate, \mathbf{K} approaches $\mathbf{0}$.
- **Measurement update.** In this step, the previously predicted parameters (and their covariance matrix) get updated with newly gathered observations from a suitable sensor environment. The impact of these new observations is determined by the previously introduced gain matrix \mathbf{K} .
- **Time update.** In the time update (or prediction step), the parameters of the next epoch and their corresponding covariance matrix are predicted using a predefined dynamic model. This model consists of a transition matrix (defining the dynamic model, e.g., a linear motion) and some matrix describing the accuracy of the model. Along with the output of the measurement update, parameters for the next epoch may be predicted.

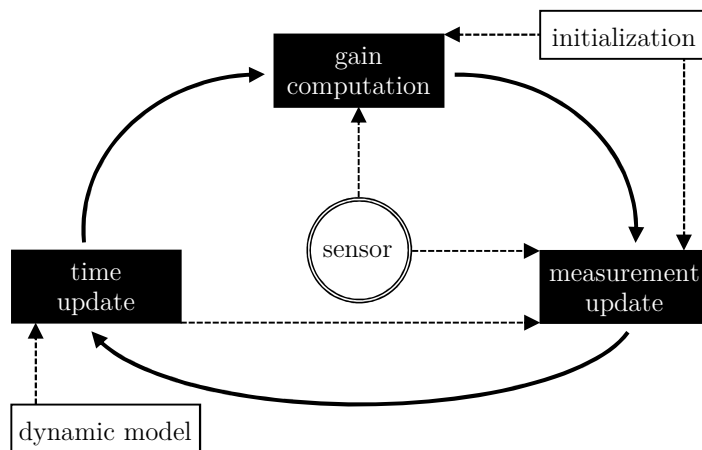


Figure 3.6: Principle of the Kalman filter [17, p. 54]

In Figure 3.6, the principle of the Kalman filter is graphically shown. Note that for the first epoch, an initialization is required since no prediction is available. For every

consecutive epoch, new measurements are received from a sensor environment. The accuracy information of those measurements is required in the gain computation step.

When performing a Kalman filter with different measurement types, one has to distinguish between various levels of coupling within the filter. Generally, there are uncoupled, loosely coupled and tightly coupled Kalman filters. While only the computed results of the individual sensors are taken into account for an uncoupled filter, raw measurement data is filtered in case of loosely and tightly coupled filters, providing a tighter sensor integration. Consequently, the maximum integration is gained in case of a tightly coupled filter.

Note that for the practical investigations performed in the context of this thesis, no Kalman filter has been applied. Thus, this section rather serves as an outlook of what to expect from future investigations, when relative positioning is considered complementing the absolute methods which are subject of this thesis.

Chapter 4

Practical investigations

Throughout this thesis, various practical investigations have been performed. This chapter shall represent an aggregation of the practical work that has been done. Unless they are considered *final results*, the findings of the various elaborations are presented directly within the corresponding section, the final outcome is displayed and discussed in Chapter 5. Throughout this thesis, content of figures is color-coded: Content related to WLAN is displayed in shades of red and Bluetooth-related content is displayed – as the reader might expect – in shades of blue.

For signal recording and processing, a prompt-based software tool has been developed. The program is briefly introduced in Section 4.2. Besides the investigations documented within this thesis, a number of smaller tests have been elaborated, primarily with the purpose of getting used to the procedure and for getting to know the capabilities of WLAN and Bluetooth for position determination. Some of the findings of these brief investigations are included throughout Chapter 2.

4.1 Used hardware

For the performed investigations, numerous pieces of hardware have been used within the measurement process. Thus, this section is subdivided into receiver hardware (i.e., laptops and antennas) and access point hardware (i.e., WLAN routers and BLE beacons). Furthermore, miscellaneous additional infrastructure is briefly mentioned.

Used receiver hardware. Throughout the measurement campaigns, the receiver base unit (i.e., a laptop) has been exchanged several times based on the requirements of the current investigation. However, due to the fact that consistent USB adapters have been

used for receiving both WLAN and Bluetooth signals, the underlying laptop does not have an impact on the measurements directly (it may, however, impact the frequency of network scans when given poor hardware specifications). The used laptops are presented in Table 4.1.

Table 4.1: Used laptops

Device name	Operating system	Kernel	CPU
Lenovo IdeaPad Z580	Linux Mint (64 Bit)	3.15.0	Intel Core i5-3210M
Asus Eee PC 1005PE	Ubuntu (32 Bit)	3.13.0	Intel Atom N450
Lenovo ThinkPad X201	ArchLinux (64 Bit)	3.17.6	Intel Core i5-540M

The use of a Linux operating system is mandatory due to the limited compatibility of the software used for signal evaluation (Section 4.2). For tracking Bluetooth signals, the power of the underlying hardware can be considered irrelevant and even the rather slow Eee PC achieved satisfying results in terms of scanning speed. For WLAN, the scanning speed depends both on the computer’s hardware and the used WLAN antenna. With the given setups, a maximum of approximately 1 Hz could have been achieved.

As mentioned before, the actual measurement is performed by external antennas, which are connected with the laptop via USB extension cables. A list of all used adapters may be found in Table 4.2.

Table 4.2: Used USB adapters for receiving WLAN and Bluetooth signals

Device name	Network capabilities
EDiMAX EW-7811UN	WLAN (2.4 GHz, IEEE-802.11b/g/n)
LogiLink BT0015	Bluetooth (Version 4.0, supports BLE)
CSL USB 2.0 WLAN Adapter	WLAN (2.4 GHz / 5 GHz, IEEE-802.11a/b/g/n)

Both the EDiMAX and LogiLink devices cost less than € 10. The CSL product is available for approximately € 20 and differs in size, as clearly visible in Figure 4.1. Its two antennas are much larger than those of the other two presented dongles. However, though the range is significantly larger than of the EDiMAX device, the stability of the RSSI shows no advantage. In addition to that, a scan for visible nearby WLAN networks takes – depending on the computing power of the laptop – at least three to four seconds, while the same scan only takes one second with the smaller EDiMAX dongle.



Figure 4.1: Used USB adapters for receiving WLAN and BLE data

Used access point hardware. Different types of access points have been used for the investigations presented in this chapter. For WLAN, a total of ten Linksys¹ E2500 routers were used. The router supports the IEEE 802.11n standard and features four internal antennas to support simultaneous 2.4 GHz and 5.2 GHz transmissions. It can be seen in Figure 4.2, along with cables for an external, portable power source making it independent from the local electricity infrastructure for the duration of the test runs.



Figure 4.2: Linksys E2500 router with cables for an external, portable power source

For Bluetooth, several different access points (BLE beacons) have been investigated, namely the devices shown in Figure 2.2. For the main investigations in the parking garage, a total of 60 beacons manufactured by Accent Advanced Systems have been used. Due to the release of a new generation of beacons during the term of this project, the

¹Formerly owned by Cisco Systems, Inc., Linksys is in possession of Belkin International, Inc. since 2013 — <http://www.linksys.com/>

beacon (model: iBKS101) displayed in Figure 2.2(b) is outdated and the new iBKS105 has been used. Its major advantages are the significantly increased battery lifetime as well as the closure system without the need for screws. The form factor has not changed between the two models. Whether or not the battery lifetime actually improved over the predecessor can not be determined yet, since both models are still running on their first battery.

Miscellaneous. Aside from the hardware required for the actual positioning, two GPS receiver and a modern tachymeter have been used for obtaining the layout plan of the parking deck. Additionally, the tachymeter (Leica MS50) has been further used to create a reference trajectory of the vehicle equipped with WLAN and BLE antennas.

4.2 Software for signal recording and evaluation

For measuring and recording the RSSI of WLAN and BLE signals, a prompt-based software tool entitled *Wireless Kit* has been developed using the programming language C++. It is designed to match the requirements of the various investigations. A sample screenshot of *Wireless Kit* may be seen in Figure 4.3.

The main features of *Wireless Kit* are:

- Scanning for nearby access points and saving them within the current radio map (available within the command `new`)
- Recording of fingerprints for a variable amount of time (also available via `new`)
- Recording of measurements for positioning (online phase) along with an implementation of a basic fingerprinting algorithm (available within the command `pos`)
- Repeated observation of selected access points only (using the command `watch`)
- Capability of editing points (coordinates, name) and removing access points and/or fingerprints (available within the command `edit`)
- Selection of the network adapter (available within the command `setup`)
- ASCII export of all taken observations for further procedure in different applications (prompted immediately after observations were taken)
- Export and import of radio maps as either binary or ascii file (via the commands `save` and `load`)

```

WIRELESS KIT
> A simple tool for absolute positioning driven by
  wireless signals. Created by Roman Wilfinger.
> Version 1.3.2

Troubles getting started? Enter help for a list of commands.

wirelesskit> load -b ble.bin
Radio map [interface:hci0] [author:Roman]
containing 6 AP(s) and 0 FP(s) successfully loaded!

wirelesskit> watch 1,2,4,5 10

Now logging RSSI values.....DONE

#          iBeacon 1          iBeacon 2          iBeacon 4          iBeacon 5
1          -70.3 dBm         -75.8 dBm         -66.3 dBm         -66.6 dBm

Do you want to export the raw measurements? (y/N): _

```

Figure 4.3: Sample screenshot of *Wireless Kit*. First, an existing binary file with previously saved access points is loaded using the command `load`, then using the command `watch` some of those access points are observed for a total of ten seconds.

For signal recording purposes, the software reverts to Unix system commands, therefore the software only is fully compatible with Unix-based operating systems. On Windows, no measurements can be taken at all due to the absence of these commands. For tracking WLAN signals, the command `iwlist`² has been incorporated; for BLE, a combination of `hcidump`³ and `hcidump`⁴ has been used. Note that those commands require administrator privileges, therefore *Wireless Kit* has to be launched with `sudo` to grant administrative privileges throughout the whole application.

4.3 Relationship between distance and RSSI

The relationship between metrical distance and RSSI (i.e., how the signal strength diminishes with increasing distance between access point and receiver) is worth to be

²For getting information from a wireless interface: <http://linux.die.net/man/8/iwlist>

³Permanently scan for Bluetooth devices in range: <http://linux.die.net/man/1/hcidump>

⁴For parsing HCI data: <http://linux.die.net/man/8/hcidump>

known for several reasons. First of all, it is essential for position determination using the lateration approach because the distance between access point and receiver must be known (see Section 3.4 and especially Section 3.4.3). For fingerprinting, only the RSSI values are of interest. However, knowing how the RSSI behaves with increasing distance is useful for designing the access point density: Since the noise level of a signal increases with greater distance, it might be a reasonable idea to increase the number of access points so that at all time enough access points are considered to be close enough.

The test arrangement is rather simple: At numerous known distances between access point and receiver (e.g., in a constant interval of 1 m) the RSSI has been observed for some minutes. After a simple 3σ outlier detection and elimination, the mean RSSI has been saved together with the current distance.

4.3.1 Wireless LAN

Figure 4.4 shows the arrangement described in the previous paragraph: To avoid potential interference and, most importantly, multipathing, the measurements have been performed on even grassland surrounded by cultivated areas. The white line visible in the photograph is a metal tape measure with a maximum length of 50 m.



Figure 4.4: Arrangement for determining the relation between distance and RSSI for WLAN signals using a Lenovo Z580 and both WLAN antennas simultaneously. The arrangement for Bluetooth is analogous.

To compare different WLAN receivers and also the performance of the 2.4 GHz and the 5.2 GHz band, both WLAN devices listed in Table 4.2 have been used simultaneously and were mounted on the back of the laptop’s display with red duct tape. Applying (3.15) with respect to the observation distances yields the theoretical path loss which is visualized as a dashed black line together with the empirical RSSI in Figure 4.5. An attenuation factor of $n = 2$ has been used for all investigations within this section. According to [21], this value for n represents free air conditions.

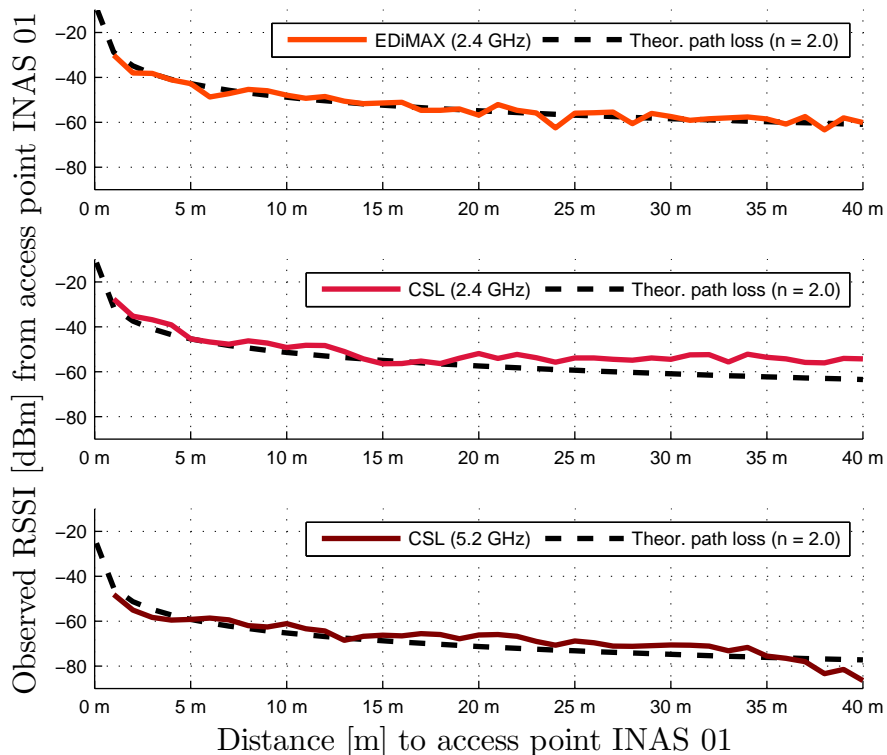


Figure 4.5: Empirically determined relation between distance to access point INAS 01 and observed RSSI in comparison with the theoretical path loss for both investigated WLAN devices.

According to Figure 4.5, the EDiMAX antenna (top graph of Figure 4.5) performs best in terms of reflecting the theoretical path loss up to the maximum observed distance of 40 m. As expected, the CSL antenna features a wider coverage area, which can be seen by means of the slowly attenuating RSSI in the 2.4 GHz band (middle graph of Figure 4.5). Due to the fact that the RSSI does not decrease significantly within 15 m and 40 m, it is expected to yield badly distinguishable fingerprints. The RSSI from the 5.2 GHz band (bottom graph of Figure 4.5) better fits to the theoretical path loss, however, the observations significantly depart from the dashed line for distances greater

than 35 m.

Based on the findings of aforementioned investigation and the fact that the CSL antenna features a considerably longer scan time, the EDiMAX antenna is favored for further measurements. On the downside however, measurements within the 5.2 GHz band are therefore omitted.

4.3.2 Bluetooth Low Energy

The same investigation has been performed for BLE on another day. In this case only one antenna has been used but – in contrary to the WLAN setup – three different access points (i.e., BLE beacons from different vendors). The result can be seen in Figure 4.6. The displayed values are a result of observations for several minutes and are computed by averaging with a preliminary 3σ outlier detection and elimination.

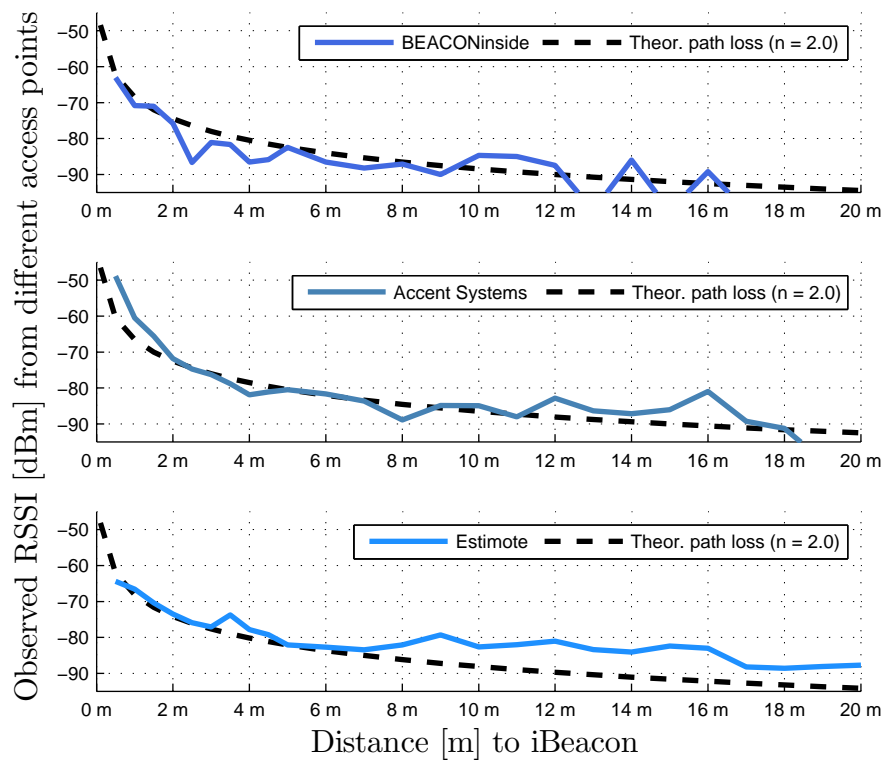


Figure 4.6: Empirically determined relation between distance to different BLE beacons and observed RSSI in comparison with the theoretical path loss.

For Bluetooth, the Spanish beacon manufactured by Accent Advanced Systems (middle graph of Figure 4.6) has been favored. It reflects the theoretical path loss better than

the other two beacons, though for distances greater than 10 m, the signal to noise ratio gets worse significantly and the RSSI behaves unexpected. However, this is also true at an even larger scale for the other investigated devices.

The German device (BEACONinside, top graph of Figure 4.6) yields an unsatisfying performance since the RSSI significantly differs from the theoretical curve even for close distances. Although the Estimote beacon (bottom graph of Figure 4.6) seems somewhat stable, the fact that it costs about twice as much as the Spanish fabricate disqualifies it from being the primary choice for further large-scale investigations.

4.4 Simple fingerprinting test bed

In advance to the main investigations in the Thondorf parking garage, a simple fingerprinting and lateration test bed has been established in a lecture room at Graz University of Technology (Neue Technik, Steyrergasse 30, first floor). The observations for the radio map creation (offline phase) took place on September 10th, 2014 and some simple positioning tests (online phase) on September 11th.

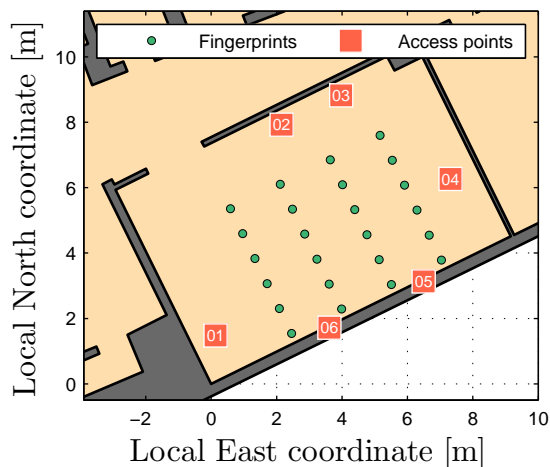
The major goals of this setup were the development of computation and visualization tools to draw first conclusions regarding the capabilities of standard fingerprinting algorithms in a simple and known environment. Additionally, it was intended to design the software in a way to be of further use in subsequent investigations.

Due to the absence of BLE devices at the time this investigation took place, only WLAN has been considered for radio map creation and positioning.

4.4.1 Test bed overview

This section shall illustrate the test bed established in the lecture room A111 at Steyrergasse 30. For visualization purposes, the walls in the lecture room and in its vicinity have been georeferenced using a simple tape measure. Based on a local, north-oriented coordinate system, both the access points and the reference points were georeferenced as well using the same technique as for the room geometry. This resulted in a relative accuracy of the point coordinates and the room geometry of a few centimeters. The visualization of the test bed can be seen in Figure 4.7(a).

In total, six WLAN access points were installed, fairly evenly distributed along the side walls of the room. The access points enclose an array of 24 reference points, placed in



(a) Overview created in Matlab



(b) Lecture room A111

Figure 4.7: Overview of the positioning test bed established in a lecture room at Graz University of Technology (Steyrergasse 30, first floor) in September 2014

a regular grid of four rows. This results in a grid spacing of 0.85 m in direction of the shorter wall of the room (where the blackboard is mounted) and 1.70 m along the other wall. To test the performance of the two investigated WLAN antennas, two radio maps were generated simultaneously by running two instances of *Wireless Kit* at the same time. At each reference point, observations were taken over the time of five minutes and averaged (under consideration of outliers based on a tolerance range of 3σ) thereafter. Due to practical reasons, the reference points were placed on top of the tables visible in Figure 4.7(b). For observation purposes, the laptop was then simply placed on top of the tables, with the antennas (mounted at the back side of the display) being centered on each reference point.

4.4.2 Results

In this section, the results of this simple configuration are shown. In advance to the positioning results, the created radio map is visualized for selected access points. Therefore, the RSSI of a certain access point is examined at all reference points and then interpolated to generate a homogeneous intensity map, as seen in Figure 4.8. The interpolation has been performed using Matlab's `v4` method, i.e., a bi-harmonic spline interpolation that is not based on a triangulation. This method has been chosen because it produced the most visually appealing solution compared to other alternatives. Since the interpo-

lation is merely due to visualization, the underlying interpolation method does not alter the positioning in any way.

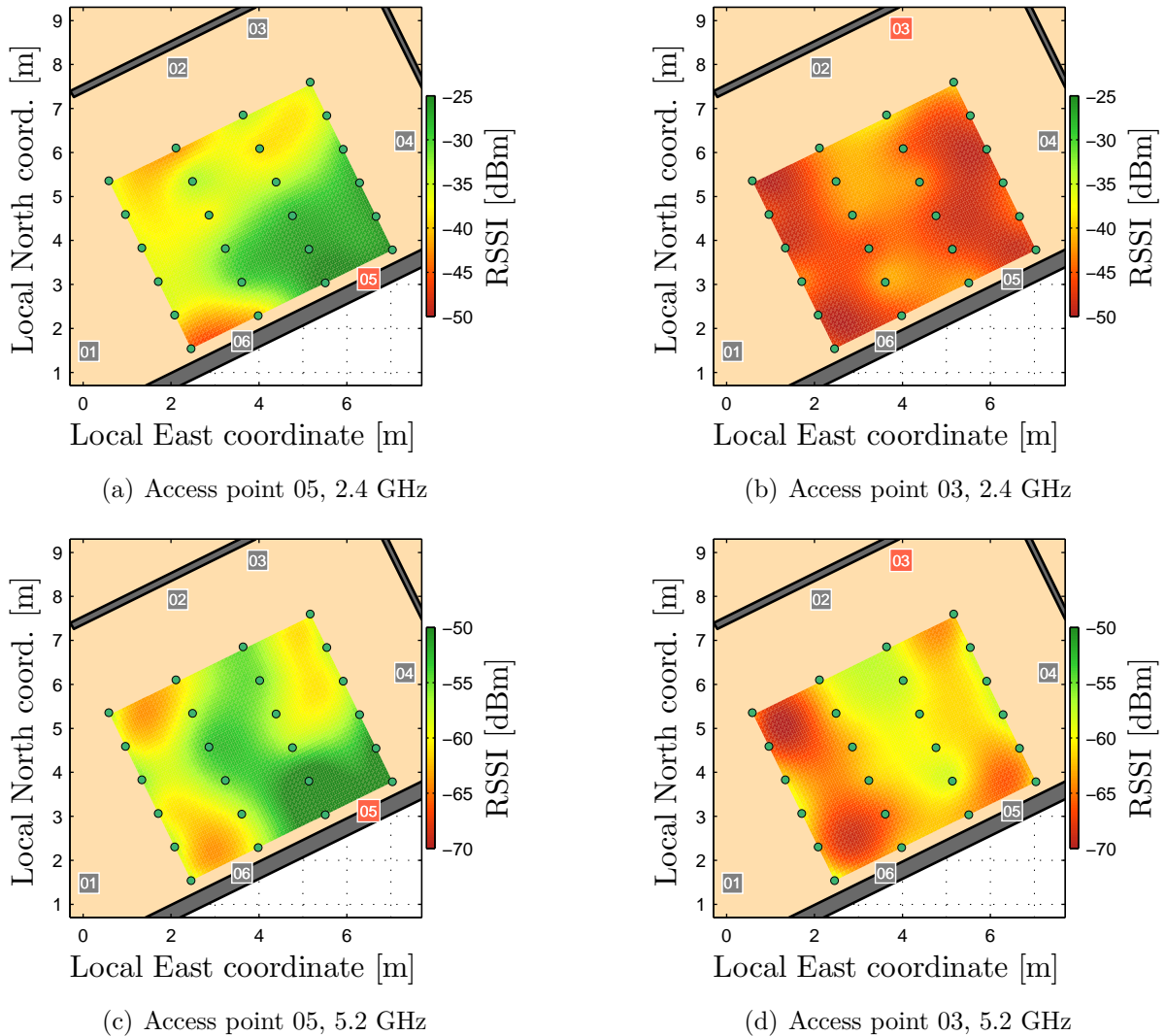


Figure 4.8: Radio map visualization by interpolation of RSSI for selected access points. For the displayed examples, the used WLAN antenna was the CSL product.

The radio map produced by access point 05, which is located on top of the window sill at the south wall of the room, shows a somewhat expected behavior: The RSSI is mitigated roughly concentric around the access point with increasing distance. This may be seen both in the 2.4 GHz band in Figure 4.8(a) as well as in the 5.2 GHz band, Figure 4.8(c). For the other presented access point (access point 03), the computed radio map seems to be dominated by signal noise and multipath effects and thus it is not meaningful.

Additionally, the overall RSSI is lower than for the other shown access point. This applies to both frequency bands (see Figure 4.8(b) for 2.4 GHz and Figure 4.8(d) for 5.2 GHz), even though the distance of the access points from the reference point grid is roughly the same. Using a larger grid space for the reference points and an overall larger grid area, respectively, more significant differences between individual grid points and thus a reduction of the ratio of the noise component is expected. However, a wide meshed reference point grid ultimately limits the achievable positioning accuracy. Thus, a compromise tailored to the particular location had to be found.

As for the positioning, several tests with static positions and 60 seconds observation time have been conducted. Representative results from two of those test points are presented in Figure 4.9. The individual solutions (approximately one position fix per second) are displayed as red crosses, the true position is denoted as a pink triangle.

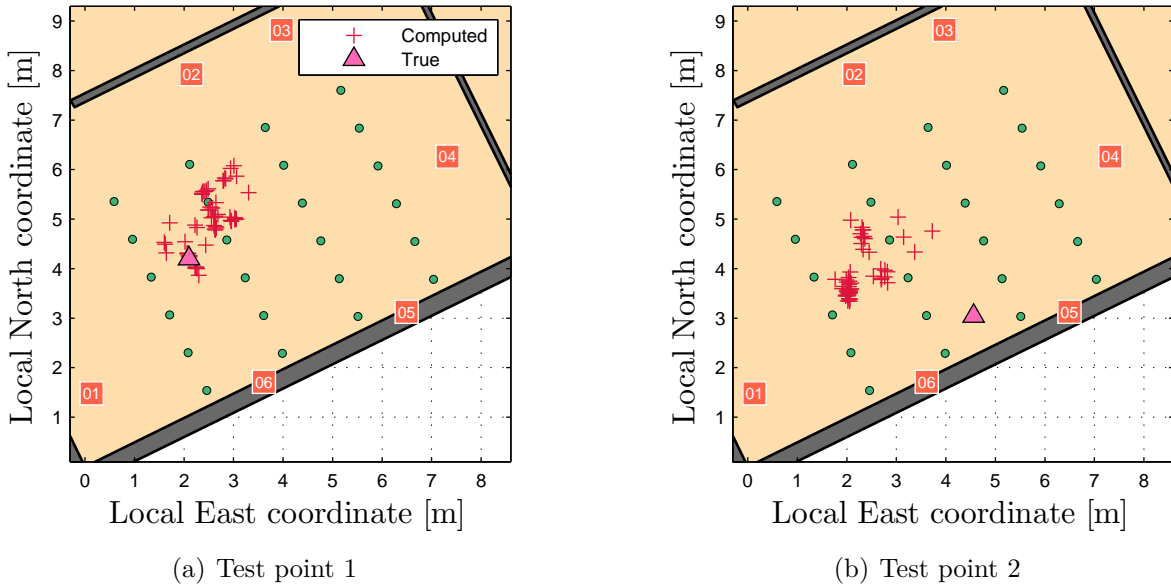


Figure 4.9: Static positioning (60 seconds) on selected test points marked as pink triangles, the used WLAN antenna was the EDiMAX dongle. Positions were computed using a WKNN fingerprinting with $K = 4$ nearest neighbors.

In Figure 4.9(a), the true position is somewhat centered with respect to the reference point grid. The computed solutions are scattered within an area approximately 2 m around the true position, but with the addition of a significantly decentralized distribution. Due to the similar signal patterns of adjacent grid points, the position fixes differ from the true position. In the given radio map, this is a crucial factor since the

grid points are very close to each other and thus the difference in the signal strength is mostly vanishing. The result is a cluster of individual solutions, which is slightly offset from the true position. Thus, the result can be interpreted as *precise*, but not *accurate*⁵. The second test point, as seen in Figure 4.9(b), is located closer to the edge of the grid. This impacts the computation when dealing with multiple ($K > 1$) nearest neighbors, because then the resulting position is likely to be drawn towards the center of the grid. The reason for this lies within the WKNN algorithm: In an idealized setting, the nearest neighbors are chosen evenly distributed around the actual position. However, if no points are available at one side of the actual position, the result is inevitably drawn towards the other side.

4.5 Setting up a radio map in a parking garage

The major practical investigation for this thesis is to set up a WLAN- and Bluetooth-based fingerprinting test bed in a sufficiently large parking garage, preferably with real life conditions (e.g., moving and parking cars) to perform various test runs. Such a testing environment has been found in Thondorf (South of Graz, Austria), next to the premises of Magna Steyr. It is briefly described in Section 4.5.1. The deliberations regarding the quantity and placement of access points and reference points are discussed in Section 4.5.2.

4.5.1 Overview of the parking garage

The garage itself is owned by the city of Graz and features a total of six floors, each with an area of approximately 4 800 m² and a room height of 2.10 m. Among those, the top three floors are exclusively rented by Magna Steyr and thus serve as a parking space for their employees. This means that heavy traffic occurs only during shift changeovers. The investigations have been performed on the fifth floor. Each floor is separated into two mezzanines, showing a height difference of approximately 1.5 m. They are connected by two ramps. While the parking garage is open on three sides (only delimited by some metal fencing), each floor is separated into three areas, divided by concrete walls and connected by large fire doors (large enough so that vehicles may easily pass through). An outside view of the whole building is given in Figure 4.10.

⁵Precision refers to the variance of the sample, meaning a sample is considered precise if the computed values are similar to each other. Accuracy, on the other hand, refers to the true value of a sample, therefore a sample is accurate if it (or its mean) is close to the true value.



Figure 4.10: Outside view of the parking garage at Liebenauer Hauptstraße 316 (Thondorf). The test bed is located on the fifth floor and has an area of roughly 4 800 m².

The garage is mainly built of concrete with multiple supportive steel girders across the ceiling of each floor. Those beams are good spots for access point placement, as seen in Figure 4.11 and Figure 4.12.



Figure 4.11: Photograph showing the inside of the Thondorf parking garage

Apart from the shadowing effects caused by the steel, placing the access points as seen in Figure 4.12 has three major benefits:

- The access points are easily installed and removed, which means that they only have to be deployed in the parking garage when measurements are taken.
- All access points are guaranteed to be higher than any vehicle in the parking garage, reducing time-variable shadowing effects caused by vehicles.
- Since the parking deck is a public place, all used hardware is at risk of being stolen. By placing the access points in the described manner, they are not visible at first glance and are therefore less likely to be removed or vandalized.

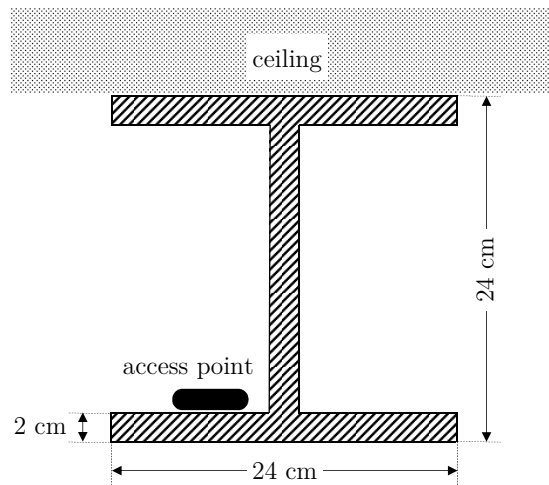


Figure 4.12: Schematic view of the steel girders located at the ceiling of each floor and the placement of an access point

A digital plan of the investigated area has been created in advance to the actual radio map creation. Therefore, a tachymetric survey has been performed on November 12, 2014 with approximately 300 detail points being recorded. To obtain absolute coordinates, two GPS receivers have been used at points in the proximity of the building. Using relative GPS, the obtained positions (WGS 84) are in the accuracy of approximately 1 cm and thus sufficient for this project. The plan layout has been drawn using AutoCAD 2015 and has then been exported as an ASCII-file containing descriptive points for further procedure in Matlab.

4.5.2 Recording the radio map

When designing a fingerprinting radio map, time (and thus cost) is usually the limiting factor, especially for large projects. It is therefore important to find a trade-off between expenditure and reference point density. In addition, the observation time per point has to be chosen, whereas a longer observation time has the benefit that outliers may be detected more reliable. Considering those criteria, a total of 568 reference points have been recorded on two days of December 2014 (offline phase). Assuming a covered area of 4800 m², this yields approximately an average 8.5 m² per reference point. The spots of the fingerprints were chosen considering two aspects: On the one hand, a more or less regular grid was aspired and, on the other hand for convenience, the points shall be easily determinable in the parking garage for convenience. Thus, the lines separating

individual parking spaces have been used for the placement of the reference points. As mentioned in Section 4.5.1, the access points have been placed along the steel girders on the ceiling. The resulting spots of fingerprints and access points are visualized in Figure 4.13.

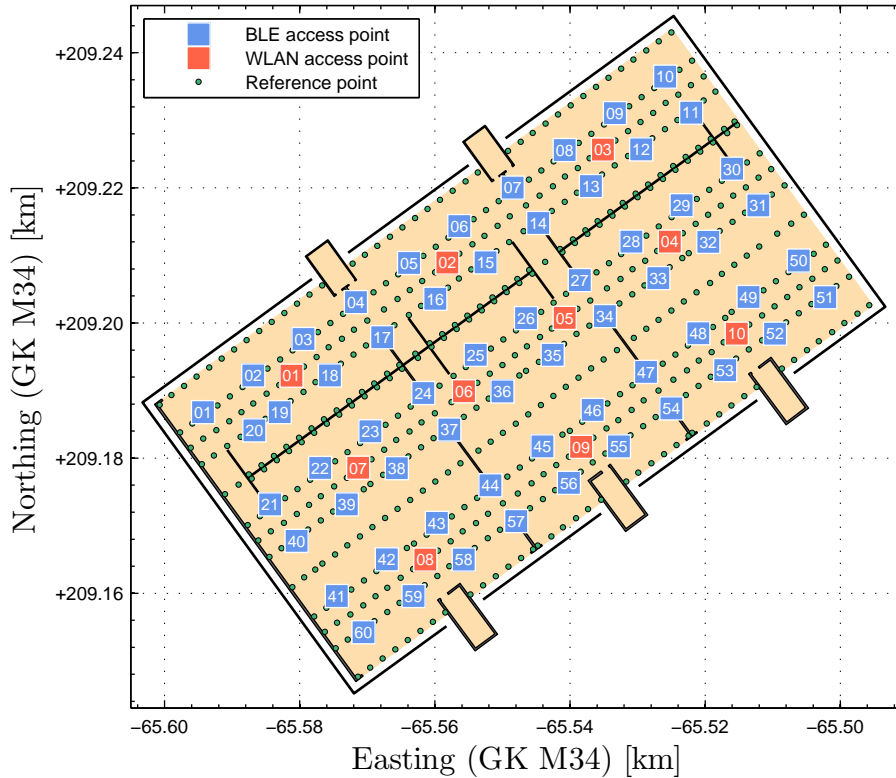


Figure 4.13: Overview of the radio map established on the 5th floor of the Thondorf parking deck in December 2014. The access points are placed along steel girders that run across the ceiling of each floor, e.g., the BLE access points 10, 11, 30, 31, 50 and 51 are placed on the same beam. The used coordinate system is Gauß-Krüger M34.

Due to a mistake, the BLE beacon 20 was misplaced during the radio map creation (the beacons usually are placed on every second steel girder). Thus, it had to remain in that position for the rest of the radio map creation as well as for the entire online positioning phase. Another problem occurred with BLE beacon 50, which showed a malfunction on the second day of the radio map creation and did not broadcast a signal. It was therefore no longer installed during further tests and existing observations were discarded.

The radio maps for both Bluetooth and WLAN have been recorded simultaneously, with two instances of *Wireless Kit* running parallel. Due to the large number of reference points, the observation time per point has been scheduled with 30 seconds, yielding

approximately 30 observations from each beacon at the configured data rate of 1 Hz. Due to the limited number of observations, the EDiMAX WLAN antenna has been chosen over the CSL antenna. Even though measurements in the 5.2 GHz band could therefore not be recorded, the significantly higher number of observations has been the decisive factor. Another approximately 30 seconds per point were required due to relocation and command inputs for a new point. Thus, the sheer radio map creation took about ten hours, which has been portioned into two days of work. The financial effort of the infrastructure is shown in Table 4.3.

Table 4.3: Used infrastructure for the parking deck

Network type	Access points	Cost per AP	Total cost
BLE	60	€ 12.50	€ 750
WLAN	10	€ 60.00	€ 600

The used number of access points has been chosen based on the findings of Section 3.4.3. The greater coverage of WLAN implies a lower necessary access point count to provide an equivalent amount of observations as BLE throughout the test site.

4.5.3 Results

For every reference point the RSSI fingerprint was computed as the mean value of all relevant observations with an outlier elimination (3σ method) done in advance. The radio map was then saved for being used in the positioning phase described in Section 4.8. For visualization purposes, the RSSI for single access points was interpolated and then plotted by means of an intensity map. The techniques used are the same as described in Section 4.4.2. Two exemplary radio maps are shown in Figure 4.14 and 4.15. A RSSI value of -100 implies that no signal has been received at that point.

Due to the much larger test area compared to the investigations in Section 4.4, the RSSI now shows expected behavior in terms of attenuation and shadowing mainly caused by walls. Though for regional sections of the test area, the measurement noise is present at roughly the same magnitude as the radio maps shown in Figure 4.8. The difference in the transmission range between WLAN and Bluetooth is clearly visible: While a WLAN access point is observable in a good portion of the test area (cf. Figure 4.15), a Bluetooth beacon only covers a small region (cf. Figure 4.14). Furthermore, for Bluetooth, the RSSI attenuation with increasing distance from the access point is not as apparent as in the case of WLAN. This is caused by the worse signal to noise ratio that decreases significantly with increasing distance.

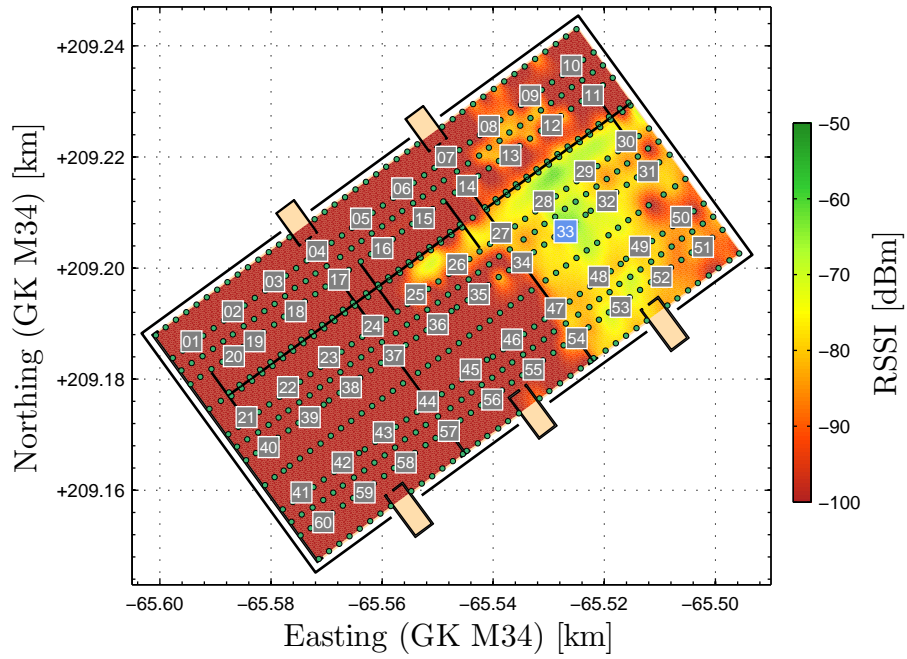


Figure 4.14: Interpolated radio map for Bluetooth access point 33

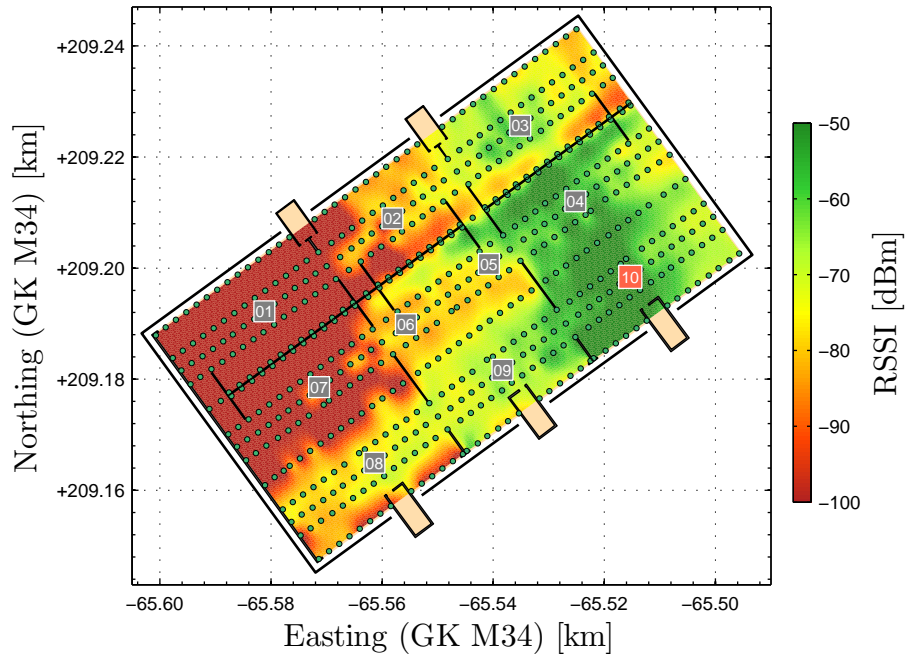


Figure 4.15: Interpolated radio map for WLAN access point 10

4.6 Measurement data processing

This section covers filtering and interpolation of the raw measurement data to obtain a smoother and more consistent signal. Due to the poor signal-to-noise ratio in the received electromagnetic waves of WLAN and Bluetooth, the RSSI shows high fluctuations. Those inconsistencies lead to less accurate positioning results. To reduce this unwanted behavior, some approaches are presented here.

4.6.1 Applying a moving average filter

Moving average filters act as a low pass filter and are therefore commonly used for noise reduction and trend estimation. The parameters of a moving average filter are the window width (i.e., how many measurements are to be considered for each epoch) and, optionally, any weighting options. The latter is used to grant measurements located towards the window's center a higher influence.

In its basic formula, the window width is expressed in terms of a number of observations that shall be considered for each epoch, reading

$$\hat{x}_{\text{MAV}}(t) = \frac{1}{2n+1} \cdot \sum_{i=-n}^{i=n} x(t+i). \quad (4.1)$$

An example for this filter is given in Figure 4.16, showing two different moving average filters (with different window width n) applied onto a noise-affected sine oscillation. It can clearly be seen that with an increasing n , the resulting time series gets smoother. Due to the filter function in (4.1), the first and the last n epochs of the original time series can not be computed.

Equation (4.1) represents a moving average function with a window width of n , resulting in $2n+1$ observations within the window. The current epoch t is centralized with respect to the window, making the filter not suitable for real time applications, since future observations are obviously not known. To overcome this, (4.1) is remodeled in a way that only data from the past is used:

$$\hat{x}_{\text{MAV}}(t) = \frac{1}{n} \cdot \sum_{i=0}^{n-1} x(t-i). \quad (4.2)$$

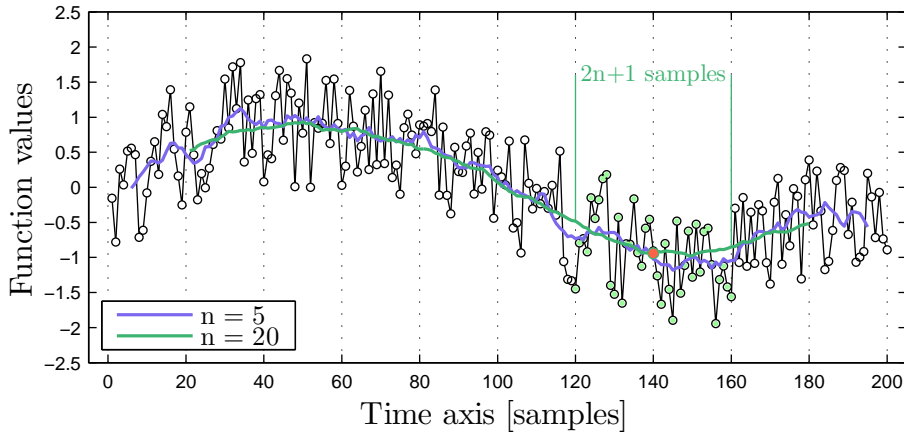


Figure 4.16: Example for two different moving average filters applied onto a noise-affected sine oscillation. The filter window for $t = 140$ (red dot) is visualized for a width of $n = 20$ ($2n + 1$ samples total).

In the case of the non-centralized filter, the total number of observations within the window is solely n , since the window is only one-sided.

In the case of a nonuniform distribution of samples, the moving average functions in (4.1) and (4.2) do not produce an optimal result, especially when the time series features larger data gaps. If that is the case, a time-based filter window shall be used: The window width is then expressed in terms of a time specification, e.g., 5 seconds, meaning that all observations that are within ± 5 seconds of t are considered for $\hat{x}(t)$. The function may be used with a centralized window or be adapted for real time applications.

4.6.2 Data interpolation

Especially for BLE, the recording interval is not perfectly constant and the observation time series often features gaps, at which the respective access point could not be recorded properly. Moreover, a scan for BLE devices doesn't retrieve all the results at once, but one after another (with a time difference of usually a few milliseconds). This aggravates the task of assigning observations to certain epochs, as needed for a kinematic positioning (otherwise, observations can not be properly assigned to certain, distinct epochs).

To overcome this unwanted behavior, the given data is interpolated at evenly distributed time points. This is realized via the filtering process described in Section 4.6.1: The time window that is responsible for selecting the relevant observations for mean computation is moved along the time series using a constant time interval. Thus, smaller gaps (where

the access point is expected to be in range but is locally obstructed by an obstacle) are being filled with the information of observations within the moving average time window. On the other hand, larger gaps will remain in the interpolated time series due to a lack of observations. However, this behavior is not unintended, as the example in Figure 4.17 suggests. Here, observations from a BLE access point representing a circuit through the Thondorf parking deck is displayed. The circuit can be seen in Figure 4.20, displayed as a thick gray line. In Figure 4.17, the time bar on top of the observations shows the period of time where the respective access point is visible proportional to the whole trajectory. The raw measurements are displayed as a thin black line, the filtered and interpolated data is represented in blue.

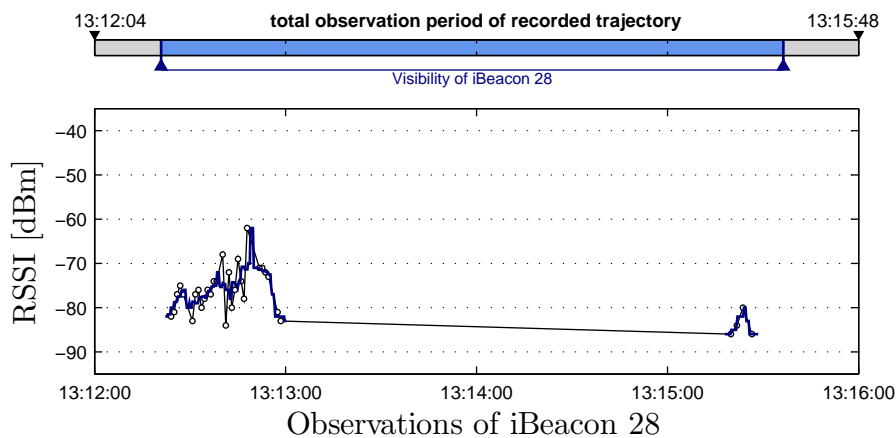


Figure 4.17: Filtered and interpolated observations (1 Hz) from BLE access point 28, showing a circuit through the Thondorf parking deck. Used filter window width is ± 2 s and interpolation interval is 0.25 s. The computed data is displayed as a blue line.

The noticeable gap between the two clusters of observations results from the layout of the circuit: In the first half, the access point (28) is passed directly; and in the second half, the access point is visible again (this time, however, it is passed at a greater distance and thus the RSSI is lower as before). In the given case, one would not want an interpolation algorithm to fill this gap, since the gap reflects the actual situation appropriately. As a result of the moving average filter, the time series is smoothed.

As for WLAN, the smoothing effect can also be clearly seen. In Figure 4.18, observations from WLAN access point 09 from the same trajectory as for the Bluetooth example are displayed. Due to the much larger coverage area of WLAN access points, data has been recorded throughout all stages of the circuit.

The short periodic oscillations, which appear along the whole time series, can be classified

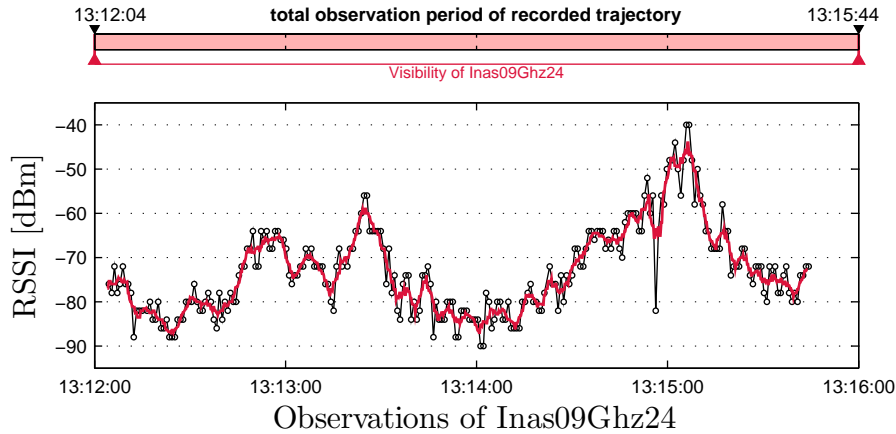


Figure 4.18: Filtered and interpolated observations from WLAN access point 09, showing a circuit through the Thondorf parking deck. Used filter window width is ± 2 s and interpolation interval is 0.25 s. The computed data is displayed as a red line.

as a signal and are caused by the numerous steel pillars that are placed throughout the parking deck. Since the fingerprints are affected by those shadowing effects as well, they should remain in the time series. However, for a lateration-based positioning, it might be reasonable to use an even stronger filtering to further cancel out higher frequencies.

4.6.3 RSSI truncation

With decreasing signal strength, a RSSI observation becomes less and less reliable due to the increasing noise. Thus, truncating measurements lower than a certain threshold increases the overall reliability of the RSSI, with the drawback of having fewer measurements available. The threshold value depends on many factors such as the used hardware or the complexity of the environment in terms of obstacles and can thus not be determined across the board. It has to be determined empirically by testing different configurations.

In Figure 4.19, the mean number of visible access points per reference point (with respect to the radio map of the Thondorf parking deck, cf. Section 4.5) is shown along the y -axis. Along the x -axis, several RSSI thresholds are displayed (e.g., a value of -80 dBm suggests that all observations with a lower signal strength than -80 dBm are omitted).

Regarding Figure 4.19, two aspects should be pointed out: First, the number of visible access points always depends on the amount and density of access points within the test area, meaning that the displayed numbers are not meaningful without knowing

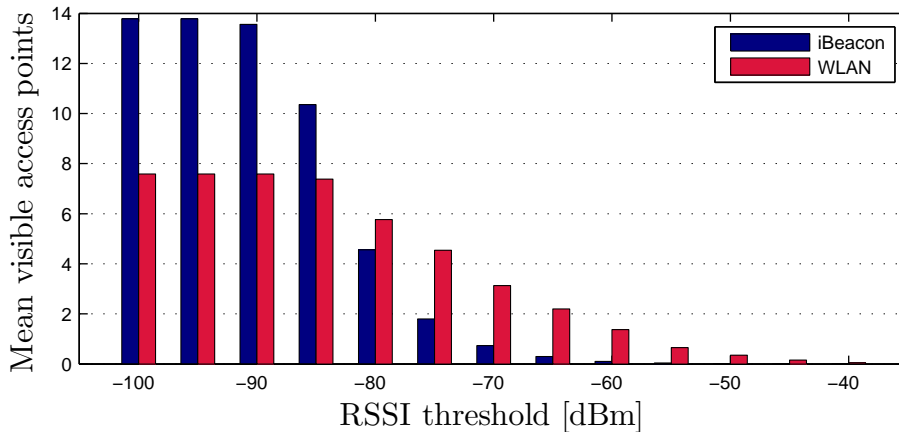


Figure 4.19: Mean number of visible access points per reference point of the radio map representing the Thondorf parking deck under the effect of various RSSI thresholds

the test area and the radio map design. Secondly, the displayed access point counts refer to the fingerprints and not a kinematic observation (e.g., a trajectory). The mean number of visible access points for the latter is, generally speaking, lower than displayed in Figure 4.19. This is caused by the fact that if observations are taken at a certain location over a period of time (as it is for the reference points), weak signals are more likely to be recorded.

For the practical investigations at the Thondorf parking deck, a RSSI threshold of -80 dBm has turned out to be most efficient for a BLE trajectory. For WLAN, a higher truncation (e.g., a threshold of -75 dBm) might be promising since the overall signal strength of WLAN is higher, as seen in Figure 4.19.

4.6.4 Impact of data processing

The impact of data post-processing as discussed in the previous sections on the resulting trajectory is shown in this section. The measured test data represents a circuit through the fifth floor of the Thondorf parking deck. In this test setup, the distance was covered by foot and the laptop (with WLAN and Bluetooth antennas) was held at chest height. In Figure 4.20, the computed trajectory using the raw measurements is shown. The starting point is in the eastern corner and the circuit has been walked counter-clockwise.

The circuit has been chosen because of several reasons. It does not only cover wide areas of the test area (including both mezzanines and both ramps), it also follows the

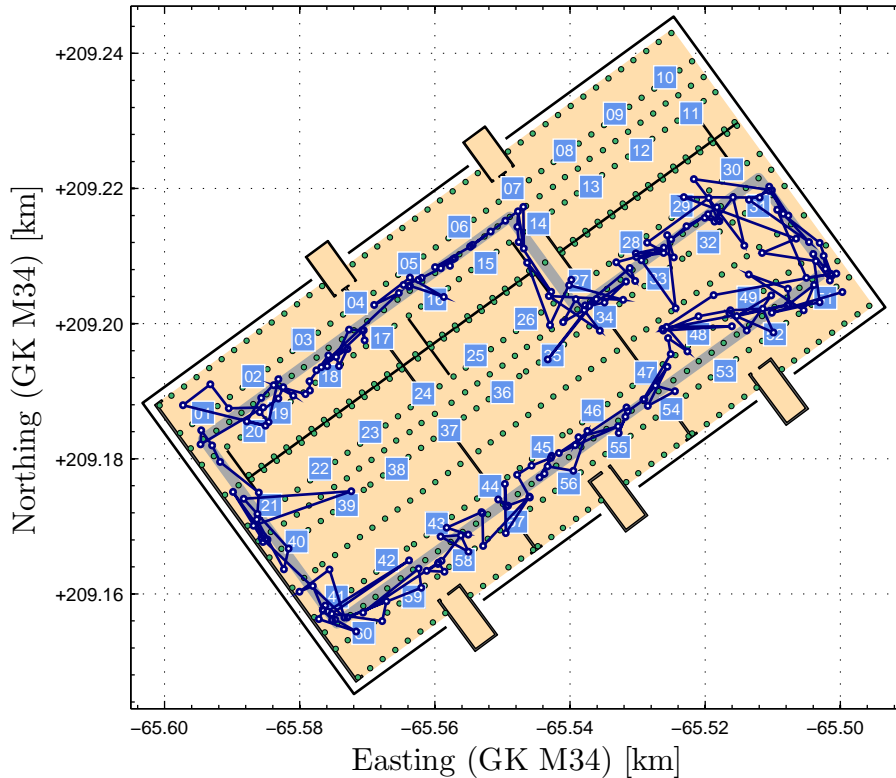


Figure 4.20: Computed trajectory resulting from fingerprinting with raw BLE measurements. Observations were taken by foot, with a sampling rate of approx. 1 Hz.

local traffic rules (one-way streets) and may thus be used for investigations involving a driving car as well. Having no stop sign or yield sign along the way allows to more or less maintain a constant velocity and hence the measurement density is expected to be roughly the same for the whole circuit.

The computed trajectory shows deviations from the reference trajectory (displayed as a thick gray line) in the magnitude of some meters, plus scattered blunders with a significantly larger deviation (both along track and across track) of up to approximately ten meters. Especially around the start/end point, the representation of the true trajectory is worse; this might be caused by the unintentional absence of the BLE access point 50, as mentioned in Section 4.5.2.

When the raw data is processed as described earlier, the resulting trajectory gets somewhat smoothed. The parameters of the post-processing applied to the measurements are listed in Table 4.4. The denoted values provided the best results compared to other configurations.

Table 4.4: Used parameters for the BLE measurement data processing

Property	Value
Window width	± 2 sec
Interpolation interval	0.25 sec
RSSI truncation	-80 dBm

The window width of ± 2 seconds provides a smoothing of the noisy RSSI time series without eliminating too much of the actual signal. Also, the RSSI truncation value of -80 dBm reduces the noise, which is significantly higher for lower RSSI. For WLAN, if enough access points are in the vicinity of the user, this threshold value could even be higher, according to the overall higher signal strength of WLAN. The result of the trajectory computed with the parameters listed above is displayed in Figure 4.21.

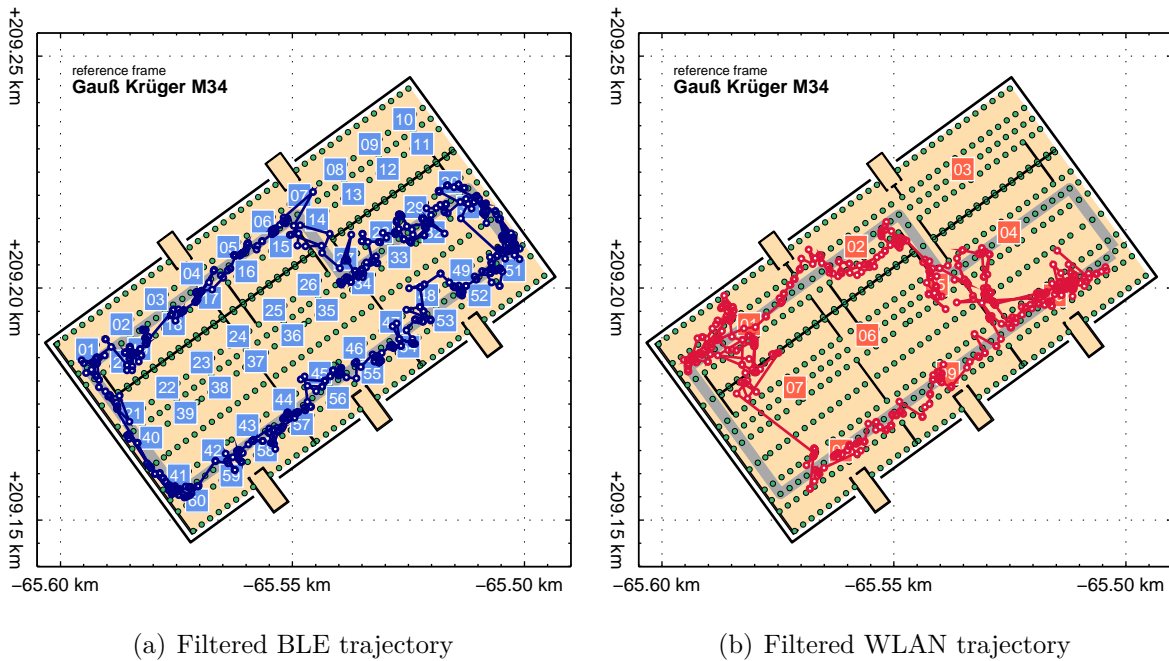


Figure 4.21: Computed trajectory resulting from fingerprinting with preprocessed BLE and WLAN measurements. Observations were taken by foot, with a sampling rate of approximately 1 Hz. The preprocessing parameters are listed in Table 4.4.

In comparison with the trajectory computed from the raw measurements (cf. Figure 4.20), the filtered BLE trajectory in Figure 4.21(a) is much smoother and the large outliers are eliminated completely. With the exception of one occurrence, the result is accurate enough to not violate the building's constraints and narrow points are passed

correctly, without intersecting walls. The WLAN trajectory in Figure 4.21(b) looks rather different. The actual circuit is reproduced poorly, especially in the Southwest and the Northeast of the building. Other filter configurations did not change this for the better. For more sophisticated readings on the accuracy of the result, the reader is referred to Chapter 5.

The reason for the low performance of WLAN is found in its high spatial availability: According to Figure 4.19, an average of eight access points are visible throughout the parking deck, that means, their signals are highly impaired by the complex environment of the test site. Bluetooth features a much shorter range and is thus not as badly influenced as WLAN. Consequently, a BLE-based radio map demands a higher amount of access points (in the given test site, the number of BLE access points is six times higher).

Remark. The example accentuates the need for suitable data preprocessing. At least for BLE, the reference trajectory is better reproduced with the filtered data and large blunders are eliminated effectively. Even if different filter configurations were used to enhance the WLAN results, they were not as accurate as the BLE trajectory. It turns out that the greater range is a problem in complex environments, because the signal is affected by more obstacles. While the filtering performed in the example is not capable of real time positioning, small changes to the filter window and the data interpolation will grant this feature. The real time capability is mandatory for applications like an automated parking pilot but is not of prior interest within this thesis.

4.7 Combination of BLE and WLAN

In this section, a combination of WLAN and BLE is shown. Thus far, trajectories obtained from WLAN measurements featured a very low accuracy compared to the BLE results. The question arises whether or not the accuracy of the trajectory can be improved by those additional measurements, regardless of their poor performance, as previously seen in Figure 4.21(b). The individual data sets introduced in Section 4.6.4 are combined by merging the two data files into one single file. This ultimately results in more access points and in less epochs with only a few or no observations at all. The combined raw data is then again filtered and interpolated by means of Table 4.4. The computed trajectory can be seen in Figure 4.22.

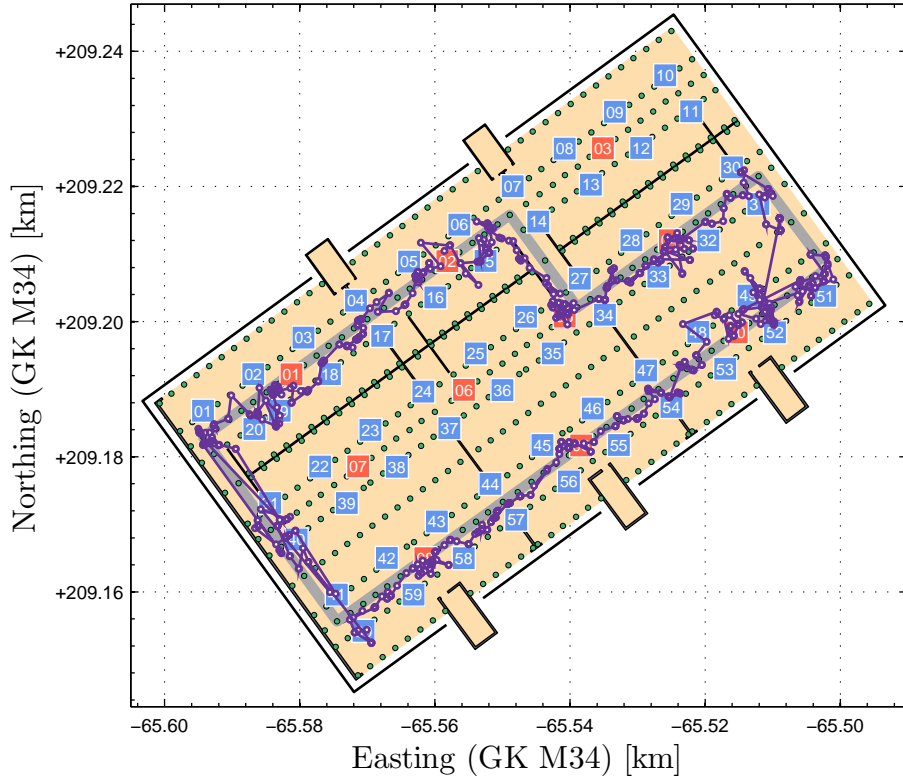


Figure 4.22: Trajectory obtained from combination of WLAN and BLE measurements

The gain of the combined radio map in terms of observations is shown in Table 4.5. Note that for practical reasons, interpolation is needed to obtain discrete epochs. The different number of epochs results from slightly different start and end times of the measurement process. Due to data preprocessing, none of the two trajectories contains epochs without any measurements.

Table 4.5: Comparison between data sets containing either BLE, WLAN or a combination of both. The displayed values refer to the interpolated data set by means of Table 4.4, but without any truncation threshold – Example 1 (by foot).

	Example 1	BLE	WLAN	Combination
mean visible access points		10.3	9.4	19.6
number of epochs		893	881	897
epochs with < 8 obs.		230	67	7
epochs with ≥ 8 obs.		663	814	890
epochs without data		0	0	0

Although the number of measurements did increase by a reasonable amount, the accuracy of the result does not improve at a comparable ratio. While the trajectory got smoother in some areas, other parts still suffer from big jumps or even got worse than the BLE-only solution. The issue is that WLAN produces a highly inaccurate result and is not able to compensate this with additional observations. However, in scenarios where only a limited amount of BLE measurements are available, the combination of BLE and WLAN might be beneficial. Such an example is shown in Table 4.6, where the antennas were placed inside a car which results in a much higher number of epochs with < 8 observations than in the WLAN-only counterpart.

Table 4.6: Comparison between data sets containing either BLE, WLAN or a combination of both. The displayed values refer to the interpolated data set by means of Table 4.4, but without any truncation threshold – Example 2 (inside a car).

	Example 2	BLE	WLAN	Combination
mean visible access points		1.5	9.2	10.3
number of epochs		553	521	553
epochs with < 8 obs.		500	44	51
epochs with ≥ 8 obs.		0	477	502
epochs without data		53	0	0

Here, the BLE signals get largely obstructed, resulting in a mere amount of 1.5 visible access points per epoch (compared to over 10 from the previous example). WLAN however still is received in most instances and hence the 53 epochs without data vanish for the data combination. The resulting trajectories for the individual radio maps may be seen in Figure 4.23. The WLAN trajectory shows again large deviations which consequently also occur in the combined result.

4.8 Vehicle positioning in a public parking garage

In this section, the actual position determination at the Thondorf parking deck by means of fingerprinting is discussed. After successfully creating a radio map for both WLAN and BLE, several positioning test runs have been performed to properly test the capabilities of fingerprinting in a complex environment such as a crowded parking garage. The findings of the previous sections in terms of data preprocessing and signal obstruction are applied here. Due to the weak performance of WLAN, the focus is laid on results derived from BLE measurements. To meet realistic conditions, the positioning

scenarios were performed using a moving car, with the antennas being mounted centered on the front part of the roof. For comparison, several tests were performed with the antennas placed inside, i.e., at the center of the car dashboard (see also Table 4.6). This resulted in a considerably large loss of observations, with many gaps and large jumps in the computed trajectory. The filtered result can be seen in Figure 4.23. Note that even though the data is interpolated at 0.25 seconds according to Table 4.4, the gaps persist due to an insufficient window width of the filter.

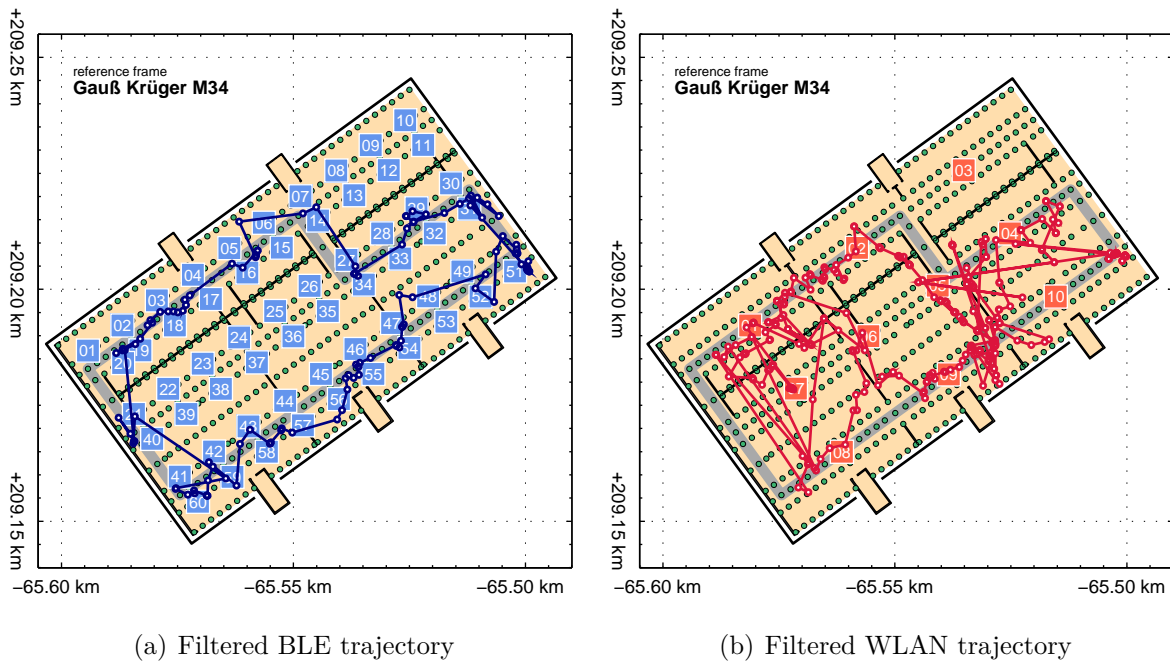


Figure 4.23: Computed trajectory resulting from fingerprinting with preprocessed BLE and WLAN measurements. Observations were taken inside a car, with a sampling rate of approximately 1 Hz. The preprocessing parameters are listed in Table 4.4.

It is obvious that none of the results shown in Figure 4.23 are close to being reliable for autonomous driving. When comparing the results with those shown in Figure 4.21 (where the antennas were exposed while walking), it becomes clear that the car itself causes drastic signal corruption. To overcome this issue, the antennas were mounted on the roof of the car for the upcoming investigations. This has been realized using USB extension cables, so that the laptop may remain inside the car. Additionally, the BLE access points were configured in a way that they emit their beacon signal at a rate of 10 Hz. WLAN on the other hand could not be measured at higher rates than 1 Hz; the limiting factor is the used laptop and the used network adapter. In Figure 4.24, the resulting trajectories are shown.

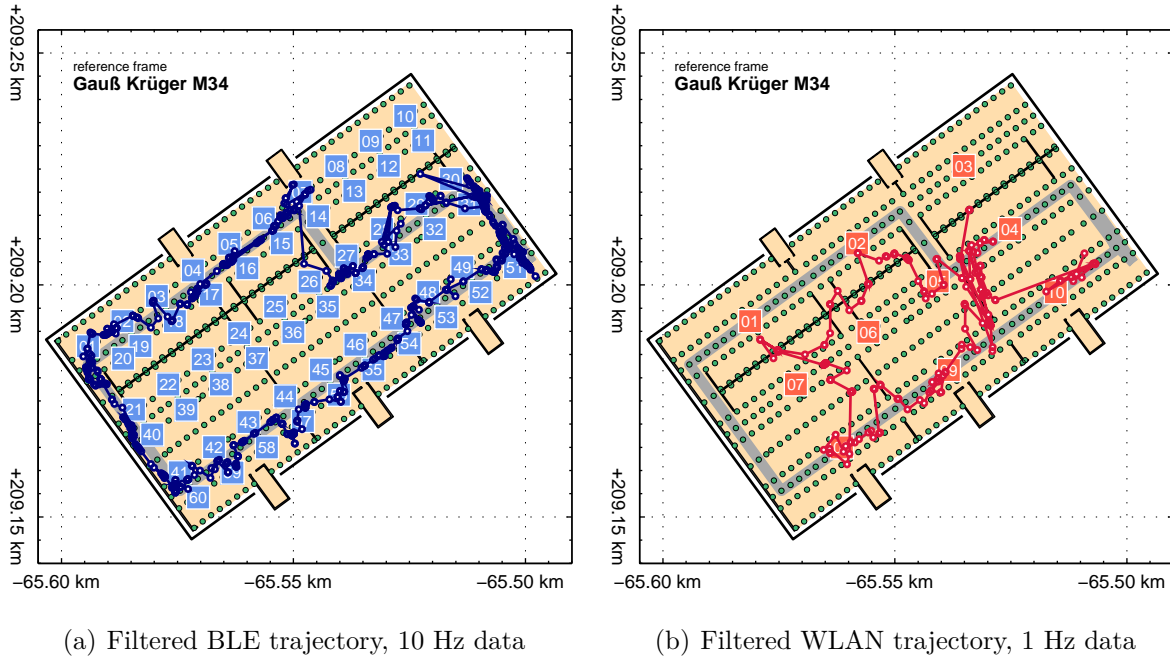


Figure 4.24: Computed trajectory resulting from fingerprinting with preprocessed BLE and WLAN measurements. The antennas were mounted onto the vehicle’s roof. Besides the parameters in Table 4.4, an interpolation interval of 0.1 sec has been used.

The overall quality of the result is comparable to the result shown in Figure 4.21. Due to the weak performance of WLAN, the combination of the two radio maps did not increase the accuracy of the BLE-only solution. Also, using different filter parameters did not change that. Due to the overall high observation count, the necessity of a combined radio map does not emerge. This is illustrated by means of Figure 4.25, where the amount of individual visible access points over the observation period is shown.

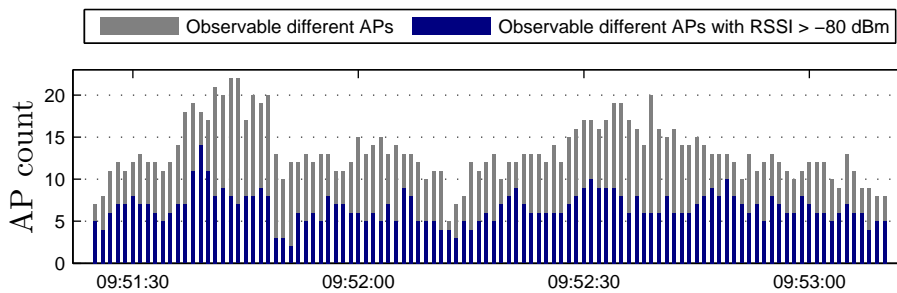


Figure 4.25: Count of different BLE access points throughout the test circuit with roof mounted antennas

An average of 13.3 different access points (6.6 with an RSSI ≥ -80 dBm) is observed each second. After interpolation at 0.1 seconds, this translates to an average of 17.6 visible access points per epoch. Compared with the numbers in Table 4.5, the increment occurs due to the higher sampling interval: For a moving receiver, some distant access point might not be recorded at lower sampling rates. Additionally, the antenna positioning (car roof vs. chest height) is beneficial for the reception, since the antennas are more likely to be in LOS with the access points due to their higher placement.

4.9 Lateration

In this section, position determination using the other eligible positioning technique⁶, lateration, is discussed. In contrary to fingerprinting, no reference points are required, but one has to be aware of the coordinates of the access points. Those had been obtained by georeferencing using the digital layout plan in the same manner as for the reference points. Thus, the position accuracy is in the magnitude of a few decimeters, which can be considered sufficiently accurate to prove whether or not this technique is appropriate for indoor vehicle positioning. Since both fingerprinting and lateration rely on the RSSI as the measured quantity, the exact same raw data that has been recorded for the fingerprinting investigations is used here.

The section is now subdivided into two parts, whereas in the first part, results of lateration performed in a simple and small environment are presented. In the second part, results obtained in the Thondorf parking garage are shown and discussed. As mentioned in Section 3.4.3, from the measured RSSI, metrical distances to the received access points are computed using the path loss model in (3.16). The used parameters can be found in Table 4.7.

Table 4.7: Used parameters for the rearranged path loss model used to obtain distance estimations from RSSI between receiver and access points

Symbol	Description	Value
d_0	Reference distance	5 m
n	Attenuation coefficient	2
PL_{d_0}	Path loss at d_0	-42.859 dBm (WLAN) -80.475 dBm (BLE)

⁶As postulated in Section 3.3, only fingerprinting and lateration are valid positioning methods for RSSI obtained by WLAN or Bluetooth using ordinary antennas.

The values for PL_{d_0} have been empirically determined within the investigations presented in Section 4.3 and correspond to the data in Figure 4.5 and Figure 4.6, respectively.

4.9.1 Lateration in A111 lecture room

As an initial test, lateration has been performed in the A111 lecture room at Graz University of Technology (the associated layout plan is shown in Figure 4.7). With data from six nearby WLAN access points, a static position has been computed for 60 seconds with a sampling rate of approximately 1 Hz. In Figure 4.26, results from two positioning tests are shown. The equivalent results for a fingerprinting-based positioning may be seen in Figure 4.9 for comparison.

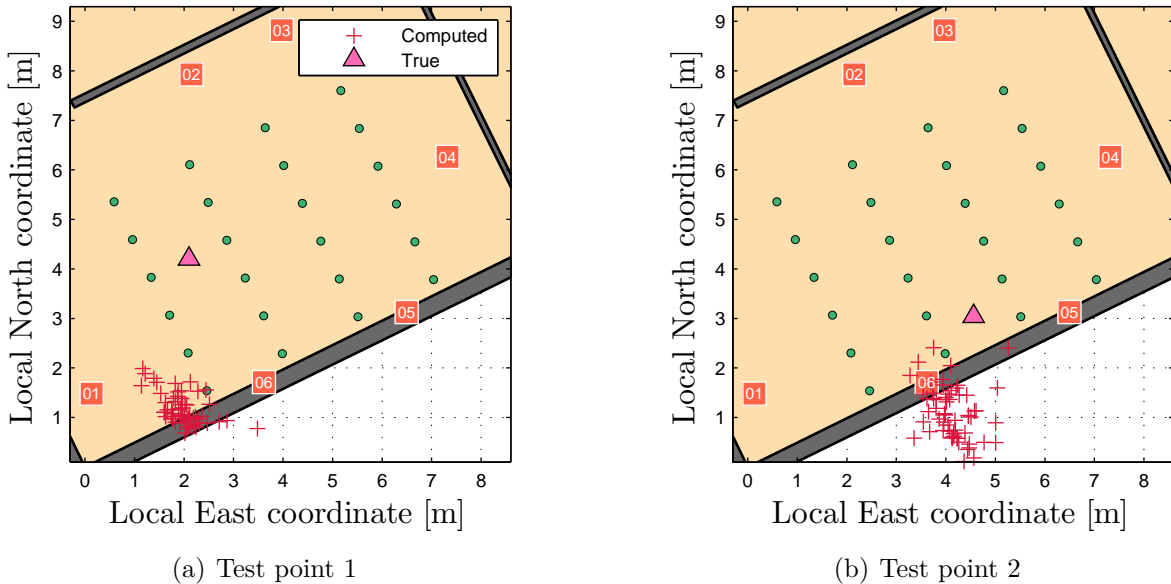


Figure 4.26: WLAN-based lateration in the A111 lecture room, using the EDiMAX dongle. The access points are shown as orange squares, the green circles represent the fingerprinting reference points and do not serve a purpose here.

When looking at the individual computed positions, one easily notices an offset of the cluster of position fixes from the true position, which is present for both test points. This is caused by the access points 2 and 3, which are placed on top of a high cabinet close to the ceiling and thus provide a significantly lower signal strength in the test area compared to the other access points. Hence, the estimated distance is much larger than it

actually is (since lower RSSI implies larger distance) and this ultimately causes an offset away from aforementioned access points. The result could theoretically be improved by dismissing observations from access points where the overall signal strength is diminished by obstacles and is thus not in line with the RSSI from other access points at a similar distance.

4.9.2 Lateration in Thondorf parking garage

In addition to the fingerprinting-based positioning performed in the Thondorf parking garage, a simple lateration was conducted as well. The positions are computed from the same data that was also used for fingerprinting. As an example, the circuit through the parking deck (by foot) is shown here (cf. Figure 4.27). For most parts of the circuit, the trajectory is poorly represented, and big jumps in the computed position occur frequently between consecutive epochs.

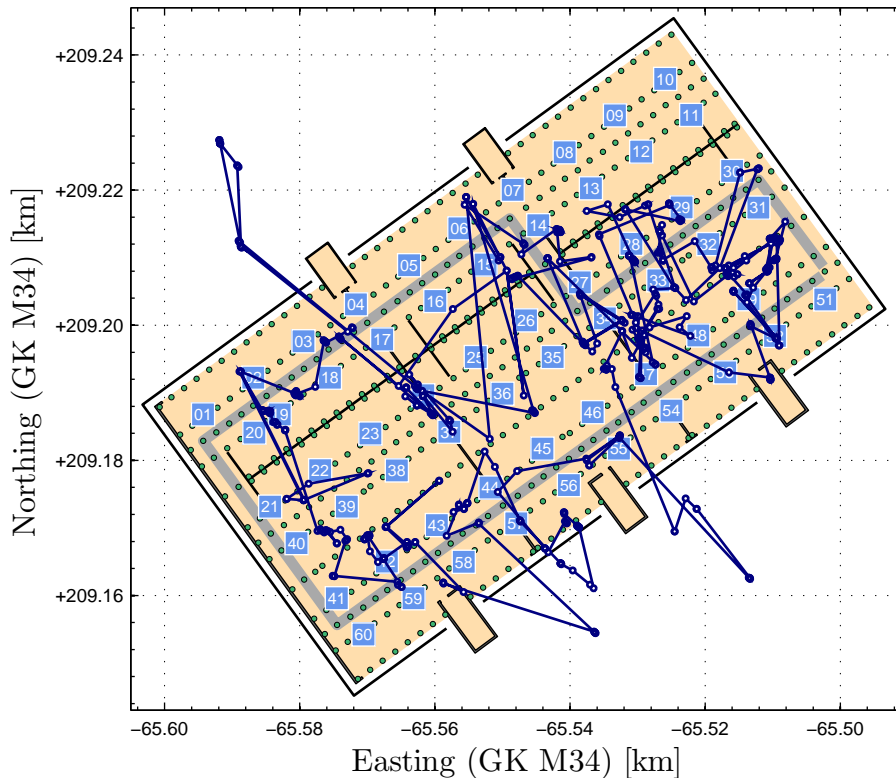


Figure 4.27: Lateration results using BLE data (filtered with a 2 s window, interpolated at 0.25 s and truncated at -85 dBm). The displayed trajectory is a circuit through the parking deck by foot.

It shall be noted that even with different filter parameters or truncation values, the result could not be improved. A major issue for the poor performance of lateration is the complex environment with concrete, metal and glass. As seen in Figure 4.12, the RSSI depends on the placement of the access point on the steel girder. While this is not a serious problem for fingerprinting, the computed spatial distance greatly suffers from it. Lateration is therefore not further considered.

4.10 Time synchronization between different measurement systems

This section deals with the problem of asynchronous clocks of different measurement systems. Whenever time-dependent quantities of different measurement systems shall be compared, the clocks of these systems have to be synchronized. In this thesis, synchronized observation times are required for comparing the fingerprinting result with a reference trajectory obtained by a Leica MS50 tachymeter, tracking a 360° reflector mounted on the car. Each group of observations (i.e., RSSI and tachymeter readings) is recorded by a separate laptop and, thus, relies on a different internal clock. Two important aspects arise in the context of asynchronous clocks:

- The clocks are separated by an offset. Depending on the magnitude of the offset and the targeted accuracy, the time difference needs to be taken into account.
- This offset is not constant over time, meaning that one clock runs faster than the other. Furthermore, the rate at which the offset grows or shrinks is not necessarily a linear process.

The ideal solution to overcome this problem is to use a third, common clock for both measurement systems. This is often realized using GPS, which is not only a positioning system, but also a timekeeping tool. GPS clocks are highly stable, with an error of about one nanosecond per day [23]. For receiving the GPS time, only one satellite has to be visible after an initial position fix with at least four satellites, and signal obstructions and multipath do not influence the readouts. Nevertheless, in situations where no GPS is available at all, the synchronization has to be accomplished in a different way. One possible empirical method is to compare distinctive, simultaneously taken measurements of both systems and then compare their recorded observation times. This requires a suitable test setup to easily distinguish the experiment from other data. Figure 4.28 shows such an example: A trackable reflector and a BLE antenna are both moved

relative to an emitting BLE access point. A horizontal movement, that approaches the access point and then moves further away again, creates a noticeable peak in both observed signal domains. The observation times of the two peaks are then compared to compute the time offset of the two clocks.

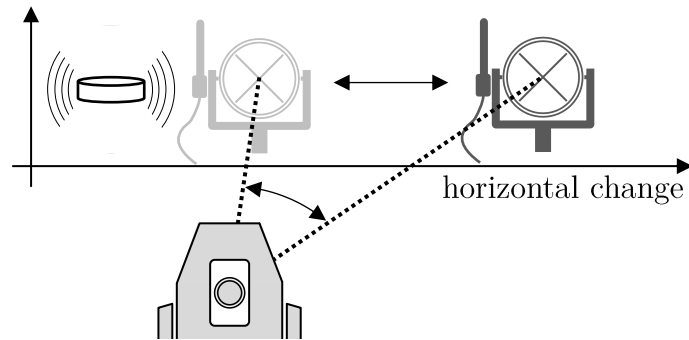


Figure 4.28: Test setup for time synchronization using distinctive observations in both signal domains

BLE has been favored over WLAN because of the higher sampling rate (up to 10 Hz versus 1 Hz for WLAN) and the faster degrading signal strength, resulting in a easier detectable maximum. The used tachymeter supports automatic tracking at a rate of approximately 3 to 8 Hz. The two signal sequences and their determined time offset Δt can be seen in Figure 4.29.

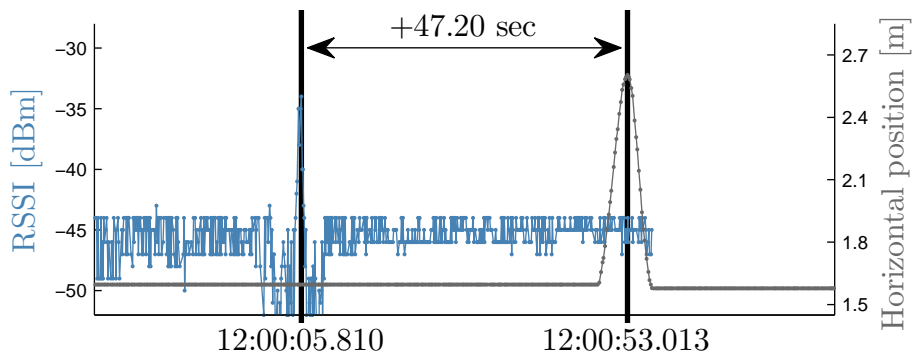


Figure 4.29: Results for time synchronization setup using distinctive observations in both signal domains

If the time offset between the two clocks is not constant, additional measurements have to be performed. For a linear change, the experiment is repeated immediately before and after the positioning tests. If the change is non-linear, time synchronization in between

the individual positioning tests might be essential. However, the required effort of time synchronization always depends on the magnitude of the offset, its change over time, and the targeted accuracy. For the sake of convenience, the horizontal movement of the reflector and the antenna may be induced by the car, so that they do not have to be dismantled in between positioning tests.

The foundation for a successful time synchronization is the stability of each individual clock with respect to an accurate reference time. Here, GPS proves useful. By recording the GPS time with a u-blox 6 GPS engine and a small ANN-MS-0-005 GPS antenna, the laptop's time stability has been evaluated. The result for the Lenovo Z580 laptop is shown in Figure 4.30. The time offset (plotted on the y -axis) has been observed over approximately four hours.

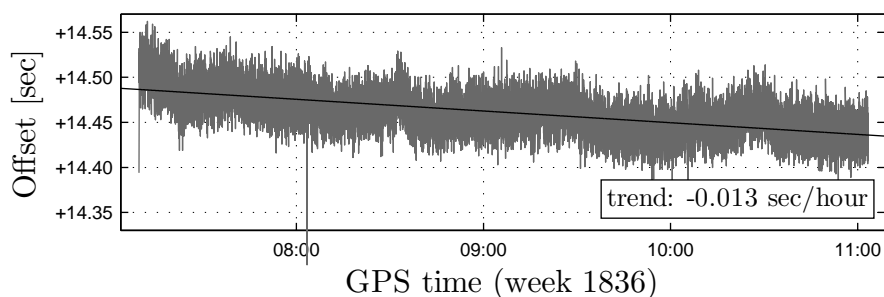


Figure 4.30: Time offset of the Lenovo Z580 relative to the GPS time

The figure shows that over the observation time, the laptop's clock is approximately 14.5 seconds ahead of the GPS time over the observation period. The offset changes at an estimated rate of -0.013 seconds per hour, implying that the laptop's clock runs slightly slower. Thus, for the investigations in this thesis the offset and hence the internal clock of the Lenovo Z580 can be treated as constant. The source of the outliers seen in Figure 4.30 is unclear and is probably due to rounding errors. Concerning their sparse occurrence, their treatment has been considered negligible.

The situation is quite different for the laptop that was used to process the data from the Leica tachymeter, an Asus Eee PC similar to the model mentioned in Table 4.1. Presumably caused by the limited performance, the internal clock shows large drifts with respect to the GPS time. As seen in Figure 4.31, the drift follows a periodic behavior. Due to a yet unclear reason, the system time seems to be corrected after reaching a too large offset (according to the graph, this threshold lies somewhere between four and five minutes). Time synchronization over the internet had been turned off, so it is assumed that Matlab (which is used to run the script) does some time corrections on its own.

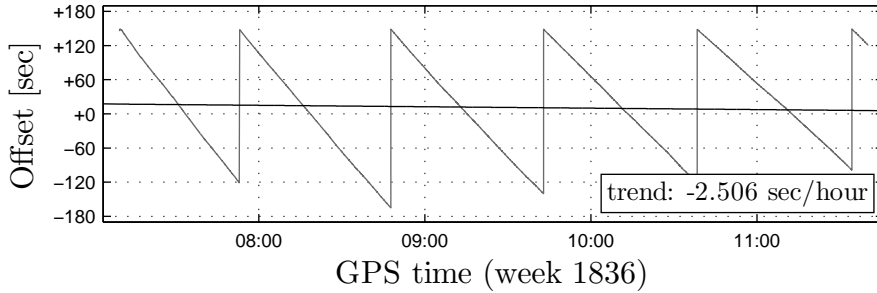


Figure 4.31: Time offset of the Asus Eee PC relative to the GPS time

Obviously, the recorded system time of the Asus netbook can not be used for synchronized time series due to its non-linear behavior. To overcome this issue, a fourth time system is introduced: The system time of the Leica MS50 tachymeter. Despite the fact that it does not provide absolute points in time but rather the elapsed time since the last switching on, the clock is nevertheless as stable as the previously investigated Lenovo laptop. Hence the epochs at which tachymetric observations are taken can be corrected by the reciprocative time offset⁷ between the Asus netbook and the MS50. Using this technique, the time offset between the two laptops can now be treated as constant within the scope of the achievable measurement rate and the total observation time. This is documented in Table 4.8, where multiple time synchronization experiments have been performed over the duration of approximately four hours.

Table 4.8: Comparison of the time offsets Δt between the two laptops computed from multiple time synchronization experiments. The third column is computed from corrected tachymeter observation epochs (considering the Leica MS50’s system time).

Test	Δt_{uncorr} [sec]	Δt_{corr} [sec]
1	52.77	47.41
2	76.21	47.39
3	89.86	47.43
4	92.16	48.42
5	102.19	47.50
6	130.22	47.20
7	142.48	47.43
8	150.95	47.19

⁷The offset is computed by subtracting the first epoch of the tachymeter clock from all successive epochs recorded with the tachymeter clock. Thus, the correction for the first epoch is 0.

The offset Δt_{corr} for the fourth test is noticeable and differs from the other results by a significant number. By looking at the respective RSSI observations, no distinct peak has been recorded in the signal strength domain and hence this test is neglected. The remaining valid time offsets add up to a mean of $\bar{\Delta t}_{\text{corr}} = 47.37$ seconds with a standard deviation of $\sigma = \pm 0.12$ seconds. Keeping in mind the sampling rates of the two measurement devices, the offset can be seen as constant over the observed period of time.

After applying this offset to the recorded tachymeter observations, the measurements are now given in the same time frame. Since both systems take observations at different, irregular intervals, interpolation at common epochs is required to compare computed positions. In the case of the signal strength measurements, this is done within the process of data filtering (cf. Section 4.6). Consequently, the positions computed by the tachymetric observations are then interpolated at the same epochs. Thereafter, deviations between the position fixes of the two observation groups may be computed by means of the explanations in Section 4.11.

4.11 Comparison with a reference solution

After the position fixes of both the fingerprinting and the tachymeter reference are synchronized, deviations between the two solutions may be computed. Given the reference coordinates $x_{\text{ref}}(t), y_{\text{ref}}(t)$ for each epoch t , the deviations $\Delta x, \Delta y$ along the coordinate axes may be computed by

$$\begin{aligned}\Delta x(t) &= x_{\text{ref}}(t) - x(t), \\ \Delta y(t) &= y_{\text{ref}}(t) - y(t).\end{aligned}\tag{4.3}$$

In order to do so, the two position fixes must also refer to the same point. Initially, this was not the case: With the intention to avoid further signal obstructions by the reflector, the reflector r and the two antennas a were not mounted in the same place, but roughly $d = 1.3$ m apart along one of the car's roof rails. Thus, the measured reference trajectory had to be corrected by that offset. The offset refers to the car's local coordinate system (*body system*), but the computed position refers to the Gauß-Krüger coordinate system. Apart from the origin, the two systems differ in a rotation around the e_3 axis, which is the heading of the vehicle. The relationship between the two coordinate systems along with the placement of reflector (r) and the antennas (a) can be seen in Figure 4.32.

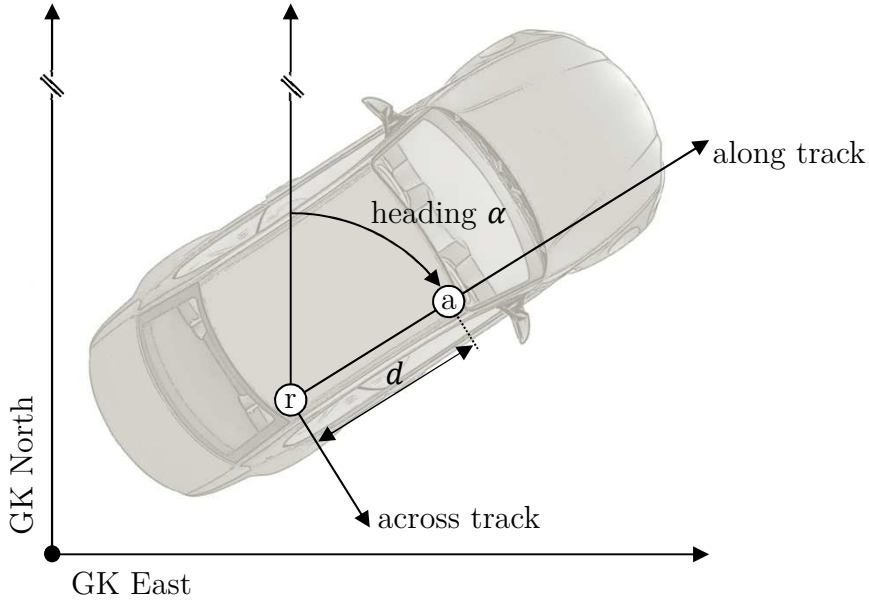


Figure 4.32: Relationship between the geodetic coordinate system and the car system

To compute the heading $\alpha(t)$, one simply computes the angle between the two adjacent positions $P_{\text{ref}}(t)$ and $P_{\text{ref}}(t+1)$:

$$\alpha(t) = \arctan \frac{y_{\text{ref}}(t+1) - y_{\text{ref}}(t)}{x_{\text{ref}}(t+1) - x_{\text{ref}}(t)}. \quad (4.4)$$

To reduce the impact of errors and measurement noise, $P(t+5)$ rather than $P(t+1)$ is used. This increases the distance between the two points and hence the impact of erroneous positions diminishes. Additionally, if the slant distance between the two points is below 3σ (and thus the vehicle is classified as not moving), the heading from the previous epoch is used:

$$\alpha(t) = \alpha(t-1). \quad (4.5)$$

This constraint is necessary because for a stationary position, the computed heading is expected to be normally distributed in the range of $0^\circ \leq \alpha \leq 360^\circ$. The computed heading is then simply linearly interpolated at each epoch, yielding an α for each epoch in the reference trajectory.

With the heading obtained, the reflector offset can be corrected. Since both reflector and the antennas are mounted at the car's roof rails, the displacement occurs (within the

accuracy of some centimeters) only in the along track component. Hence, the correction reads

$$\begin{aligned} y_{\text{corr}}(t) &= y_{\text{ref}}(t) + d \cdot \sin \alpha(t), \\ x_{\text{corr}}(t) &= x_{\text{ref}}(t) + d \cdot \cos \alpha(t) \end{aligned} \tag{4.6}$$

with d being the distance between the reflector and the antennas.

Now (4.3) can be computed with the corrected values. Since the deviations along the coordinate axes are only partially meaningful (because the heading does not follow one of the coordinate axes in general), the deviations are rather combined to a single value Δp . This Point Position Error (PPE) is simply computed by

$$\Delta p(t) = \sqrt{\Delta x(t)^2 + \Delta y(t)^2} \tag{4.7}$$

and represents the slant distance between the computed position and the reference solution. Visual representations in the form of time series of these PPEs are shown throughout Chapter 5.

Remark. Although the accuracy of the MS50 tachymeter is in the magnitude of a few millimeters [11] and hence insignificant, the computed differences Δp must not be treated as completely error-free due to the uncertainty in the time synchronization. Given an empirically found mean tachymeter sampling rate of approximately 0.2 seconds, the synchronization is in the worst case only accurate up to half of that number. Assuming a speed of approximately 10 km/h, an uncertainty of 0.1 seconds adds up to a potential error of some decimeters. This error is inevitable with the used infrastructure and techniques, but it affects each Δp in a consistent manner. The static measurements do not rely on time synchronization, hence their Δp 's can be assumed to be error-free (except from the tachymeter's measurement error). For kinematic Δp 's, the uncertainty is present, however the results are still meaningful since the mean PPE lies in order of some meters, rendering the synchronization error much less significant. Another error accrues as a result of the offset between the reflector and the antennas, however its impact is much smaller than the error caused by the time synchronization.

Chapter 5

Results

This chapter summarizes the findings of the measurements documented in Chapter 4 and presents the final results of this Master’s thesis. Therefore, the position fixes derived from fingerprinting using WLAN and BLE are compared with equivalent reference positions of superior accuracy. Those have been obtained by tracking the test vehicle with a Leica MS50 tachymeter featuring an angle measurement accuracy of 0.3 mgon and a distance measurement accuracy of 1 mm + 1.5 ppm [11]. Compared to the achievable accuracy of the fingerprinting, the reference can therefore be considered as *exact*. In a number of both static and kinematic tests, the accuracy of the fingerprinting is evaluated by means of Section 4.11. To complete the thesis, a conclusion and an outlook is presented in Section 5.3.

Throughout this chapter, consistent data filtering parameters have been used. They were empirically adapted for both BLE and WLAN and are listed in Table 5.1. The raw data is recorded at a rate of approximately 10 Hz for BLE and at a rate of approximately 1 Hz in the case of WLAN.

Table 5.1: Used parameters for the final measurement data processing

Property	BLE	WLAN
Filter window width	± 2 sec	± 2 sec
Interpolation interval	0.25 sec	0.25 sec
RSSI truncation	-85 dBm	-75 dBm

To preserve the impact of the data preprocessing for each observation type, the filtered observation groups were merged for the combined evaluation of BLE and WLAN rather than the raw data.

5.1 Static positioning

In this section, the results of static positioning experiments are presented. In a series of test runs on different locations the accuracy of the position fixes and their variance is determined. The test points have been distributed across the visible areas of the parking deck¹ in a way that the results represent different areas with a varying access point visibility.

The results are listed in Table 5.2. While the results are grouped by observation type, the number (#) represents the test point on which WLAN and BLE have been measured simultaneously (cf. Figure 5.1). The table shows the mean PPE of the various test runs as well as additional statistical parameters describing the results (i.e., the standard deviation σ , the percentage of position fixes better than the mean PPE and the maximum PPE). The observation time was three minutes for each test point. With an interpolation interval of 0.25 seconds applied, this yields a maximum of 720 position fixes per observation type.

Table 5.2: Results for three static positioning tests. The Point Position Error (PPE) refers to a point position of superior accuracy.

Type	#	mean PPE	σ_{PPE}	below mean PPE	max PPE
WLAN	1	9.9 m	± 0.9 m	83.9 %	14.4 m
	2	9.1 m	± 1.4 m	43.1 %	12.8 m
	3	11.9 m	± 2.8 m	42.0 %	16.3 m
BLE	1	6.7 m	± 1.1 m	33.8 %	17.4 m
	2	3.9 m	± 0.2 m	95.0 %	5.3 m
	3	2.8 m	± 0.6 m	77.8 %	8.3 m
Combination	1	6.3 m	± 1.2 m	83.5 %	17.4 m
	2	4.0 m	± 0.5 m	73.9 %	12.3 m
	3	2.7 m	± 0.9 m	22.9 %	13.9 m

The table illustrates the different accuracy capabilities of WLAN and BLE. While WLAN yields a mean PPE of 9 – 12 m, the BLE solution is capable of a mean PPE better than 3 m. This is achieved at test point 3, however the cause of the difference in accuracy is unclear. By reason of the significant difference in accuracy, the combined evaluation does not improve the BLE-only solution.

¹The tachymeter has been positioned in the South corner, thus only a fraction of the parking deck is visible from that point. The tachymeter placement for the kinematic test runs has been the same as well.

The visual representation of the data shown in Table 5.2 can be seen in Figure 5.1. Each investigated test point is shown in a separate figure, whereas the true position is marked as a pink circle. The test point numbers correspond with those listed in Table 5.2.

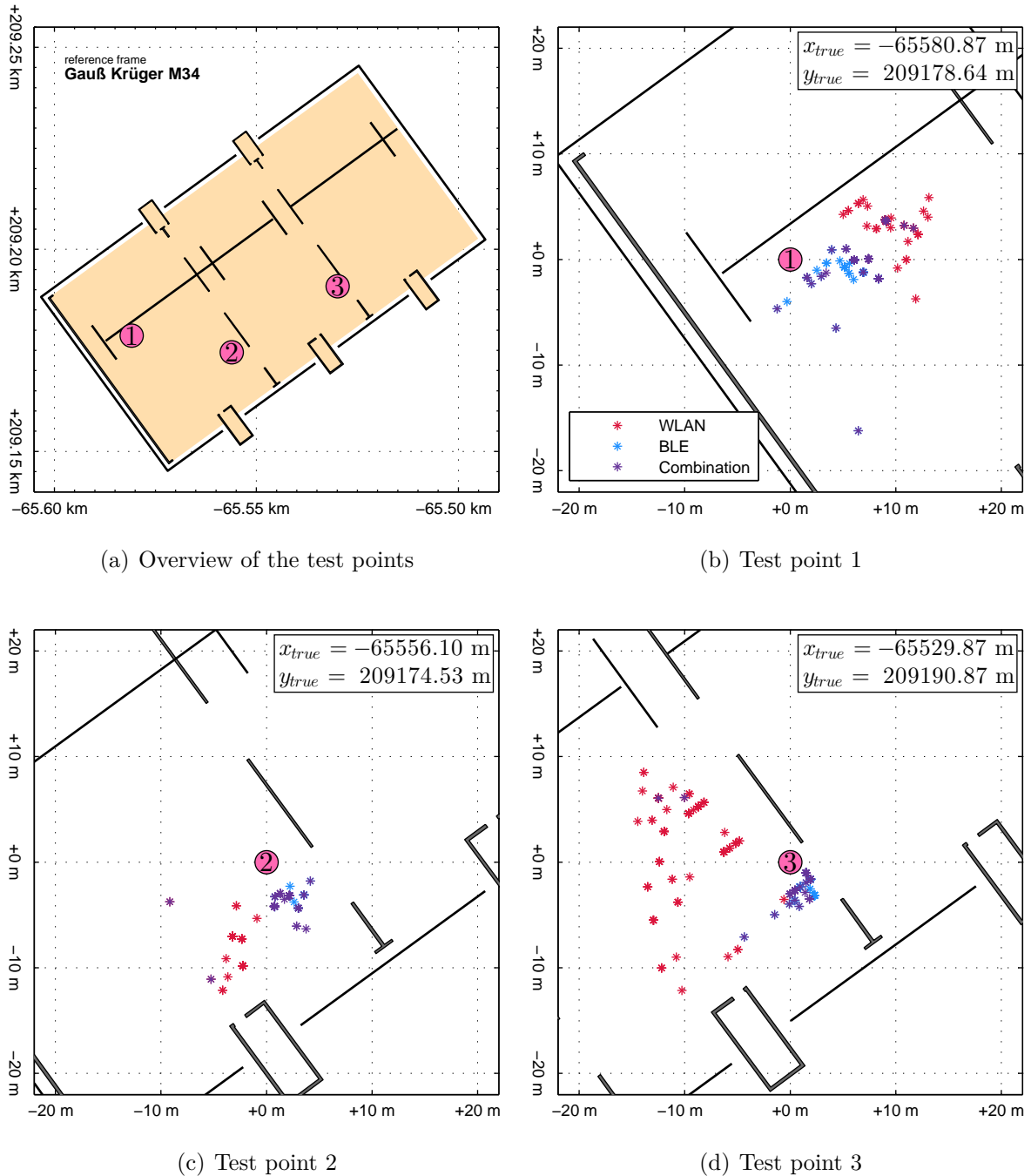


Figure 5.1: Static positioning results on three selected test points

The individual position fixes are displayed as colored asterisks. Note that due to overlapping of individual position fixes, the visible amount of position fixes may be rather small. Especially in Figure 5.1(d), the difference in both accuracy and precision of WLAN and BLE is apparent. This can also be seen in Figure 5.2, where the PPE is shown for test point 3. Both accuracy and precision of the WLAN-solution are considerably worse than the BLE counterpart.

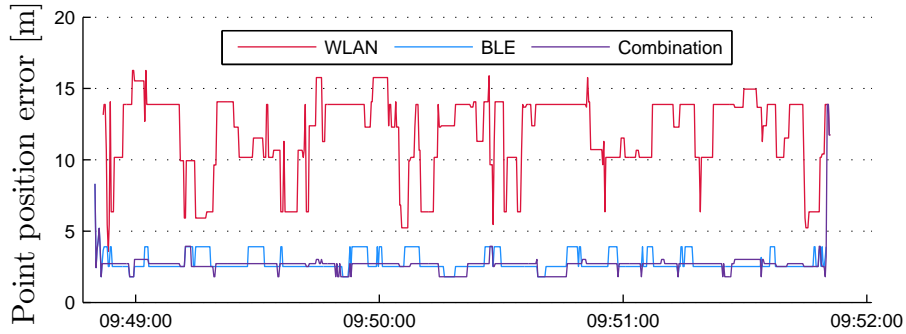


Figure 5.2: Time series of the PPE for test point 3

In all test runs, a displacement of the solution clusters from the true position is visible, which results in a decentralized distribution. The reason for this behavior is assumed to be found in the time-variability of the environment: At the time of the radio map creation, the distribution of occupied parking spaces was different than at the time of the positioning tests, yielding differently obstructed signal paths. This problem has emerged throughout the various investigations in this thesis and can not be controlled effectively.

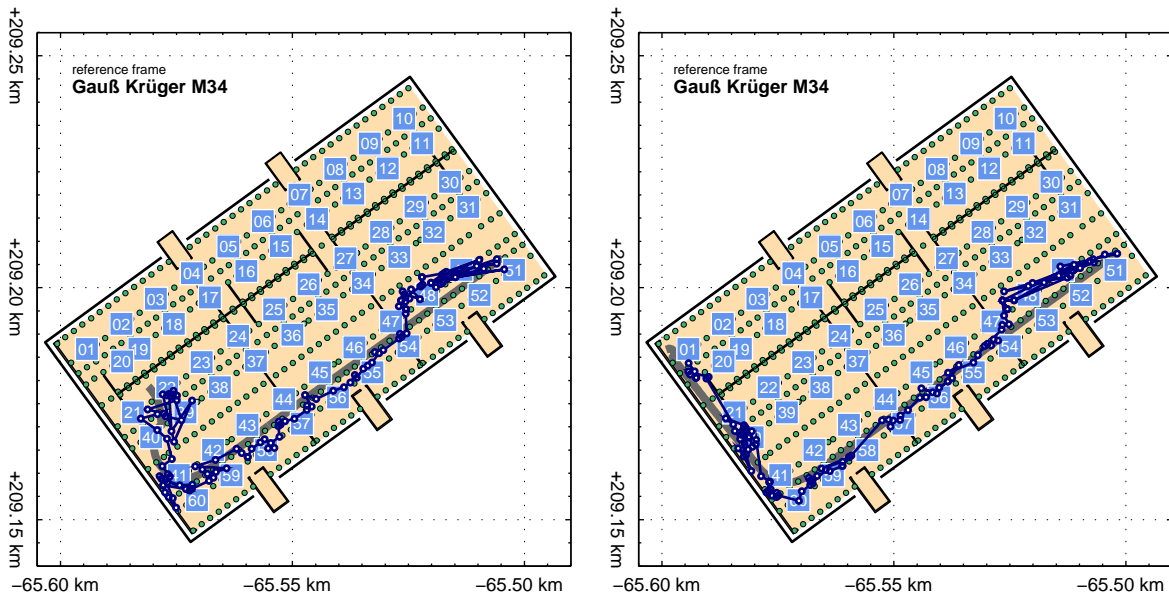
5.2 Kinematic positioning

This section covers the results of the kinematic positioning inside the Thondorf parking deck. In a number of test runs, the computed trajectories were evaluated and compared with each other. With respect to a reference solution with superior accuracy, the quality of the results is listed in Table 5.3. In total, four trajectories have been evaluated, whereas in one test run the recording of WLAN signals failed and thus no WLAN trajectory (and, consequently, no combined solution) could be evaluated. Due to the placement of the tachymeter and hence the limited amount of observable space, only two different trajectories in both directions have been investigated. Compared to the results shown in Section 5.1, the differences between WLAN and BLE are not as prominent.

Table 5.3: Results for three kinematic test runs. The Point Position Error (PPE) refers to a reference trajectory of superior accuracy.

Type	#	mean PPE	σ_{PPE}	below mean PPE	max PPE
WLAN	1	6.2 m	± 5.5 m	68.4 %	34.6 m
	2	6.9 m	± 5.9 m	63.3 %	34.6 m
	3	5.7 m	± 5.1 m	64.1 %	28.5 m
BLE	1	4.8 m	± 3.7 m	61.9 %	22.5 m
	2	4.5 m	± 3.5 m	64.8 %	14.7 m
	3	6.2 m	± 5.5 m	65.8 %	25.2 m
	4	6.3 m	± 4.9 m	61.3 %	28.7 m
Combination	1	4.1 m	± 2.9 m	63.0 %	22.5 m
	2	4.4 m	± 3.6 m	66.5 %	16.0 m
	3	5.5 m	± 4.9 m	68.4 %	26.1 m

By comparing results of different observation types it becomes clear that in the kinematic case, the combination of WLAN and BLE positively affects the result. The same can be seen in the two exemplarily visualized trajectories (2 and 3) shown in Figure 5.3 (BLE results), Figure 5.4 (WLAN results) and Figure 5.5 (combined results).



(a) Trajectory 2

(b) Trajectory 3

Figure 5.3: Kinematic positioning, exemplary BLE trajectories

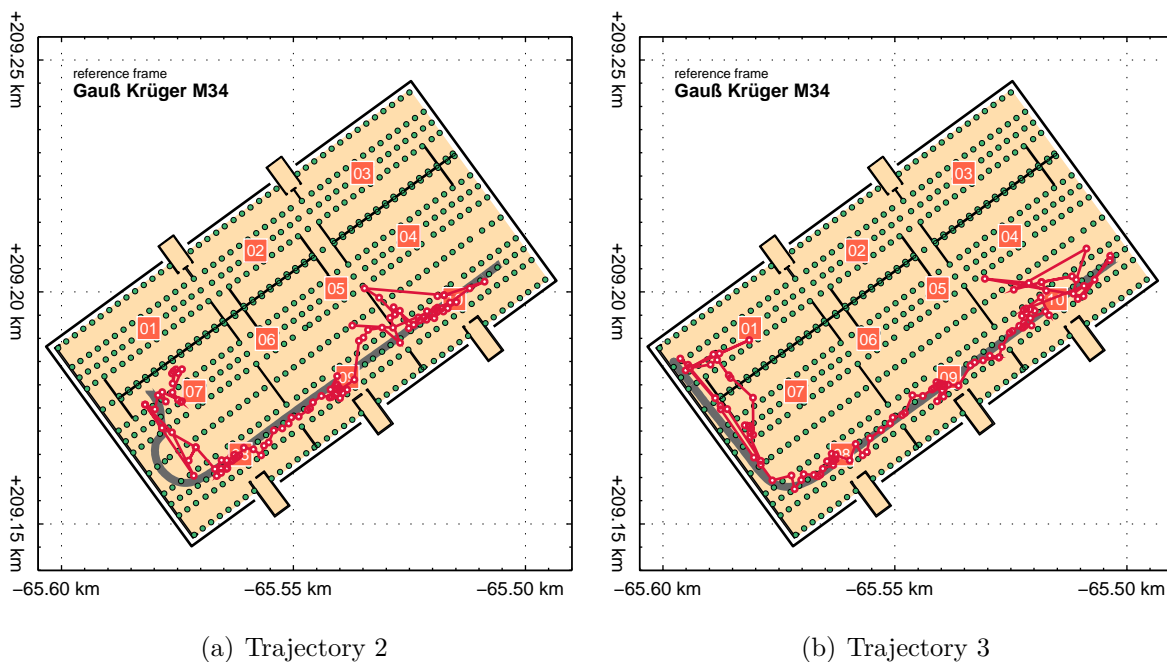


Figure 5.4: Kinematic positioning, exemplary WLAN trajectories

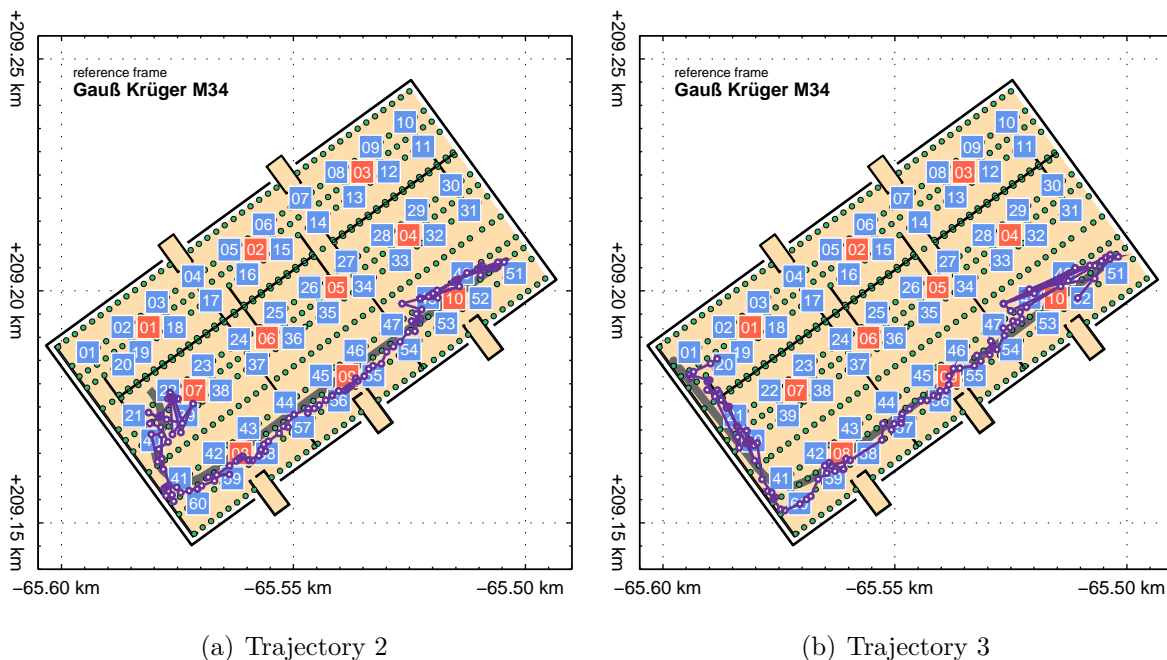


Figure 5.5: Kinematic positioning, exemplary BLE+WLAN combined trajectories

By comparison with the static test runs, it turns out that now the combination of WLAN and BLE improves the result. On the one hand, this is due to the overall better performance of WLAN than in the static case. On the other hand, the number of visible BLE access points per epoch is lower now and, hence, additional measurements are beneficial. On average, 15.17 BLE observations are available at each epoch in the static case, while only a mean of 11.09 observations is being recorded now. Looking at the displayed trajectories, different levels of accuracy in reproducing the reference trajectory become visible inside the parking deck. The location of these *good* and *bad* areas more or less remained the same throughout all investigations. Having a roughly constant access point and reference point distribution throughout the test site, this leads to the conclusion that the signal obstruction at the time of the offline phase was highly atypical and is hence hardly reproducible. This assumption is further emphasized by the fact that the pattern is similar for WLAN and BLE. The effect can be seen by looking at the time series of the PPE, exemplarily shown for trajectory 3 in Figure 5.6.

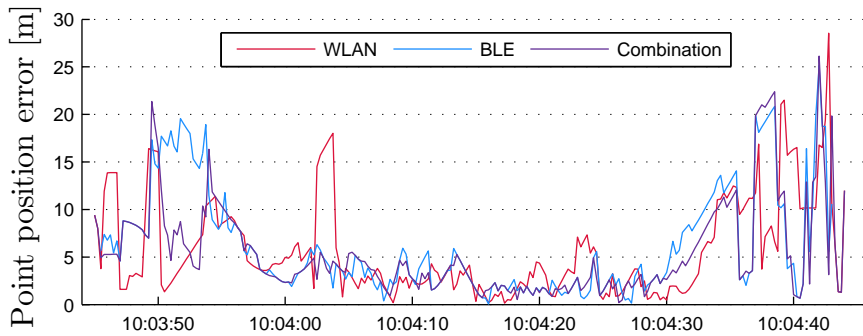


Figure 5.6: Time series of the PPE for test trajectory 3

The errors are significantly larger at the beginning and the end of the time series, while the middle part (which represents the long straight along the South side of the parking deck) is reproduced with a PPE clearly below the mean value.

Remark. For the kinematic results it has to be noted that the displayed PPE values are affected by a certain degree of uncertainty, mainly caused by the time synchronization as explained in the final paragraph of Section 4.11. However, since the error in the PPEs is of much smaller scale than the PPEs itself and since it occurs in a similar way for all computed PPEs, the results are still meaningful.

5.3 Conclusion and future work

This section briefly summarizes the findings gathered within the process of work. Since intermediary results were usually discussed aside their appearance in Chapter 4, in general, those are not mentioned here again. Rather the applicability of WLAN and Bluetooth for vehicular position determination is discussed and potential error sources are mentioned in Section 5.3.1. In Section 5.3.2 an outlook is presented, briefly introducing follow-up investigations that build on the results of this thesis and further enhancing the positioning accuracy. Additionally, strategies to improve the fingerprinting itself are mentioned.

5.3.1 Valuation of the results

The backbone of a self-driving vehicle is an accurate and reliable position determination. Combined with knowledge of the environment and other traffic participants (vehicles and pedestrians), local traffic rules, the route, and the vehicle's geometry, autonomous driving can be accomplished.

According to the expectations, the position determination solely relying on WLAN and BLE fingerprinting does not meet the requirements for safely maneuvering a car through a narrow parking garage. It is nonetheless an emerging technology and is expected to be capable of achieving a higher accuracy over the course of the future research and development. The current capabilities are in the magnitude of the GPS single point positioning some 30 years ago, which has greatly evolved since then. Caused by the complex and uncontrollable environment, the accuracy that has been achieved with fingerprinting throughout various investigations is in the magnitude of a few meters. Static positioning tests show that the precision (i.e., the variance of the sample) is high, with a standard deviation of approximately $\sigma \approx 1$ m or better for the BLE result. This suggests that the different environmental conditions between the offline and the online phase that inevitably occurs in a public parking garage has a significant impact on the position computation. Unfortunately, this is an unpredictable and uncontrollable aspect and greatly limits the capabilities of the fingerprinting-based positioning. On the other hand, though, lateration-based positioning is completely unfeasible by reason of the highly obstructed signal paths. Hence, no model for the signal attenuation can be formulated and therefore the derived distances are profoundly defective.

As shown throughout the thesis, BLE performs better than WLAN and hence is put in favor. It has been shown that the combination (i.e., merging the two radio maps

and the observations) of both network technologies does in general enhance the result. However, the humble gain of accuracy (cf. Table 5.3) might not be worth the large effort of incorporating an additional radio map². For the given test site, a total of 60 BLE beacons and ten WLAN routers have been installed. The chosen density has been derived from investigations regarding the range of the access points (cf. Section 3.4.3). In an attempt to reduce the infrastructure, half of the access points (i.e., the access points 02, 04, 06, etc.) were temporarily erased from the radio maps for the exemplary evaluation of the third trajectory, exemplarily shown in Figure 5.3(b)³. For BLE, the mean PPE slightly increased from 6.2 m to 6.4 m. In the case of WLAN, the difference is enormous: The mean PPE increased from 5.7 m to 17.8 m with a maximum error of 60 m. These figures suggest that the number of WLAN access points must not be reduced, but also that a higher amount of access points could potentially increase the accuracy. Even though the accuracy of the BLE result did not decrease by a large amount, it has to be noted that for many epochs, no position could be computed. Thus, the reliability is in any case reduced.

5.3.2 Outlook

Although the absolute position determination is hereby concluded and the goals are met, the research on the subject must not be treated as finished. To really comply with the requirements in terms of position accuracy and reliability needed for an autonomous parking pilot, additional sensors are mandatory. Hence, the accuracy will be enhanced by means of a multiple sensor environment. The absolute positions obtained in this thesis are going to be combined with relative positions derived from an IMU or odometry and steering angle readings as well as with a digital, navigable map. Due to the multi-sensor environment, the large blunders with a PPE of 10 m or worse that occur throughout the trajectory are expected to vanish, yielding an overall smoother and more accurate result. By establishing a particle filter, the geometry of the building will be embedded within the positioning algorithm to eliminate implausible position guesses. Research concerning this matter is subject to a number of follow-up investigations, which are scheduled after the completion of this thesis.

To refine the results of the absolute positioning, one could consider a few improvements over the current routine. As seen in Figure 4.12, the placement of the access points results

²The measurement process itself does not increase the expenditure of time by a large amount, but the monetary effort is roughly doubled when using a second set of access points.

³Note that the Figure only shows the course of the trajectory, the result with reduced access points is not shown separately.

in a shadowing of the signal in one direction. However, the signal is still receivable and the shadowed (and thus weakened) signal can be seen as a characteristic of the signal pattern used for fingerprinting. Thus, no immediate drawback results from the current situation of access point placement. On the second glance, however, the attenuated signal strength implies a reduced coverage area for the access point, ultimately lowering the average visible access point count per reference point. In [24] the authors claim that the number of access points, as long as it is the same in offline and online phase, does not affect the positioning accuracy significantly. Caused by the constant changes of the environment that necessarily occur in parking garages, the indirect signal path may be highly deviating from the offline phase. Thus, LOS signal paths are to be favored. This can be (partly) realized by mounting the access points on the bottom side of the steel girders. Also, for a lateration based positioning, this is an inevitable step as a result of the necessity of LOS signal paths.

Another aspect, that is worth additional research, is the actual fingerprinting algorithm, namely the computation of fingerprint candidates. The common algorithm, also used in this thesis, might not ideally adapt to the characteristics of BLE. Whether or not the introduction of proximity zones as mentioned in 2.3 and thus a classification of the RSSI into multiple distance levels positively influences the positioning accuracy is to be investigated.

Bibliography

- [1] M. Altini, D. Brunelli, E. Farella, and L. Benini. Bluetooth indoor localization with multiple neural networks. In *Wireless Pervasive Computing (ISWPC), 2010 5th IEEE International Symposium on*, pages 295–300, May 2010.
- [2] Apple, Inc. *Getting Started with iBeacon (Version 1.0)*, June 2014.
- [3] Bluetooth SIG. Bluetooth specifications 1.0 a-4.0 (2013), 2013.
- [4] Bluetooth SIG. Basics | Bluetooth Technology Website, 2015. [<http://www.bluetooth.com/Pages/Basics.aspx>; visited on Mar 10th, 2015].
- [5] Bluetooth SIG. Bluetooth Smart | Bluetooth Technology Website, 2015. [<http://www.bluetooth.com/Pages/Bluetooth-Smart.aspx>; visited on Mar 9th, 2015].
- [6] Mark Campbell, Magnus Egerstedt, Jonathan P. How, and Richard M. Murray. Autonomous driving in urban environments: approaches, lessons and challenges. *Philosophical Transactions of the Royal Society A: Mathematical, Physical and Engineering Sciences*, 368(1928):4649–4672, 2010.
- [7] Ruizhi Chen. *Ubiquitous Positioning and Mobile Location-Based Services in Smart Phones*. Premier reference source. Information Science Reference, 2012.
- [8] H Stewart Cobb. *GPS pseudolites: Theory, design, and applications*. PhD thesis, Citeseer, 1997.
- [9] Roland Dutzler, Martin Ebner, and Robert Brandner. Indoor Navigation by WLAN Location Fingerprinting-Reducing Training-Efforts with Interpolated Radio Map. In *UBICOMM 2013, The Seventh International Conference on Mobile Ubiquitous Computing, Systems, Services and Technologies*, pages 1–6, 2013.
- [10] Alexander George. Volvo Thinks Magnetic Roads Will Guide Tomorrow’s Autonomous Cars, Mar 17 2014. [<http://www.wired.com/2014/03/volvo-magnets-autonomous/>; visited on Feb 23rd, 2015].

- [11] Leica Geosystems. *Leica Nova MS50 Datasheet*. Leica Geosystems AG, Heerbrugg, Switzerland, 2013.
- [12] N. Golmie, N. Chevrollier, and O. Rebala. Bluetooth and WLAN coexistence: challenges and solutions. *Wireless Communications, IEEE*, 10(6):22–29, Dec 2003.
- [13] Erico Guizzo. How Google’s Self-Driving Car Works — IEEE Spectrum, 2011. [<http://spectrum.ieee.org/automaton/robotics/artificial-intelligence/how-google-self-driving-car-works>; accessed 18-February-2015].
- [14] Petra Hafner, Thomas Moder, Manfred Wieser, and Thomas Bernoulli. Evaluation of Smartphone-based Indoor Positioning Using Different Bayes Filters. *2013 International Conference on Indoor Positioning and Indoor Navigation*, 2013.
- [15] S. Haykin. *Neural Networks: A Comprehensive Foundation*. International edition. Prentice Hall, 1999.
- [16] Robin Henniges. Current approaches of Wifi Positioning. *Service-Centric Networking – Seminar WS2011/2012*, 2012.
- [17] B. Hofmann-Wellenhof, K. Legat, and M. Wieser. *Navigation: Principles of Positioning and Guidance*. Springer Wien New York, 2003.
- [18] D. Jiang and L. Delgrossi. IEEE 802.11p: Towards an International Standard for Wireless Access in Vehicular Environments. In *Vehicular Technology Conference, 2008. VTC Spring 2008. IEEE*, pages 2036–2040, May 2008.
- [19] K. Kaemarungsi and P. Krishnamurthy. Properties of Indoor Received Signal Strength for WLAN Location Fingerprinting. In *Mobile and Ubiquitous Systems: Networking and Services, 2004. MOBIQUITOUS 2004. The First Annual International Conference on*, pages 14–23, Aug 2004.
- [20] R. Kummerle, D. Hahnel, Dmitri Dolgov, S. Thrun, and W. Burgard. Autonomous driving in a multi-level parking structure. In *Robotics and Automation, 2009. ICRA '09. IEEE International Conference on*, pages 3395–3400, May 2009.
- [21] A. Kushki, K.N. Plataniotis, and A.N. Venetsanopoulos. *WLAN Positioning Systems: Principles and Applications in Location-Based Services*. WLAN Positioning Systems: Principles and Applications in Location-based Services. Cambridge University Press, 2012.
- [22] H. Leppakoski, S. Tikkinen, and J. Takala. Optimizing radio map for WLAN fingerprinting. In *Ubiquitous Positioning Indoor Navigation and Location Based Service (UPINLBS), 2010*, pages 1–8, Oct 2010.

BIBLIOGRAPHY

- [23] W. Lewandowski, Jacques Azoubib, and William J. Klepczynski. GPS: primary tool for time transfer. *Proceedings of the IEEE*, 87(1):163–172, Jan 1999.
- [24] Juraj Machaj, Peter Brida, and Barbora Tatarova. Impact of the number of access points in indoor fingerprinting localization. In *Radioelektronika (RADIOELEKTRONIKA), 2010 20th International Conference*, pages 1–4. IEEE, 2010.
- [25] R. De Maesschalck, D. Jouan-Rimbaud, and D.L. Massart. The mahalanobis distance. *Chemometrics and Intelligent Laboratory Systems*, 50(1):1 – 18, 2000.
- [26] John Markoff. Google Cars Drive Themselves, in Traffic. *The New York Times*, October 9 2010.
- [27] Rainer Mautz. *Indoor positioning technologies*. PhD thesis, ETH Zurich, Department of Civil, Environmental and Geomatic Engineering, Institute of Geodesy and Photogrammetry, 2012.
- [28] Matt McFarland. Sorry, Volvo. Magnetic roads for self-driving cars are a pipe dream., Mar 18 2014. [<http://www.washingtonpost.com/blogs/innovations/wp/2014/03/18/sorry-volvo-magnetic-roads-for-self-driving-cars-are-a-pipe-dream/>; visited on Feb 23rd, 2015].
- [29] Thomas Moder, Petra Hafner, Karin Wisiol, and Manfred Wieser. 3D Indoor Positioning with Pedestrian Dead Reckoning and Activity Recognition Based on Bayes Filtering. In *International Conference on Indoor Positioning and Indoor Navigation*, October 2014.
- [30] Kevin J. Negus and Al Petrick. History of Wireless Local Area Networks (WLANs) in the Unlicensed Bands. *George Mason University Law School Conference, Information Economy Project, Arlington, VA.*, 2008.
- [31] Lang Peng, Junyi Han, Weixiao Meng, and Jingyu Liu. Research on Radio-Map Construction in Indoor WLAN Positioning System. In *Pervasive Computing Signal Processing and Applications (PCSPA), 2010 First International Conference on*, pages 1073–1077, Sept 2010.
- [32] Teemu Roos, Petri Myllymäki, Henry Tirri, Pauli Misikangas, and Juha Sievänen. A Probabilistic Approach to WLAN User Location Estimation. *International Journal of Wireless Information Networks*, 9(3):155–164, 2002.
- [33] P. Schnabel. *Netzwerktechnik-Fibel: Grundlagen, Übertragungstechnik und Protokolle, Anwendungen und Dienste, Sicherheit*. Schnabel, 2004.

BIBLIOGRAPHY

- [34] John C. Stein. Indoor Radio WLAN Performance – Part II: Range Performance in a Dense Office Environment. *Harris Semiconductors*, 2401 Palm Bay, Florida 32905.
- [35] Chris Urmson, Joshua Anhalt, Drew Bagnell, Christopher Baker, Robert Bittner, M. N. Clark, John Dolan, Dave Duggins, Tugrul Galatali, Chris Geyer, Michele Gittleman, Sam Harbaugh, Martial Hebert, Thomas M. Howard, Sascha Kolski, Alonzo Kelly, Maxim Likhachev, Matt McNaughton, Nick Miller, Kevin Peterson, Brian Pilnick, Raj Rajkumar, Paul Rybski, Bryan Salesky, Young-Woo Seo, Sanjiv Singh, Jarrod Snider, Anthony Stentz, William "Red" Whittaker, Ziv Wolkowicki, Jason Ziglar, Hong Bae, Thomas Brown, Daniel Demitrish, Bakhtiar Litkouhi, Jim Nickolaou, Varsha Sadekar, Wende Zhang, Joshua Struble, Michael Taylor, Michael Darms, and Dave Ferguson. Autonomous driving in urban environments: Boss and the Urban Challenge. *Journal of Field Robotics*, 25(8):425–466, 2008.
- [36] Long Vu-Hoang, Hung Nguyen-Manh, Chinh Phan-Duy, Dung Le-Quang, Thanh Do-Van, and Vinh Tran-Quang. A new technique to enhance accuracy of WLAN fingerprinting based indoor positioning system. In *Communications and Electronics (ICCE), 2014 IEEE Fifth International Conference on*, pages 270–275, July 2014.